Identification of cell cycle-regulated *Drosophila* microtubule-associated proteins using quantitative mass spectrometry

Heather Syred

Presented for the Degree of Doctor of Philosophy

The University of Edinburgh

August 2010

Declaration

I hereby declare that I alone have composed this thesis and that the work presented is my own, except where otherwise stated.

Heather Syred

August 2010

ACKNOWLEDGEMENTS

I would first like to thank my two supervisors Hiro Ohkura and Juri Rappsilber for their help and support throughout my PhD. My thanks go especially to Hiro who has been a patient and supportive teacher and has made my first lab experience an enjoyable one.

I should also thank those many people who have made going to work fun, the Ohkura and Rappsilber labs, Jimi and Karen for keeping my MS in check and especially Ana, Nathalie, Judith and Jo whom without I would not be typing this today.

Lastly I would like to thank my family who, with their support, have got me here in the first place and have always supported me through hard times. But most importantly I would like to thank Pete, 'my chef', who has fed and supported me through these 4 years and without whom I would not be as happy as I am today. Thank you.

CONTENTS

FIGURES AND TABLES

ABBREVIATIONS

ATP	adenosine triphosphate
bp	base pairs
BSA	bovine serum albumin
cDNA	complementary DNA
DAPI	4,6-Diamidino-2-phenylindole
Df	deficiency
DNA	deoxyribonucleic acid
dsRNA	double-stranded RNA
FBS	foetal bovine serum
GDP	guanosine diphosphate
GFP	green fluorescent protein
GTP	guanosine triphosphate
HURP	hepatoma upregulated protein
LC	liquid chromatography
MAP	microtubule associated protein
MBP	maltose binding protein
MS	mass spectrometry
NES	nuclear export signal
NLS	nuclear localisation signal
NuMA	nuclear mitotic apparatus protein
NuMAP	nuclear microtubule associated protein
NuSAP	nucleolar spindle associated protein
PBS	phosphate buffered saline
PCR	polymerase chain reaction
RNA	ribonucleic acid
RNAi	RNA interference
S2 cells	Schneider 2 cells
SDS	sodium dodecylsulphate
SDS-PAGE	SDS – polyacrylamide gel electropheresis
TPX2	targeting protein for Xklp2
Tris	2-amino-2-(hydroxymethyl)-1,3-propanediol
UAS	upstream activating sequence

ABSTRACT

The microtubule network is the central framework in multiple cellular processes. The microtubule array undergoes dramatic changes as cells progress through the cell cycle. In mitosis the interphase microtubule array is reorganised into the dynamic mitotic spindle which mediates chromosome segregation. This reorganisation is co-ordinated by microtubule associated proteins (MAPs). However, little is known about the cell cycle regulation of MAPs and how it plays a role in mitotic spindle formation.

In this thesis, I describe the development of a method to determine the profiles and relative quantities of MAPs purified from mitotic and interphase *Drosophila* culture cells. This method utilises mass spectrometry combined with stable isotope labelling by amino acids in cell culture (SILAC) for protein quantification. This study identified MAPs whose association with microtubules increased during mitosis and revealed a new mitotic MAP, which I have named NuMAP.

NuMAP localises to the nucleus in interphase and to microtubules only in mitosis, covering the entire spindle. Truncation analysis identified two protein domains sufficient but not essential for nuclear localisation and one C-terminal domain vital for microtubule localisation. Interestingly, creation of an interphase cytoplasmic pool indicated that the interphase form of NuMAP has low affinity for microtubules, suggesting a cell cycle-related post-translational modification. A deletion mutant of the NuMAP gene was generated by P element excision and will be valuable to define the role of NuMAP in fly development.

1. Introduction

1.1 Microtubule structure and polymerisation

Microtubules are essential cytoskeletal components in all eukaryotic cells. The microtubule network functions as the central framework of a number of different cellular processes such as cell division, morphogenesis and migration (Valiron et al., 2001). The diversity of microtubule function is possible due to the number of different arrays that microtubules form in cells: parallel, staggered linear arrays or radial arrays. This depends on cell type. One of the most remarkable structures formed by microtubules is the mitotic spindle. The mitotic spindle is a very dynamic structure and is crucial to segregate chromosomes correctly during cell division.

1.1.1 Microtubule structure

Microtubules are composed of α- and β-tubulin heterodimers (Weisenberg et al., 1968). This subunit was first purified using its affinity for colchicine, a strong mitotic inhibitor (Weisenberg et al., 1968). The dimer bound one mole of colchicine and two moles of nucleotide, guanosine triphosphate (GTP). It was identified that there were two nucleotide binding sites. The first site allowed rapid exchange of bound and free GTP. Nucleotide exchange at the second site proceeds very slowly. By measuring the binding activity of colchicine, Weisenberg *et al* (1968) found that GTP was necessary to maintain the native protein configuration.

Further biochemical studies showed that the β-subunit hydrolyses GTP during polymerisation (Weisenberg et al., 1968). Hydrolys takes place in the fast exchanging site (the E-site) and occurs when the tubulin subunit becomes integrated into the microtubule lattice. Following hydrolysis, the E-site contains guanosine diphosphate (GDP), which is not exchangeable while the β-tubulin remains within the microtubule (David-Pfeuty et al., 1977). When the microtubule is depolymerised, this GDP-containing dimer becomes free and GDP-GTP exchange can take place. The resulting GTP dimer is then free to undergo another round of polymerization. The α-tubulin subunit also binds GTP (Spiegelman et al., 1977) the second site identified by Weisenberg *et al* (1968). GTP in this site is non-exchangeable and is not hydrolysed during microtubule polymerisation (Spiegelman et al., 1977).

The amino acid sequence of these two globular proteins, α- and β-tubulin, is approximately 45 % identical (Burns, 1991) and each has a molecular mass of about 50 kDa. This remarkable similarity in primary structure suggests similar tertiary structures. The few differences between the proteins are thought to lie on the exterior of the protein, with the GTP binding sites remaining highly conserved (Burns, 1991). Tubulin heterodimers associate in a head to tail arrangement, interacting through hydrophobic and polar contacts (Nogales et al., 1999). This head-to-tail association has been shown to be the structural basis of the protofilament (Figure 1.1a) (Amos and Klug, 1974). Protofilaments come together in a lateral arrangement to form a 25 nm wide hollow cylindrical structure; the microtubule (Amos and Klug, 1974). Purified tubulin polymerised spontaneously *in vitro* produces structures which mainly contain 14 protofilaments. However, negative

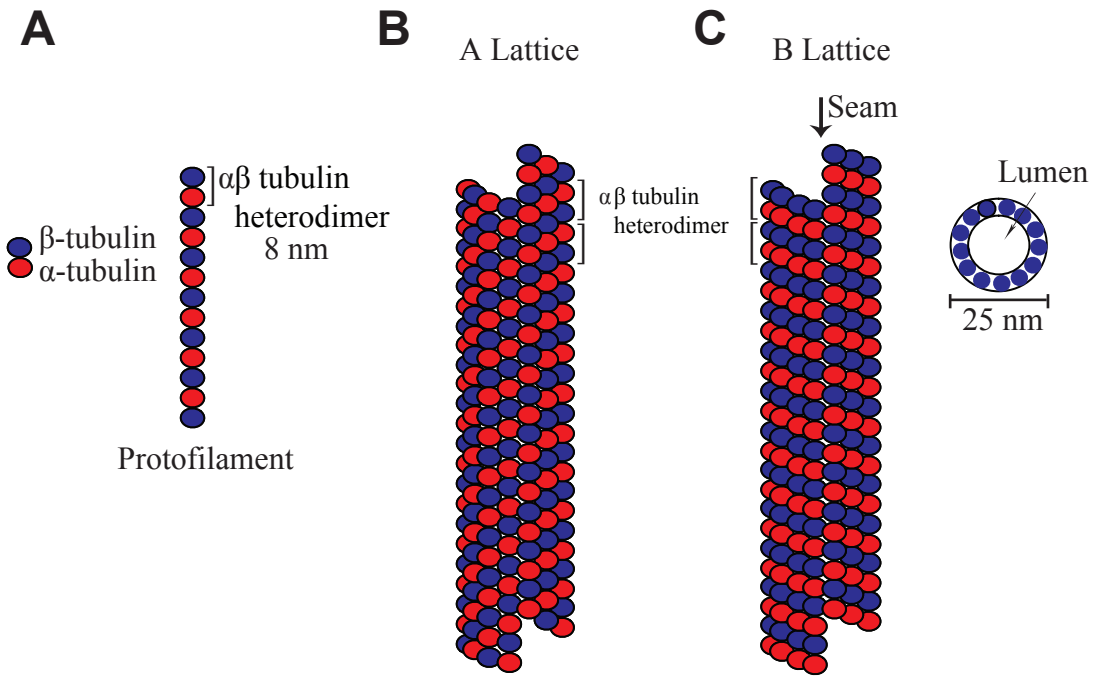

Figure 1.1 The microtubule structure, the protofilament and their subunit. (A) A schematic representation of the tubulin heterodimer and the protofilament. The heterodimers composed of α- and β- tubulin proteins associate in a head-to-tail arrangement to form the protofilament. **(B)** A schematic representation of the A lattice. Lateral associations form between the α-monomers of one protofilament and the β-monomers of the adjacent protofilment. **(C)** A schematic representation of the B lattice. Lateral interactions are between α- and β-monomers (a dimer) of adjacent protofilaments. 13 protofilaments aligned in parallel create a hollow cylindrical structure with a diameter of 25 nm. (Adapted from Desai and Mitchison 1997)

staining of microtubules polymerised *in vivo* or nucleated *in vitro* from centrosomes, showed that 13 protofilaments form the microtubule structure. It is thought that the pericentriolar material of the centrosome nucleates microtubules, creating a uniform polarity and favouring this specific structure. (Amos and Klug, 1974; Evans et al., 1985),

The head-to-tail association of the tubulin dimer leads to structural polarization of the protofilament (Amos and Klug, 1974). Parallel alignment of protofilaments to form the microtubule structure establishes this polarity within the microtubule (Amos and Klug, 1974). This integrated polarity results in distinct microtubule ends with structural and kinetic differences. The two ends of the microtubule have different polymerisation rates, with the faster-growing end known as the plus end and the slower-growing end as the minus end (Allen and Borisy, 1974). The α-tubulin subunit is exposed at the minus end of the microtubule (Fan et al., 1996), which is associated with microtubule organising centres (MTOCs) usually located towards the centre of the cell. In contrast, the faster growing plus end of the microtubule is not anchored and the β-tubulin subunit exposed (Mitchison, 1993). This orientation of the tubulin dimer in the protofilament is also supported by studies of kinesin motor domain binding. A microtubule coated with the kinesin head, the motor domain, a region of kinesin known to bind β-tubulin was examined. Electron microscopy of the decorated microtubule showed the main mass of kinesin head to be associated with the tubulin subunit closer to the plus end. This confirmed the dimer orientation to be α-tubulin to the minus end and β-tubulin to the plus end. *In vivo* the plus end of the microtubule is peripheral and selectively interacts with cellular components such as kinetochores and the cell cortex (Hayden et al., 1990).

The polarity within the microtubule is also critical to the function of motor proteins such as kinesin.

There are two possible arrangements of protofilaments with regard to the lateral interactions, the A-lattice and the B-lattice. For the A-lattice it is proposed that lateral associations are between α-monomers of one protofilament and β-monomers of adjacent protofilaments (Figure 1.1b). In comparison, the lateral interactions of the B-lattice are proposed to be between α- and β-monomers (dimer) of adjacent protofilaments (Figure 1.1c). Structural analysis of a kinesin decorated microtubule confirmed the correct structure to be that of the B-lattice (Kikkawa et al., 1994). The bonds between tubulin monomers do not lie horizontally, they in fact have a 10° angle. This creates a helical path of monomers which travels along the microtubule in a 3-start helix formation. With this arrangement the adjoining monomers in the helix are both either β- or α-subunits for a single helical turn. At this point the change in monomer creates a seam where an α- and β-tubulin are neighbouring (Figure 1.1c) (Kikkawa et al., 1994).

1.1.2 Microtubule polymerisation

The microtubule is formed by the head-to-tail association of the tubulin dimer. However, although the microtubule is described as a helical structure, it does not have to assemble by the classical helical formation. Tubulin dimers often first form a curved sheet like lattice of protofilaments (Detrich and Jordan, 1986). Multiple studies have observed the presence of jagged/C-shaped protofilament sheets at the distal end of microtubules (Detrich and Jordan, 1986; McIntosh et al., 1985; Simon

and Salmon, 1990). This morphology has been seen *in vivo* and *in vitro* and is believed to represent an intermediate structure of microtubule assembly and not disassembly. Erickson (1974) polymerised purified tubulin and took samples for analysis at regular time points during assembly. At early time points he observed these large sheets containing up to 13 protofilaments. However, they rarely saw those sheets containing 13 protofilaments. Closer analysis showed the frequency of protofilament sheets to decrease as microtubule assembly progressed. They therefore hypothesised that microtubule assembly begins with a small aggregate of filaments. This then elongates with the addition of more tubulin dimers to existing filaments, along with the slower addition of protofilaments to the side. This curving structure, with the addition of a 13^{th} filament, will close and form bonds creating the intact cylindrical structure of the microtubule (Erickson, 1974).

The formation of sheets of parallel protofilaments has been observed in conditions lacking associating proteins. This therefore suggests their formation to be an intrinsic property of microtubule assembly (Simon and Salmon, 1990). The presence of these protofilament sheets has been suggested to stabilise microtubules, and when closed the microtubule is more likely to undergo a catastrophe. (Chretien et al., 1995).

1.2 Microtubule dynamics

Microtubules are dynamic structures and undergo significant changes through the cell cycle. It has long been established that the dynamic properties of microtubules are essential for their function, specifically during mitosis (Inoue and Sato, 1967).

Therefore the characterisation of microtubule dynamics and their function has been thoroughly studied. Here I will summarise four main features of microtubule dynamics: treadmilling, dynamic instability, the GTP cap and the importance of microtubule dynamics *in vivo*.

1.2.1 Treadmilling

Microtubules were primarily analysed with respect to treadmilling, a process which had been observed in actin filaments (Wegner, 1976). The idea of treadmilling in microtubules was introduced after Margolis *et al* (1978) observed the continuous incorporation of tubulin into the steady state microtubule using ^{3}HGTP as a tubulin marker. The microtubule poison podophyllotoxin, which interferes with microtubule function in cells, prevented the incorporation of tubulin into the microtubule matrix, but not its loss. Furthermore, pulse labelling of microtubules at steady state showed little loss of label over a significant period of time. These results indicated that microtubule assembly and disassembly occur at different sites of the microtubule (Margolis and Wilson, 1978). An increase in the disassembly rate of microtubules when sheared showed tubulin loss to be end dependent, identifying the assembly and disassembly to occur at opposite ends of the microtubule (Margolis and Wilson, 1978). The plus end of the microtubule incorporates tubulin dimers containing GTP and the minus end loses tubulin dimers containing GDP during treadmilling (Figure 1.2). When microtubule minus ends are fixed in structures such as MTOCs, treadmilling results in the appearance of a flux of tubulin dimer through the microtubule. When microtubule ends are free, treadmilling results in an apparent

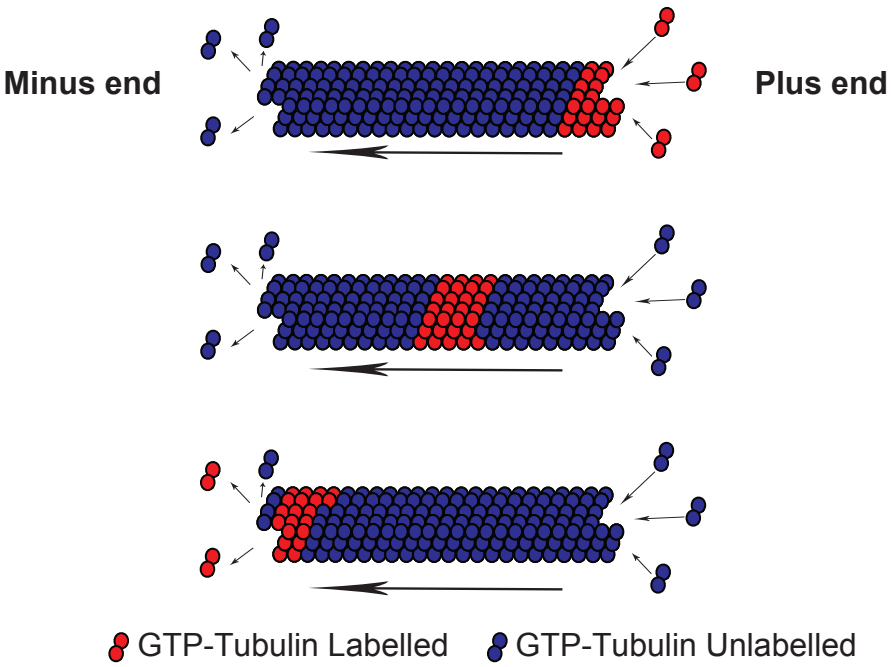

Figure 1.2 A schematic representation of microtubule treadmilling. The plus end of the microtubule incorporates tubulin dimers containing GTP and the minus end loses tubulin dimers containing GDP. When microtubule minus ends are fixed in cell structures, treadmilling results in the appearance of a flux of tubulin dimer through the microtubule.

migration of the microtubule within the cell (Margolis and Wilson, 1981; Rodionov and Borisy, 1997).

1.2.2 Dynamic instability

Dynamic instability is a behaviour whereby microtubules are proposed to alternate stochastically between polymerisation and depolymerisation. This mechanism was first put forward by Mitchison and Kirschner in 1984. The shearing of steady state microtubules and depolymerisation in the absence of re-nucleation decreased the number of microtubules, but created monomers available for incorporation, and resulted in longer microtubules. This indicated that the steady state microtubule network results from the existence of two phases; the majority of microtubules polymerising slowly at equilibrium and a minority of microtubules depolymerising rapidly (Mitchison and Kirschner, 1984). If transition between these phases is frequent, little elongation or number loss would be observed. Mitchison *et al* (1984) concluded that the phase transition occurs infrequently. This was also observed by Horio and Hotani (1986) and was later confirmed by Walker *et al* (1988) with analysis of individual microtubules by video light microscopy. Transitions were not only infrequent but also abrupt and random.

The transition from elongation to rapid shortening is known as a 'catastrophe' and the transition from shortening to elongation as 'rescue'. Walker *et al* (1988) also observed microtubules to 'pause', a period of time when the microtubule length remained constant. However, this occurred very rarely. Observations of individual microtubules have led to the description of dynamic instability by four parameters:

the rates of polymerisation and depolymerisation and the occurrence of catastrophes and rescues (Walker et al., 1988). The microtubule plus end polymerises approximately three times faster than the minus end and undergoes a higher rate of 'catastrophe'. In contrast, the minus end of the microtubule undergoes faster depolymerisation and an increase in the frequency of 'rescue'(Horio and Hotani, 1986). These significant differences of dynamic instability at microtubule ends contribute to the previously described treadmilling effect (Hotani and Horio, 1988). The mechanism of dynamic instability appears to be unique to microtubules and has become established as the main mechanism for the regulation of microtubule dynamics (Desai and Mitchison, 1997).

The hydrolysis of GTP by β-tubulin during polymerisation is thought to be the source of energy for dynamic instability. Kinetic data has shown GTP hydrolysis to be two successive reactions (Carlier and Pantaloni, 1981): chemical cleavage of the γ-phosphate group, followed by the release of phosphate. Although hydrolysis of GTP is thought to provide energy, microtubule polymerisation does not require GTP hydrolysis to occur (Caplow et al., 1994). GTP hydrolysis is also independent of free tubulin concentration, unlike polymerisation, and, when present within the microtubule, GTP is still able to be exchanged. Upon hydrolysis the remaining product, GDP, is locked into the E site of tubulin (Carlier and Pantaloni, 1981). The replacement of GTP with GDP causes a tubulin conformational change, resulting in a more ordered structure (Howard and Timasheff, 1986).

Tubulin-GDP has a stronger tendency to form a double ring structure than tubulin-GTP. Analysis of this structure shows it to be equivalent to pairs of curved protofilaments coiled sideways which are tensioned within the microtubule. This

structure causes functional instability within the microtubule and increases the possibility of depolymerisation (Diaz et al., 1994). Structural analysis of dynamic microtubules revealed structural differences between polymerising and depolymerising microtubule ends. Cryo-electron microscopy showed growing microtubule ends to have straight protofilaments, whereas those undergoing depolymerisation had protofilaments coiled inside-out (Mandelkow et al., 1991).

Caplow *et al* (1994) identified conditions in which guanylyl-(a,b)-methylenediphosphonate (GMPCPP), a GTP analogue, was hydrolysed upon integration into the microtubule lattice. Comparison of the disassociation of GMPCPP and its hydrolysed product GMPCP, showed GMPCP to dissociate faster than its counterpart. They also observed that the energy release upon GMPCPP hydrolysis was close to zero, indicating that the potential energy produced by hydrolysis is stored within the microtubule (Caplow et al., 1994). This system is thought to apply to GTP hydrolysis and potentially regulates microtubule dynamics. Within the cell, the energy stored in microtubules could be utilized to move structures in the cell such as chromosomes during anaphase.

The use of GTP-hydrolysis is proposed to function as the main regulator of microtubule dynamics. Evidence shows that the hydrolysis of GTP induces weakening of the microtubule lattice, increasing the probability of catastrophes. However, the mechanism for prolonged microtubule polymerisation is not addressed here. There are multiple models for the maintenance of microtubule stability, with the key mechanism suggested to be a GTP cap at the plus end of the microtubule.

1.2.3 The GTP cap

Free tubulin has a slow rate of GTP hydrolysis. Integration into the microtubule lattice increases the rate of this reaction (Caplow and Shanks, 1990; David-Pfeuty et al., 1977). As the hydrolysis of GTP is thought to be a main regulator of microtubule dynamics, it was suggested by Mitchison *et al* (1984) that microtubules were stabilised by a cap of tubulin-GTP. This hypothesis was supported by the earlier observation that tubulin is integrated into the microtubule lattice before GTP hydrolysis (Carlier and Pantaloni, 1981). However some studies have indicated that there is little, if any, lag between polymerisation and hydrolysis (Caplow, 1992).

The GTP cap could be made up of either GTP-tubulin or GDP.Pi-tubulin. It is not always the cleavage of GTP that induces a conformational change in protein structures. It can also be the release of phosphate (Pi). Melki *et al* (1990) observed direct evidence for GTP and GDP-Pi intermediates in microtubule assembly. It was found that microtubules composed of GDP.Pi-tublin were very stable, losing subunits at a very slow rate. This led to the conclusion that the release of Pi and not the cleavage of GTP induced a conformational change in tubulin and subsequent destabilisation of the microtubule lattice (Melki et al., 1990). These results supported evidence showing little lag time between microtubule polymerisation and GTP hydrolysis (Caplow and Shanks, 1990). It is therefore proposed that microtubules growing at rates relevant to dynamic instability have terminal GTP subunits and sub-terminal GDP.Pi subunits (Melki et al., 1990). The release of Pi from polymerising microtubules was addressed in later years. Again a lag between microtubule polymerisation and Pi release was observed using rapid taxol-driven microtubule polymerisation (Melki et al., 1996). The presence of this lag was not

confirmed under the conditions of dynamic instability, but clearly supports the model of a GTP/GDP.Pi cap.

The size of the GTP/GDP.Pi cap has also been previously investigated by Walker *et al* (1991). Polymerising microtubules were rapidly diluted and the time it took for microtubules to undergo a catastrophe was measured. Individual microtubules were observed to undergo a catastrophe only seconds after dilution, even at high rates of microtubule elongation. It was therefore concluded that the size of the stabilising cap was small, ≈ 200 tubulin dimers or less, and was independent of microtubule polymerisation rates (Walker et al., 1991). By labelling subunits with rhodamine, Drechsel *et al* (1994) measured the size of the cap to be as few as 40 subunits in order to stabilise the microtubule plus end. This supports a model in which at least one tubulin subunit at the end of all 13 protofilaments of a microtubule is bound with GTP (Drechsel and Kirschner, 1994).

1.2.4 Microtubule dynamics in vivo

Several biological functions in the cell have been suggested to gain the benefit of dynamic instability. Firstly it has been proposed that dynamic instability allows the rapid filling of newly formed cytoplasm with microtubules. Imaging of fluorescently tagged microtubules in frog embryonic neurons showed that microtubules change rapidly between configurations during growth cone extension. However, no net growth within the microtubule system was observed, with little change in the growth, shrinkage and catastrophe rates. This suggested the colonisation of newly formed cytoplasm was regulated by a high rescue frequency of microtubules. Translocation

of polymer from the axon also appeared to be a major mechanism in generating new polymer in the growth cone (Tanaka and Kirschner, 1991).

Interestingly, dynamic instability is thought to be the mechanism by which microtubules search three-dimensional space effectively to find specific target sites, this is known as the search-capture model. Quantitative modelling showed dynamic instability reduces the time needed for microtubules to find a target; and clearly demonstrated the importance of dynamic instability in the search and capture model (Holy and Leibler, 1994). The search-capture model was formulated to account for the capture of kinetochores by microtubule plus ends during the formation of the mitotic spindle. Using interference-contrast light microscopy this process was visualised in prometaphase newt lung cells. Microtubules emanating from polar regions continuously probed chromosomes until they contacted chromosome kinetochores (Hayden et al., 1990). Captured microtubules are then thought to be stabilised, resulting in the detyrosination of α-tubulin (Bulinski and Gundersen, 1991).

The parameters of dynamic instability *in vitro* differ from those observed *in vivo*. Microtubules assembled from purified tubulin *in vitro* show reduced dynamic behaviour when compared to those polymerised *in vivo*. Microtubule elongation in sea urchin interphase extract is approximately six times faster than that observed with purified sea urchin egg tubulin. The occurrence of catastrophes and rescues were 20 times and 2 times more frequent respectively. However, the rate of shortening was equivalent between *in vitro* and *in vivo* samples (Simon et al., 1992). Therefore, sea urchin extract must contain factors that stimulate elongation velocity and induce microtubule catastrophe (Simon et al., 1992).

The parameters of microtubule dynamics also change extensively through the cell cycle, specifically at the interphase-mitosis transition. Incorporation of labelled bovine tubulin into cultured mammalian cells occurs in a matter of seconds during mitosis. However, in interphase cells, fluorescent microtubules are only obtained after minutes. Photo-bleaching has also confirmed this difference in microtubule dynamics (Saxton et al., 1984). Analysis of microtubule dynamics in interphase and mitotic *Xenopus* extracts showed a significant difference in microtubule dynamics between the two cell states. Quantitative analysis determined polymerisation and depolymerisation rates to be similar, with an increase in the frequency of catastrophe (Belmont et al., 1990). Cell differentiation also induces different microtubule dynamics. Microtubules are selectively stabilised during cell differentiation, becoming labelled by post-translational modifications of phosphorylation and acetylation (Baas et al., 1991; Bulinski and Gundersen, 1991).

The control of microtubule dynamic instability appears to be achieved through regulatory molecules targeted to control the frequency of microtubule transition between phases. Activation of *Xenopus* extracts with cyclin B results in shortening of centrosome-nucleated microtubules with increased catastrophe rates (Verde et al., 1992). Computational simulation demonstrated that an increase in catastrophe and a decrease in rescue frequencies could reproduce microtubule dynamic changes observed *in vivo* between interphase and mitosis (Gliksman et al., 1993).

Evidence that microtubules are also regulated by signal transduction pathways has been observed. Cell stimulation of macrophages with phorbol esters results in an increase in the level of microtubule polymer and number (Robinson and

Vandre, 1995). Studies on the regulation of microtubule dynamics have suggested that phosphorylation and transcriptional regulation play significant roles. Treatment of sea urchin egg extract with a potent phosphatase inhibitor resulted in the elimination of microtubule rescue and the production of short dynamic microtubules, typical of mitosis (Gliksman et al., 1992). In neurite growth, nerve growth factor has been suggested to promote microtubule assembly through the synthesis of microtubule regulating factors (Drubin et al., 1985).

To understand fully the dynamics of microtubules *in vivo*, significant work has been carried out to identify the proteins regulating microtubules. A large number of these proteins are known to associate with microtubules. This group of proteins are collectively called microtubule-associated proteins, (MAPs). Below I discuss a number of MAPs, how they regulate microtubules, and the roles they play in cellular processes.

1.3 Microtubule-associated proteins

Microtubule-associated proteins are the main regulators of microtubule dynamics and organisation and are defined as proteins which associate with microtubules (Solomon et al., 1979). They were first identified as proteins which fractionate with microtubules after cycles of assembly and disassembly (Borisy et al., 1975) with the more prominent proteins having high molecular weights.

MAPs are classified into 2 groups, motor and non-motor MAPs. Motor MAPs generate force through adenosine-triphosphate (ATP) hydrolysis and move along the microtubule, often carrying cargo (Amos and Cross, 1997). Non-motor

MAPs are a varied group of proteins and do not contain any force-generating domains. These proteins regulate microtubules by binding directly and through their associating proteins.

The movement of motor MAPs along the microtubule is directional due to the polymer's polarised structure and are classified by their direction of translocation. There are two families of motor MAPs; dynein and kinesin, which are defined by their motor domain structure. One form of dynein, cytoplasmic dynein 1, is a minus end-directed complex with a range of functions, including spindle positioning and organisation during mitosis (Eshel et al., 1993). Dynein is regulated through its interaction with accessory proteins such as dynactin (Gonczy et al., 1999; Goshima et al., 2005; Morales-Mulia and Scholey, 2005). The kinesin family of motors are classified into 14 groups and are mostly plus end-directed motors (Amos and Cross, 1997; Lawrence et al., 2004; Miki et al., 2005). One exception is kinesin-14 which is a minus end-directed kinesin (Miki et al., 2005). Like dynein, kinesins play essential roles in a number of cellular processes, including organelle transport (Brady et al., 1990), nuclear movement (Holzinger and Lutz-Meindl, 2002), chromosome segregation and bipolar spindle formation (Enos and Morris, 1990).

Non-motor MAPs are a diverse group of proteins with no common structural or functional motifs. They are classified by the roles they play in microtubule regulation and can be divided into two main groups. Firstly there are those that stabilise microtubules, for example the key neuronal protein tau. Tau increases the polymerisation rates of individual microtubules and *in vitro* enhances a reduction in the rate of microtubule transition to the depolymerisation (Drechsel et al., 1992). In

neurons, tau influences net microtubule assembly, increasing neurite extension and stability (Esmaeli-Azad et al., 1994).

Secondly there are MAPs that destabilise microtubules. These proteins are important for the rapid change of microtubule organisation through the cell cycle. Microtubule destabilisation is induced through multiple mechanisms. For example, the protein Katanin induces rapid depolymerisation by removal of the GTP cap through microtubule severing. This leaves the microtubule prone to rapid disassembly (Hartman et al., 1998; McNally et al., 1996; McNally and Vale, 1993). In contrast the protein stathmin prevents microtubule polymerisation by sequestering the tubulin dimer inhibiting microtubules polymerisation (Belmont and Mitchison, 1996) and inducing catastrophes.

1.4 Biochemical identification of microtubule-associated proteins

Microtubule-associated proteins regulate microtubule organisation, dynamics and, in turn, their function in the cell. Due to their key roles in microtubule cytoskeletal function, the identification of MAPs has become an important goal in research.

MAPs were first identified in porcine brain tissue as high molecular weight proteins which co-purify with microtubules in assembly/disassembly cycles (Borisy et al., 1975), however this identified very few proteins. The conditions of microtubule assembly/disassembly cycles excluded the isolation of specific groups of MAPs such as microtubule destabilising proteins. Further improved microtubule purification methods have therefore been developed.

In 1982, Vallee investigated the use of taxol, a microtubule stabilising drug, in the purification of MAPs. Using taxol, microtubules were assembled and purified in conditions for rapid and high yield of MAPs which were previously unsuitable for microtubule polymerisation (Vallee, 1982). MAPs were shown to disassociate from microtubules when exposed to elevated concentrations of NaCl, providing a method for the separation of MAPs from microtubules (Vallee, 1982; Vallee and Bloom, 1983). Using this new taxol dependent method, Vallee and Bloom (1983) identified several mitotic spindle MAPs by generating monoclonal antibodies. This approach provided a rapid and conclusive method for the identification of MAPs in various cell systems (Vallee and Bloom, 1983). Although sedimentation of taxol-stabilised microtubules with their associating proteins is rapid, only proteins which tightly bind the entire microtubule length are identified.

In 1989 an affinity chromatography method for the identification of less-abundant MAPs was developed by Kellogg *et al* (1989). Affinity chromatography allowed the isolation of minor MAPs with weak microtubule binding and identified proteins that localised to the centrosome and kinetochores (Kellogg et al., 1989). Comparison of microtubule co-sedimentation and affinity chromatography showed these methods to be complementary to each other. Affinity chromatography identifies a larger variety of proteins with a higher protein yield. However, although a broader range of MAPs are identified using affinity chromatography, co-sedimentation still isolates unique proteins. Neither method obtains complete MAP coverage and each approach has its advantages; affinity chromatography allows close regulation of elution conditions, while co-sedimentation is rapid and robust (Kellogg

et al., 1989). Therefore these methods used in parallel could obtain a more comprehensive list of MAPs.

The above studies confirmed isolated proteins to be MAPs by a variety of methods. Borisy *et al* (1975) examined the sedimentation of the high molecular weight proteins in conditions in which microtubule assembly was prohibited. Both the Vallee and Bloom (1983) and the Kellogg *et al* (1989) studies produced antibodies against isolated proteins. Immunofluorescence microscopy confirmed protein localisation to microtubules and immunoblot confirmed protein enrichment in microtubule fractions (Kellogg et al., 1989; Vallee and Bloom, 1983).

In recent years mass spectrometry and biochemical screens have also been used in combination for the identification of MAPs. Microtubule co-sedimentation has been used to isolate MAPs from extracts of various organisms and mass spectrometry used for protein identification (Hughes et al., 2008; Mack and Compton, 2001; Sisson et al., 2000). Together these screens identified 303 MAPs, 17 of which were primarily isolated to interact with actin and therefore also bind microfilaments. Mack and Compton's (2001) use of mammalian mitotic cell extract to identify spindle-associated proteins was complemented by the isolation of structures such as the centrosome which revealed more mitotic proteins (Andersen et al., 2003; Muller et al., ; Ozlu et al., 2010; Sauer et al., 2005; Skop et al., 2004). Further proteomic analysis of human spindles confirmed the high complexity of the spindle apparatus and showed it to contain more proteins than previously predicted or identified (Sauer et al., 2005). Together these numerous screens have provided hundreds of candidate MAPs.

1.5 The regulation of microtubule associated proteins

Although significant research has been carried out to identify MAPs, little is known about their regulation. Due to the essential role MAPs play in the regulation of microtubules and the formation of the mitotic spindle, it is likely that they themselves are under tight regulation. At present, only three mechanisms have been identified to regulate MAPs: protein phosphorylation, ubiquitination and the Ran pathway.

1.5.1 The regulation of microtubule associated proteins by phosphorylation

Structural MAPs have been shown to be *in vitro* substrates of several protein kinases suggesting a major role of MAP regulation is the post translation modification of phosphorylation. However precise mechanisms have been identified and studied in very few cases.

Tau

Hyper-phosphorylated forms of the microtubule stabilising protein tau are the components of paired helical filaments. The presence of these filaments is a major hallmark of Alzheimers disease (Morishima-Kawashima et al., 1995). Due to its implication in the pathology of neurodegeneration, most published data regarding MAP phosphorylation concerns tau and its effect on microtubule binding and regulation. Tau can be phosphorylated by multiple kinases at many different sites

which effect its ability to promote the assembly of microtubules (Lindwall and Cole, 1984).

Two types of tau phosphorylation have been distinguished; phosphorylation at KXGS motifs in repeat sites and TP/SP motifs in domains flanking the repeats. Phosphorylation of TP/SP motifs accounts for approximately 80 % of tau phosphorylated residues. However, using site directed mutagenesis the phosphorylation of Ser^{262} within a KXGS motif in the first repeat has been identified to be dominant in reducing the affinity of tau for microtubules (Biernat et al., 1993; Morishima-Kawashima et al., 1995). This phosphorylation of tau specifically at Ser^{262} is essential for microtubule destabilisation and reorganisation during neuronal differentiation (Biernat and Mandelkow, 1999).

Previous studies showed C-kinase and CaM Kinase II can phosphorylate tau at Ser^{262} but it only partially reduces the microtubule binding of tau (Sengupta et al., 1998). Interestingly they showed that Thr^{231} and Ser^{235} phosphorylation with Ser^{262} gave the maximum inhibition of the microtubule binding of tau. (Sengupta et al., 2006) that the phosphorylation of tau by cyclin dependent kinase-5 (Cdk5) at Ser^{235} induces robust phosphorylation of Thr^{231} and Ser^{262} by glycogen synthase kinase-3 (GSK3). This induction of GSK activity is proposed to be regulated by inhibitory cross-talk of Cdk5 and GSK3 via phosphatases (Plattner et al., 2006).

Kinesin-5

Kinesin-5 is a key regulator of spindle assembly and has also been reported to be phosphorylated. The tail region of Kinesin-5 contains a conserved motif which in

Xenopus was shown to be phosphorylated by Cdk1 during mitosis (Cahu et al., 2008; Heck et al., 1993; Sawin and Mitchison, 1995). In *Drosophila,* the non-phosphorylated kinesin-5 protein does not localise to the mitotic spindle nor does it rescue the mutant monopolar phenotype. Kinesin-5 localisation and function are therefore phosphorylation-dependent (Goshima and Vale, 2005; Sharp et al., 1999). During interphase kinesin-5 remains diffuse and does not associate with microtubules. As cells progresses into mitosis kinesin-5 is phosphorylated by Cdk1 and associates with microtubules, regulating the formation of the bipolar mitotic spindle (Goshima and Vale, 2005).

In HeLa cells, the microinjection of antibodies against human kinesin-5 blocked centrosome migration and resulted in cell arrest in mitosis with monoastral microtubule arrays. Blangy *et al* (1995) also showed that the conserved phosphorylation site Thr^{927} was phosphorylated exclusively in mitosis and was readily phosphorylated by $p34^{cdc2}$/cyclin B *in vitro*. The microtubule association of human kinesin-5 was inhibited by the mutation of Thr^{927} to a nonphosphorylatable form. These results indicated that the phosphorylation of kinesin-5 at Thr^{927} by $p34^{cdc2}$ protein kinase is essential to promote its microtubule association.

CLIP-170

Recently the phosphorylation of the MAP CLIP-170 has been shown to be important for the formation of focal adhesions and lamellipodium created during cell polarity and migration processes. Nakano *et al* (2010) identified the majority of endogenous CLIP-170 protein to be phosphorylated at Ser^{311} by the AMP-activated protein kinase

(AMPK). Both the inhibition of AMPK and the transient expression of the non-phosphorylatable form of CLIP-170 resulted in an accumulation of CLIP-170 at slower growing microtubule tips. It was also noted that microtubule depolymerisation was reduced and the number of stable microtubules was increased (Nakano et al., 2010). Collectively the data suggests that AMPK phosphorylation of CLIP-170 is needed for the effective disassociation of CLIP-170 from microtubules and is essential for efficient microtubule polymerisation and depolymerisation. Interestingly, Nakano *et al* (2010) also demonstrated that CLIP-170 is the most important protein substrate of AMPK as phenotypes produced by AMPK depletion of inhibition could be rescued by the expression of phosphomimetic CLIP-170.

1.5.2 The regulation of microtubule associated proteins by Ran- a central player in mitosis

Ran is an abundant nuclear GTPase which was first characterised to regulate protein nuclear transport during interphase. In 1999 it was demonstrated that Ran plays a significant role in the assembly of the mitotic apparatus. The addition of RanGTP to *Xenopus* M phase extracts induced the nucleation and assembly of spindle like structures (Carazo-Salas et al., 1999). Further studies confirmed this and identified RCC1 (the Ran nucleotide exchange factor), RanBP1 (a guanine nucleotide dissociation inhibitor) and RanGAP (an activator of Ran GTPase activity) to be involved in the spindle assembly process (Kalab et al., 1999; Ohba et al., 1999). A generally accepted model is that RCC1, a chromosomal associated protein, generates a high concentration of RanGTP is the region of the chromosomes.

In the cytoplasm the protein RanGAP is thought to stimulate Ran GTPase activity. From this a RanGTP gradient is formed; a high RanGTP concentration surrounding the chromosomes reducing to a low cytoplasmic RanGTP concentration. Therefore a favourable environment for microtubule nucleation and spindle assembly is created in the vicinity of chromosomes. The existence of this gradient has been demonstrated in *Xenopus* egg extract and cells. Using fluorescence energy transfer based biosensors, RanGTP was shown to have a steep nuclear cytoplasm concentration gradient in interphase and a steep chromosome cytoplasm gradient in mitosis (Kalab et al., 2002). Long range gradients were later demonstrated and predicted to result from the RanGTP importin-β complex preventing RanGAP induced GTP hydrolysis until the association of importin-α (Caudron et al., 2005). In cells, this long range gradient kinetically promotes spindle formation (Kalab et al., 2006).

Ran is known to associate with the nuclear import receptors importin-β and importin-α. Analysis of Ran's role in spindle assembly showed these receptors to play significant roles. Investigation into protein regulation by Ran and the nuclear import receptors, revealed the protein NuMA (nuclear mitotic apparatus protein) as a target. Alongside this, the purification of Ran-dependent nucleation activity from HeLa cells using *Xenopus* egg extract depleted of importin-α, identified the protein TPX2 (Gruss et al., 2001).

From this work it was proposed that in low RanGTP concentrations the cargo, such as MAPs regulating spindle assembly, bind importin-α and -β. In high RanGTP concentrations, for example surrounding chromosomes, importin-β dissociates from the complex and binds RanGTP. This dissociation weakens the binding between

importin-α and its cargo. Spindle assembly factors are released and activate microtubule nucleation and spindle formation. Away from the chromosomes, Ran GTPase activity is activated by the RanGAP/RanBP1 complex and importin-β is released, allowing it to re-establish inhibition of spindle assembly factors distant from the chromosomes (Dasso, 2002; Gruss et al., 2001). Therefore spindle assembly factors will be predominantly released in the vicinity of the chromosomes. This model is illustrated in Figure 1.3.

During interphase, Ran and the importin proteins regulate the import of proteins into the nucleus. Therefore from this model, Ran regulated spindle assembly factors are localised to the nucleus during interphase. Indeed the spindle factors NuMA and TPX2 are located in the nucleus during interphase.

1.5.3 Mitotic Ran regulated importin cargos

Multiple proteins have been identified to be regulated directly by Ran or are related to Ran regulated factors. Here I will describe key spindle assembly factors which are regulated by the Ran pathway.

TPX2

Targeting protein for Xklp2 (TPX2) is an 82.4 kDa protein first identified as being required for the microtubule localisation of the kinesin like protein Xklp2. A point mutation of Xklp2 suggested TPX2 to be a receptor for the Xklp2 leucine zipper and regulates the mitotic specific association of Xklp2 with microtubules (Wittmann et

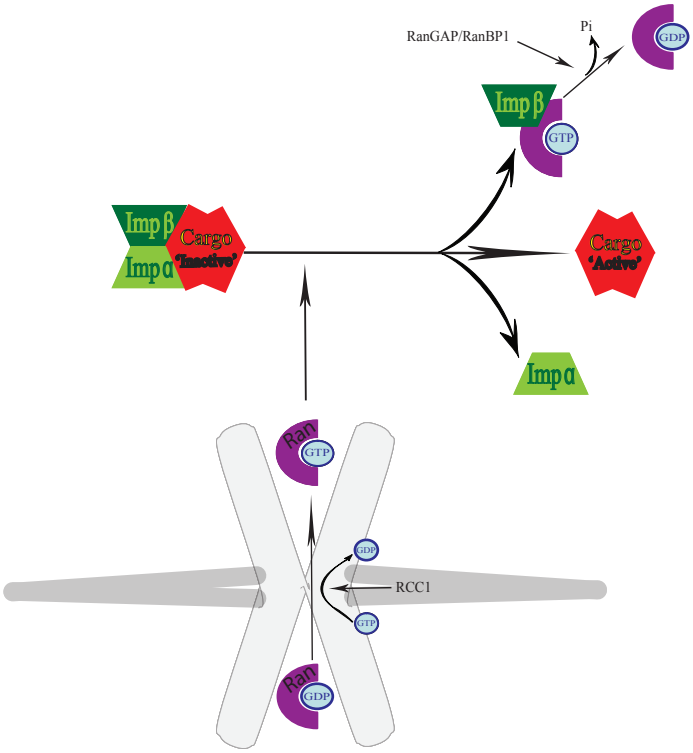

Figure 1.3 Model of Ran regulation of spindle assembly factors.
At low RanGTP concentrations importin-α and -β form a complex with their cargo. In high RanGTP concentrations, for example around chromosomes, importin-β dissociates from the complex and binds RanGTP. The interaction of importin-α and its cargo is weakened and the active cargo is released. In the cytoplasm the RanGAP/RanBP1 complex activates Ran's GTPase activity releasing importin-β, allowing the re-estabilshment of cargo inhibition.

al., 1998). During interphase TPX2 is localised in the nucleus and during mitosis becomes localised to the spindle poles. This pole localisation requires activity of the dynein-dynactin complex. In late anaphase TPX2 is relocated to the spindle midbody(Wittmann et al., 2000). Immunodepletion of TPX2 in mitotic *Xenopus* egg extract induced bipolar spindle structures with disintegrating poles and a decreased microtubule density. In contrast, excess TPX2 created monopolar spindle structures with large poles (Wittmann et al., 2000). In HeLa cells TPX2 depletion arrested cells in mitosis with multipolar spindles (Garrett et al., 2002), or no spindle formation even in the presence of duplicated centrosomes (Gruss et al., 2002). Later work has shown that depletion of TPX2 in mammalian cells blocks kinetochore associated microtubule polymerisation but does not affect chromosome capture by centrosomal microtubules (Tulu et al., 2006). However, co-depletion of TPX2 with MCAK, or the addition of excess XMAP215 can rescue spindle formation (Groen et al., 2009).

As described earlier, TPX2 is regulated by RanGTP and is required for spindle formation through the RanGTP pathway. TPX2 is inactivated by importin-α binding which is displaced by RanGTP (Gruss et al., 2001). A TPX2 mutant that shows reduced affinity for importin-α is constitutively active and induces the formation of microtubule containing aster-like structures in *Xenopus* egg extracts. However, although importin-α inhibits TPX2 induced microtubule formation, it does not inhibit TPX2 tubulin interaction or its ability to bundle microtubules (Schatz et al., 2003). TPX2 has also been identified to activate the mitotic kinase Aurora A. RanGTP stimulates an interaction between TPX2 and Aurora A resulting in the phosphorylation of both proteins in a microtubule dependent manner (Tsai et al., 2003). TPX2 and microtubules induce Aurora A phosphorylation by prevention of

protein phosphatase I. This de-phosphorylation results in a kinase gradient on the microtubules and regulates spindle assembly and dynamics (Tsai et al., 2003). The interaction of these two proteins is inhibited by importin-α resulting in no Aurora A activity or recruitment to microtubules (Trieselmann et al., 2003).

NuMA

Nuclear mitotic apparatus protein (NuMA) is a 236 kDa coiled-coil protein which is a component of the nuclear matrix and the aster promoting activity complex (Sun and Schatten, 2006). The localisation of the NuMA protein is cell cycle-regulated. In interphase NuMA is restricted to the nucleus of the cell. Indirect immunofluorescence in human cells showed NuMA to concentrate to the polar regions of the mitotic apparatus during mitosis (Lydersen and Pettijohn, 1980). This localisation is dependent on the integrity of the mitotic spindle. Closer analysis identified more specific cell-cycle localisation; in prophase NuMA localises in the vicinity of centrosomes. It becomes localised to the poles in metaphase, with a crescent shape localisation at poles in anaphase. Lastly in telophase, NuMA is localised to the newly formed sister nuclei (Kallajoki et al., 1991). Again these specific localisations are dependent on the presence of functional microtubules.

NuMA is essential for the formation and early function of the mitotic spindle. In a cell free system for the assembly of mitotic asters the depletion of NuMA results in the formation of dispersed microtubules instead of organised asters (Gaglio et al., 1995). In *Xenopus* egg extracts, depletion results in chromatin associated with irregular microtubule arrays which lack characteristic spindle poles (Gaglio et al.,

1995; Merdes et al., 1996). The injection of monoclonal NuMA antibody into interphase and prophase HeLa cells showed inhibition of the mitotic spindle formation. Cells remained in a prometaphase state (Kallajoki et al., 1991). Antibody injection during metaphase shows spindle collapse into monopolar spindles (Yang and Snyder, 1992). In contrast, antibody microinjection during anaphase resulted in fewer defects, suggesting NuMA is required early in mitosis (Kallajoki et al., 1993).

The cell cycle localisation and function of NuMA is regulated by phosphorylation. Mutation of a predicted $p34^{cdc2}$ phosphorylation site abolishes NuMA association with spindle microtubules and poles. This results in spindles that are disorganised and micronuclei are formed as seen with NuMA depletion (Compton and Luo, 1995). However this mutation does not affect NuMA localisation to the nucleus. NuMA associates with the dynein/dynactin complex (Merdes et al., 1996), which is thought to translocate NuMA to the spindle poles (Sun and Schatten, 2006). In anaphase NuMA is de-phosphorylated and dissociates from the dynein/dynactin complex and the spindle poles. NuMA dissociation from the poles, allowing spindle disassembly and the reorganisation of the microtubule network into an interphase array (Gehmlich et al., 2004).

NuMA is also thought to be regulated by RanGTP although the details of this regulation are not yet established. NuMA interacts with the nuclear transport receptor protein importin-β which inhibits microtubule aster formation in *Xenopus* egg extracts (Wiese et al., 2001). NuMA is released from importin-β by the association of RanGTP, inducing the formation of the spindle structures (Nachury et al., 2001).

NuSAP

Nucleolar spindle associated protein (NuSAP) is a 48 kDa protein which was first identified in a screen of cDNA expression patterns during proliferation of mouse MCSTSE1 oseteoblasts (Raemaekers et al., 2003). NuSAP is similar to other Ran regulated proteins and is localised in the nucleus during interphase and on the spindle during mitosis. Specifically, NuSAP localises to microtubules in the vicinity of the chromosomes during metaphase and early anaphase. This chromosomal localisation is not dependent on microtubule integrity. NuSAP was identified to directly bind DNA and it is therefore thought that NuSAP links chromosomes and microtubules (Ribbeck et al., 2007). Depletion of NuSAP protein by siRNA in HeLa results in a number of mitotic phenotypes. Prometaphase spindles are disorganised and frequently show abnormal chromosome condensation patterns. Metaphase spindles are also less dense with disorganised microtubules and misaligned chromosomes (Raemaekers et al., 2003).

NuSAP is regulated by rapid degradation and the Ran pathway. Importin-α and importin-β have been shown to associate with NuSAP and inhibit protein activity. RanGTP releases NuSAP from importin-α and importin-β allowing NuSAP to regulate spindle function, microtubule bundling and stabilisation (Ribbeck et al., 2006). The protein NuSAP is described in further detail in 4.7.2.

HURP

Hepatoma upregulated protein (HURP) is a microtubule binding protein which was first identified in 2003 due to its differential expression in human hepatocellular

carcinoma (HCC). HURP mRNA levels are regulated closely through the cell cycle and peak at the G_2/M phase transition (Tsou et al., 2003). In a functional genomic screen in HeLa cells, HURP was identified to be required for chromosome congression and alignment. In HeLa cells HURP co-localises with the mitotic spindle with an increased concentration in the vicinity of the chromosomes (Wong and Fang, 2006). The depletion of HURP results in the persistence of unaligned chromosomes and a reduced tension in inter sister kinetochore tension in HeLa cells (Koffa et al., 2006; Wong and Fang, 2006). *In vivo*, HURP stabilises microtubules, promotes polymerisation, supports bipolar spindle formation and reduces spindle turnover. As a result HURP plays an important role in spindle stability and dynamics (Wong and Fang, 2006).

HURP was also identified to be a target of the Ran pathway. HURP protein was determined to be a direct cargo of the nuclear transport protein importin-β. The overexpression of a RanGTP mimic (RanQ69L) in COS7 cells resulted in increased association of HURP with the mitotic spindle. In addition HURP is phosphorylated by the Ran regulate kinase Aurora A. This phosphorylation increases the stability of the HURP protein (Yu et al., 2005).

1.5.4 Regulation of MAPs by ubiquitination

The ubiquitin ligase anaphase-promoting complex/cyclosome (APC/C) is essential for correct formation of the mitotic spindle. Recently it was identified that the APC/C promotes the ubiquitination and degradation of four proteins required for spindle formation; Bard1, Hmmr, HURP and NuSAP (Song and Rape). Similar to

other known APC/C substrates, all four proteins accumulate in HeLa cells arrested in mitosis and are degraded upon mitotic exit. All proteins are absent from quiescent cells and co-expressed on cell cycle re-entry. As described previously, HURP and NuSAP are also regulated by RanGTP and the importin proteins. Interestingly HURP and NuSAP proteins are not degraded in HeLa cell extracts containing high levels of importin proteins. In contrast Bard1 and Hmmr are effectively degraded in these conditions. It is proposed that the degradation of NuSAP and HURP requires their release from importin-β by RanGTP. The inhibition of APC/C-dependent degradation of NuSAP and HURP by importin-β during prometaphase is essential for spindle formation. Equally, the degradation of excess HURP and NuSAP proteins by the APC/C is important to achieve accurate spindle formation (Song and Rape, 2010). The co-regulation of these proteins is therefore essential for cell cycle progression and spindle formation.

1.6 Project aims and objectives.

The microtubule network functions as a central framework in a number of different cellular processes and changes dramatically as cells progress through the cell cycle. In mitosis the interphase microtubule array is reorganised into the dynamic mitotic spindle which is crucial for the correct segregation of chromosomes during cell division. This reorganisation is regulated by a group of proteins collectively called microtubule-associated proteins (MAPs). However, little is known about the regulation of MAPs.

My hypothesis is that there are distinct groups of MAPs which associate and regulate microtubules at specific times during the cell cycle. For example, as cells progress from interphase to mitosis, an interphase group of MAPs will disassociate and a mitotic group of MAPs will associate with microtubules (Figure 1.4). This group of mitotic MAPs will be important for the correct formation and function of the mitotic spindle. The aim of this study was to identify those MAPs which associate with microtubules specifically during mitosis and to understand their regulation and function.

To fulfil this aim, I began the study with two specific objectives:

1) The development of a method for the identification of MAPs which associate with microtubules specifically during mitosis.

2) The characterisation of those proteins identified to associate with microtubules specifically during mitosis.

In this thesis I describe the work carried out to achieve these objectives and the subsequent identification of a new mitotic-specific MAP.

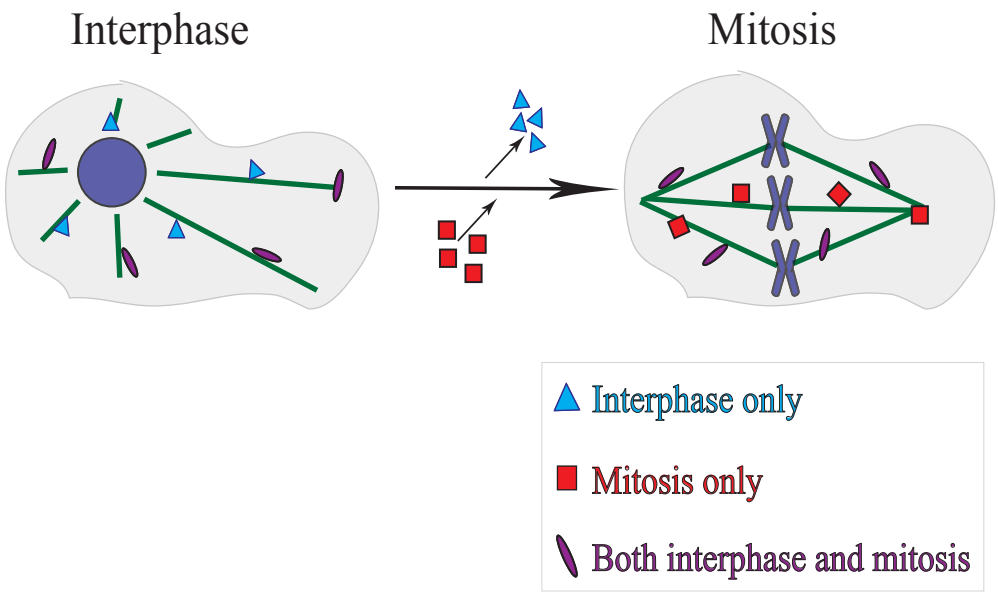

Figure 1.4 Proposed model of microtubule associated protein regulation from interphase to mitosis. There are three distinct groups of microtubule associated proteins (MAPs) which associate with microtubules at specific times during the cell cycle. As cells progress from interphase to mitosis, the interphase group of MAPs dissociate from microtubules and a group of mitotic MAPs associate with microtubules. The third group of MAPs remain associated with microtubules in both interphase and mitosis.

2. Materials and methods

2.1 Supplier information

All oligonucleotides used in this study were supplied by MWG-Biotech. All chemical reagents (if not stated otherwise) were supplied by Invitrogen, Sigma-Aldrich and Gibco. All chemicals used were analytical grade. Other kits and equipment used are stated below.

2.2 Standard buffers and stock solutions

Standard stock solutions and buffers were used throughout the study (Sambrook, 1989). Compositions of commonly used buffers were: Protein sample buffer (50 mM Tris pH6.8, 2 % SDS, 10 % Glycerol, 0.1 % Bromophenol blue); PBS (1.4 mM KH_2PO_4, pH 7.5, 4.3 mM Na_2HPO_4, 2.7 mM KCl, 137 mM NaCl); DEPC water (0.01 % DEPC added to water and stirred overnight); TBS (50 mM Tris HCl pH 7.4, 150 mM NaCl). Where necessary, buffers and solutions were sterilised by using an autoclave.

2.3 Antibodies

The working dilutions of all primary and secondary antibodies used are shown in Table 2.1.

Table 2.1 Antibodies used in this study.

Antibodies	Dilution	Blocking solution	Company
Primary antibodies			
Western blot			
MPM2	1:500	3 % milk, 0.05 % Tween in TBS	Upstate
Mouse anti-phosphotyrosine	1:1000	3 % milk, 0.05 % Tween in TBS	Upstate
Rabbit anti-GFP	1:1000	3 % milk, 0.05 % Tween in PBS	Molecular probes
Immunofluorescence			
Mouse anti-tubulin (dm1a)	1:250	10 % FBS in 0.1 % Triton X 100-PBS	Sigma
Rabbit anti-histone H3 phosphate	1:500	10 % FBS in 0.1 % Triton X 100-PBS	Upstate
Mouse anti-γ tubulin (GTU-88)	1:1000	10 % FBS in 0.1 % Triton X 100-PBS	Sigma
Rat YOL 1/34	1:10	10 % FBS in 0.1 % Triton X 100-PBS	Sigma
Rabbit anti-GFP	1:500	10 % FBS in 0.1 % Triton X 100-PBS	Molecular probes
Secondary antibodies			
Anti-mouse HRP	1:1000	Same as primary antibody used	Jackson immuno research
Anti-rabbit HRP	1:1000	Same as primary antibody used	Jackson immuno research
Anti-rabbit alexa flour 488	1:1000	10 % FBS in 0.1 % Triton X 100-PBS	Molecular probes
Anti-mouse alexa flour 488	1:250	10 % FBS in 0.1 % Triton X 100-PBS	Molecular probes
Anti-rat Cy3	1:500	10 % FBS in 0.1 % Triton X 100-PBS	Jackson immuno research
Anti-mouse Cy5	1:125	10 % FBS in 0.1 % Triton X 100-PBS	Jackson immuno research

2.4 DNA techniques

2.4.1 Generation of NuMAP entry clone

Gateway molecular cloning technology was used to generate entry clones. The NuMAP coding sequence was amplified from NuMAP cDNA (LD43724) using Exl polymerase. The primers used are listed in Table 2.2. The sequence highlighted in red corresponds to the specific sequences (*att*B sites) needed for recombination. The PCR products were purified using the PCR cleanup kit (Qiagen) following the manufacturer's instructions and used as a DNA template for a second PCR using *att*B1/*att*B2 primers shown in Table 2.2. These primers encompass the remaining *att*B site sequence needed for recombination. The PCR product was purified from agarose gel and BP recombination reactions were carried out following the manufacturer's instructions (Invitrogen), using purified PCR product and pDONR221 plasmid. Transformation was carried out using TOP10 cells (Invitrogen) as described by the bacteria manufacturer. 2.5 µl of BP reaction was used for 25 µl TOP10 cells. Bacteria were plated on LB-plates, supplemented with the appropriate antibiotic and incubated at 37 °C overnight. Correct clones were identified from transformants by colony PCR and restriction digest. Positive colonies were then confirmed by sequencing.

2.4.2 Generation of NuMAP expression plasmids

Expression plasmids were generated by LR recombination reactions using NuMAP entry clones and destination vectors (pAWG, pAGW, pPWG, pPGW obtained from

Table 2.2 Primers used for gene cloning.

Gene	Forward	Reverse
CG11120 with stop	AAAAAAGCAGGCTCCAAA ATGGAACTTAATATTGAT	GTACAAGAAAGCTGGGTCCT AATCCTCCTCCAGGTG
CG11120 without stop	AAAAAAGCAGGCTCCAAA ATGGAACTTAATATTGAT	GTACAAGAAAGCTGGGTCAT CCTCCTCCAGGTGTCG
CG11120 (548-754)	AAAAAAGCAGGCTCCAAA ATGAGCAGGATCCCCAAG	GTACAAGAAAGCTGGGTCCT AATCCTCCTCCAGGTG
CG11120 (623-754)	AAAAAAGCAGGCTCCAAA ATGCAGAGCACCACGTCT	GTACAAGAAAGCTGGGTCCT AATCCTCCTCCAGGTG
***att*B1/*att*B2**	GGGGACAAGTTTGTACAA AAAAGCAGGCTCCAAAAT G	GGGGACCACTTTGTACAAGA AAGCTGGGTC

Table 2.3 Expression plasmids generated using the gateway cloning system.

Plasmid Number	
pHS18	MBP-CG11120
pHS19	GST-CG11120
pHS20	Ap GFP-CG11120
pHS21	Ap CG11120-GFP
pHS25	pUASp CG11120-GFP
pHS26	pUASp GFP-CG11120
pHS48	MBP-CG11120(548-754)
pHS49	GST-CG11120(623-754)
pHS50	Ap GFP-CG11120(548-754)
pHS51	Ap GFP-CG11120(623-754)

Ap = Actin promoter

Drosophila Genomics Research Centre; pMAL-gateway and pGEX-4T-1-gateway previously generated in the lab). LR reactions were carried out following the manufacturer's instructions. All expression plasmids created are shown in Table 2.3.

2.4.3 Generation of plasmids to express NuMAP truncation

NuMAP truncations were created using 4 different methods. Green fluorescent protein (GFP)-NuMAP(548-754) and GFP-NuMAP(623-754) were created using the Gateway cloning system with primers suitable to amplify the corresponding region of protein. The primers used are shown in Table 2.2. GFP-NuMAP(0-44), (0-109), (0-171), (0-227) and (0-404) were created by site-directed mutagnesis using the Quick change Kit (Invitrogen) to introduce premature stop codons. All Quick change reactions were carried out using GFP-NuMAP plasmid as the template DNA following the manufacturer's instructions. Truncations GFP-NuMAP(623-729), (623-693) and (623-718) were also created by the introduction of premature stop codons from the GFP-NuMAP(623-754) expression plasmid. The primers used for site directed mutagenesis are shown in Table 2.4. GFP-NuMAP(0-57/232-754), (0-57/537-754) and (0-57/609-754) were created using EcoRI endonuclease. The GFP-NuMAP plasmid contains a single EcoRI cleavage site 57bp from the start of NuMAP's coding sequence. Additional sites were firstly introduced by Quick change reactions at approximately 100 bp intervals in the NuMAP coding sequence. The resulting plasmids were digested and the DNA purified using the QIAquick Gel Extraction Kit (Qiagen) without actually running DNA on agarose gels. The purified DNA was re-ligated at room temperature with T4 ligase (Promega) for 2 hours in a

Table 2.4 Primers used to create CG11120 truncations.

Truncation	Forwards	Reverse
(0-227)	GAATCTGGAGCAACCAATATAG ATAAAGAAGTCCTCTAGGG	CCCTAGAAGACTTCTTTATCTAT ATTGGTTGCTCCAGATTC
(0-404)	CAGCCTGTTGTTTGAGCTCCGA AGCCGGA	TCCGGCTTCGGAAGCTCAAACAA CAGGCTG
(0-545)	TTGTACGAAAAACGCTGAAAG ATGACGAGGATCCC	GGGATCCTGCTCATCTTTCAGCG TTTTCGTCCAA
(0-617)	CAGAAGCAAGTGCCAGGATAG GCGGCGAAG	CTTCGCCGCCTATCCTGGCACTT GCTTCTG
(0-44)	GGCCAGGAAAACGCGATGAGC GGTCCTCAAGCGG	CCGCTTGAGGACCGCTCATCGCG TTTTCCTGGCC
(0-109)	CCGCCAAGAAGGCTATCGTCTA AGCACTTTCAGCCGATCCCG	CGGGATCGGCTGAAAGTGCTTAG ACGATAGCCTTCTTGGCGG
(0-171)	ACGGAGTTGGAGGTCCCACAGT AAAAGGTGGATCCTTCTCAGG	CCTGAGAAGGATCCACCTTTTAC TGTGGGACCTCCAACTCC
(0-57/ 232-754)	GGAGCAACCAATATCGATAAA GAATTCTTCTAGGGCGTCTAAA AATCC	GGATTTTTAGACGCCCTAGAAGA ATTCTTTATCGATATTGGTTGCTC C
(0-57/ 409-754)	CCTGTTGTTTGCGCTCCGAATTC GGAAATTCCGGAGGAGAAGCC G	CGGCTTCTCCTCCGGAATTTCCG AATTCGGAGCGCAAACAACAGG
(0-57/ 537-754)	CCAATGTCAATAACCGGCGTAG GAATTCAAAGTCATTGGACGAA AAACGC	GCGTTTTTCGTCCAATGACTTTG AATTCCTACGCCGGTTATTGACA TTGG
(0-57/ 609-754)	GGAACGCGCCAAGGTGCTAAC GAATTCTGTACAGAAGCAAGTG CC	GGCACTTGCTTCTGTACAGAATT CGTTAGCACCTTGGCGCGTTCC
(623-650)	CCGCCGATCGGACCGTGTGAAT GGATCATCCGTCCG	CGGACGGATGATCCATTCACACG GTCCGATCGGCGG
(623-676)	CCCGCTTCTAATGTAGCTCCAT AGCCAGCTTTCAATTTGTCC	GGACAAATTGAAAGCTGGCTATG GAGCTACTTAAGAAGCGGG
(623-729)	CCAAGGACCAGAAGGAGTAAG GAGAGTTTATCCGC	GCGGATAAACTCTCCTTACTCCT TCTGGTGCTTGG
(623-693)	GTGAAGACATTCAACGCCTAGT TTTCCAGCAGACCG	CGGTCTGCTGGAAAACTAGGCGT TGAATGTCTTCAC
(623-718)	GGCGCATTGACATGTTCTAGGG TAGAACAACCAAG	CTTGGTTGTTCTACCCTAGAACA TGTCAATGCGCC
(623-630/ 713-754)	GGGGAATTCATTGACATGTTCA AGGGTAGA	CCCGAATTCCACAGACGTGGTGC TCTGCAT

volume of 40 µl. 5 µl of ligation was transformed using 50 µl of TOP10 cells (Invitrogen) as described by the manufacturer. Bacteria were then plated on LB-plates supplemented with the correct antibiotic. Positive transformants were identified by plasmid DNA purification using the QIAprep spin Miniprep kit (Qiagen) followed by plasmid digestion with appropriate restriction endonucleases.

2.4.4 Generation of plasmid containing NuMAP NES fusion

Full length NuMAP coupled to a nuclear export signal (NES) was created using two methods. The NES coding sequence used was from the human protein PKI alpha. Firstly the Gateway cloning system was used to create an entry clone containing the NES-NuMAP fusion. The forward primer used for the amplification of NuMAP coding sequence contained three specific sequences, one specific to the NuMAP gene, the NES coding sequence and *att*B1 sequence needed for the recombination reaction. Primers used here are shown in Table 2.5. An entry clone and the GFP expression plasmids were created using this amplified DNA fragment as described previously.

Secondly, full length NuMAP coupled with an NES was also created using PCR and XhoI endonuclease. PCR was used to amplify the NuMAP entry clone plasmid using primers which annealed to the beginning of the NuMAP coding sequence. Both primers contained XhoI cleavage sites and the forwards primer also contained the NES coding sequence. The PCR product was digested using XhoI and re-ligated using T4 ligase, to generate a new plasmid containing the NES-NuMAP coding sequence.

Table 2.5 Primers used to create CG11120/nuclear export signal fusion.

Construct	Forwards	Reverse
Using Gateway cloning		
NES-CG11120	AAAAAAGCAGGCTCCAAAA TGTTAGCCTTGAAATTAGCA GGTCTTGATATCGAACTTAA TATTGAT	GTACAAGAAAGCTGGGTC CTAATCCTCCTCCAGGTG
Using XhoI Digestion		
NES-CG11120	GGGCTCGAGTTAGCCTTGAA ATTAGCAGGTCTTGATATCC GCCCAAACGATGTCGGCGTC	CCCCTCGAGATTATCAATAT TAAGTTCCAT
Using EcoRI digestion		
NES-CG11120 (623-754)	GGGGAATTCTTAGCCTTGAA ATTAGCAGGTCTTGATATCG AGGATCGTGCTCGTCCAAGG	CCCGAATTCCACAGACGTGG TGCTCTGCAT
CG11120 (623-754)-NES	GGGGAATTCTTAGCCTTGAA ATTAGCAGGTCTTGATATCC GACACCTGGAGGAGGATTA G	CCCGAATTCACGGTGCTGCA TTTGGAGTTC

2.5 Techniques used for *Drosophila* cell line culture

2.5.1 Drosophila cell culture

The *Drosophila* Schneider 2 (S2) cell line was used for all RNA interference (RNAi) experiments, MAP purification and NuMAP localisation analysis. The cells used for RNAi and NuMAP localisation analysis were cultured in Schneider media (Sigma) supplemented with 10 % heat-inactivated foetal bovine serum (Gibco) at 27 ºC in a humidified incubator. Small cultures, less than 20 ml, were grown in 25 cm^2 and 75 cm^2 flasks (Iwaki), and cultures over 20 ml were cultured in a spinner flask (Sigma).

The cells used for microtubule co-sedimentation were cultured in stable isotope labelling by amino acids in cell culture (SILAC) conditions. Media was made following the recipe for Schneider media (Sigma) omitting Arginine, Lysine and yeast extract. Yeast extract at 200 mg/ml (Sigma) was dialysed overnight using dialysis tubing with a pore size of 1200 MW in a solution of 0.9 % NaCl. Media was supplemented with 10 % heat inactivated dialysed foetal bovine serum (Gibco) and dialysed yeast extract to a final concentration of 2 mg/ml. For 'heavy' culture conditions, ^{13}C arginine and ^{13}C lysine were added to 3.4 mM and 2.8 mM. For 'light' culture conditions ^{12}C arginine and ^{12}C lysine were used at the same concentrations. All S2 cell cultures were kept at a cell density between 0.5×10^6 cells/ml and 1×10^7 cells/ml.

2.5.2 S2 cell transfection

3.5×10^6 cells were transfected with 0.4 µg DNA of interest using the Effectene transfection reagent (Qiagen) following the manufacturer's instructions. Healthy growing cells at a density of 6×10^6 cells/ml were diluted to a density of $2.5\text{-}3 \times 10^6$ cells/ml. After 24 hours, 3.5×10^6 cells were seeded with fresh media in a 6-well plate at a final volume of 1.6 ml. 0.4 µg DNA of interest was diluted to a final volume of 100 µl with DNA condensation buffer (Buffer EC), 3.2 µl of Enhancer was added and the mixture incubated at room temperature for 5 min. 10 µl of Effectene solution was then added to coat DNA molecules with cationic lipids, mixed by pipetting and then incubated at room temperature for 10 min to allow transfection-complex formation. After transfection-complex formation, 600 µl of growth media was then added and the mixture added drop wise to the seeded cells. The cells and transfection complex were mixed by pipetting and swirling to ensure even distribution of DNA complexes. The cells were then cultured at 27 °C for 24-48 hours and examined by immunofluorescence.

2.5.3 Generation of a stable S2 cell line expressing GFP-NuMAP

To generate a cell line stably expressing GFP tagged NuMAP, S2 cells were transfected with 800 ng of GFP-NuMAP expression plasmid and 200 ng of vector containing blastidicin resistance gene using Effectene. The transfected cells were then cultured under normal conditions for 2 days. The culture was then diluted 2:1 with fresh media containing 25 µg/ml blastidicin for selection. Cells were cultured for a further 3 weeks in the presence of blastidicin. After this period the blastidicin

was removed and cells cultured under normal conditions. No clones were isolated resulting in a diverse population with varying expression levels between cells.

2.5.4 Mitotic arrest of S2 cells

To obtain cell cultures enriched in mitotic cells, confluent S2 cell cultures (6×10^6 cells/ml) were diluted with fresh media to a concentration of 0.5×10^6 cells/ml and colchicine added to a final concentration of 12 µg/ml. Cultures were incubated with colchicine for approximately 24 hours to obtain mitotically enriched cell populations. Longer incubations with colchicine resulted in increased frequency of cell death and unhealthy cell populations. Therefore colchicine incubation was not increased in SILAC cultures with longer generation times.

2.5.5 RNA interference in S2 cells

Double stranded RNA (dsRNA) used for silencing in S2 cells was produced by two rounds of PCR followed by *in vitro* transcription. In the first round of PCR, approximately 600 bp of the largest exon of the target gene was amplified from genomic DNA. For the preparation of genomic DNA for PCR, 1 male fly was homogenised in 40 µl of fly homogenising buffer (10 mM Tris, 1 mM EDTA pH8, 25 mM NaCl, 200 µg/ml freshly added Proteinase K, (Roche)) and incubated at 37 °C for 30 min, followed by 5 min at 95 °C. 1 µl of genomic DNA was used for a single PCR.

The primers used for the first round of PCR began with 18 nucleotides corresponding to the minimal T7 promoter sequence (27 bp) followed by 18 gene-specific nucleotides, as shown in Table 2.6. The first round PCR product therefore carried an 18 bp inverted sequence at both ends. This PCR product was then run on an agarose gel, purified using the QIAquick gel extraction kit (Qiagen) and used as template DNA in a second round of PCR. For the second round of PCR, the minimal T7 promoter sequence (27 nt) was used as the primer for both sides. This resulted in the addition of the rest of the promoter sequence at either end of the product.

The second PCR product was purified using the PCR purification kit (Qiagen), quantified by spectrophotometry at 260 nm and used as template DNA in an *in vitro* transcription of both sense and antisense strands. The transcription was performed using the MEGAscript T7 Kit (Ambion) following the manufacturer's instructions. The RNA was ethanol precipitated, re suspended in DEPC-treated water (RNase free) and the formation of dsRNA was induced by heating to 65 °C for 30 min and slowly cooling to 0 °C. dsRNA was run on an agarose gel, quantified by spectrophotometry and stored at -20 °C.

To induce gene silencing, dsRNA was transfected into cells by adding it to culture medium. Healthy cells at a density of 5-7 x 10^6 cells/ml were diluted to 1 x 10^6 cells/ml with serum free culture medium and 15 µg of dsRNA was added to 1 ml of diluted cells. After 1 hour of serum starvation, 2 ml of serum-containing media was added. Cells were then incubated with dsRNA for 5 days and examined by immunofluorescene. To obtain 8 days of gene silencing, cells were incubated with dsRNA for 5 days and then diluted back to 1 x 10^6 cells/ml in serum free media

Table 2.6 Primers used for generation of dsRNA.

Gene	Forwards	Reverse
T7 promoter	GAATTAATACGACTCACTAT AGGGAGA	GAATTAATACGACTCACTAT AGGGAGA
β-lactamase	CGACTCACTATAGGGAGATT CCTGTTTTTGCTCACC	CGACTCACTATAGGGAGAA GTGAGGCACCTATCTCA
CG11120	CGACTCACTATAGGGAGA GGTCGCCAAGAAGCAGAA	CGACTCACTATAGGGAGA GGTTCATCCAGGCCATCA
CG10641	CGACTCACTATAGGGAGA ACGATACGGCTCGTGATG	CGACTCACTATAGGGAGA TGTTCGTCCGCAGCTGTT
CG12065	CGACTCACTATAGGGAGA ACGGATGCCGACTTCAAC	CGACTCACTATAGGGAGA CGAAATGGCAGCGAAGTT
CG1681	CGACTCACTATAGGGAGA ATCTGGCACGCGAAAAGT	CGACTCACTATAGGGAGA TCGCCCATCATGAACTTG
CG3902	CGACTCACTATAGGGAGA CGGTATTGCTGCCCAGAT	CGACTCACTATAGGGAGA TGGTGCTCAGCTGCATGT
CG3415	CGACTCACTATAGGGAGA TCTGCACGGCGAACAGTA	CGACTCACTATAGGGAGA AGGTGATCCGCGCTTACA

containing 15 µg of new dsRNA. Again after 1 hour of serum starvation 2 ml of serum-containing media was added and cells cultured for a further 3 days and then examined by immunostaining.

2.5.6 Immunostaining of S2 cells

To prepare for immunostaining analysis, S2 cells were plated onto concanavalin A (Con A) coated coverslips. Con A coated coverslips were prepared as follows; Coverslips (thickness 1mm, VWR International) were washed three times for 5 min in dH_2O. Coverslips were then treated with 0.5 M HCl for 30 min, washed three more times with dH_2O (5 min each) and once with 100 % ethanol for 30 min. Coverslips were then air dried, dipped in 0.5 mg/ml con A (Calbiochem) solution, allowed to air dry again and stored at 4 °C.

The cells were diluted to 5 x 10^6 cells/ml with serum-containing media and plated onto Con A coated coverslips for 2 hours (Rogers et al., 2002). Excess media was removed and adhered cells were fixed in cold methanol fix (90 % methanol, 3.5 % paraformaldehyde, 5 mM Na_2CO_3 pH 9, prechilled on dry ice for 30 min) or paraformaldehyde fix (6.4 % paraformaldehyde in PBS). For methanol fixation, cells were incubated in fix for 15 min on dry ice, 15 min at room temperature and washed twice in washing buffer (0.1 % Triton X 100 in PBS). For paraformaldehyde fixation, cells were incubated in fix for 15 min at room temperature, in SDS solution (0.5 % SDS in PBS) for 15 min and finally washed in PBS. Fixed cells were then stored at 4 °C in PBS.

For immunostaining, fixed cells were blocked for 1 hour in blocking solution (10 % Foetal bovine serum (FBS) in washing buffer), and incubated with primary antibodies diluted in blocking solution for 1 hour. After three 5 min washes in washing buffer, cells were incubated for 1 hour with secondary antibodies diluted in blocking solution. Again the cells were washed three times for 5 min followed by a 10 min incubation with 0.4 µg/µl DAPI diluted in washing buffer. Coverslips were finally washed twice with washing solution and once with PBS and mounted onto slides with mounting medium (85 % glycerol, 2.5 % propyl gallate). Cells were then visualised using an Axioplan-2 fluorescent microscope (Zeiss) using x40 and x100 magnification. Images were obtained with a CCD camera (Hamamatsu) attached to the microscope controlled by Openlab 2.2.1 software (Improvision). Exposure times were varied depending on signal quantity and image quality. The images obtained were finally cropped and contrasted (if required) using Adobe Photoshop.

2.6 Bacterial and fly strains

2.6.1 Bacterial strains and culture

The following bacterial strains were used for DNA cloning and protein expression:

One shot TOP10 cells; Invitrogen, *F-mcrA Δ(mrr-hsdRMS-mcrBC) φ80lacZΔM15 ΔlacX74 recA1 araD139 Δ(araleu) 7697 galU galK rpsL (StrR) endA1 nupG.*

XL1Blue; *recA1 endA1 gyrA96 thi-1 hsdR17 supE44 relA1 lac* [F´ *proAB lacI*qZΔ*M15* Tn*10* (Tetr)].

BL21; *E. coli B F- dcm+ The ompT hsdS(r_B- m_B) gal λ (DE3) [pLysS Cam_r]^{a}endA Tet^r*. Bacteria were cultured in Luria-Bertani (LB) medium, or LB-agar plates supplemented with the appropriate antibiotic at 37 ºC or 18 ºC (Sambrook, 1989).

2.6.2 Drosophila melanogaster culture

Flies were grown on yeast cornmeal agar medium at 25 ºC or 18 ºC and standard techniques for *Drosophila* handling were used (Ashburner, 2005). All fly lines used are shown in Table 2.7.

2.7 Protein techniques

2.7.1 SDS- polyacrylamide gel electrophoresis

Throughout the study, standard protein techniques were used (Sambrook, 1989). Proteins were analysed by standard SDS-polyacrylamide gel electrophoresis (SDS-PAGE). Resolving gels (10 % acrylamide concentration) and stacking gels (5 % acrylamide concentrations) were made using the Mini-PROTEAN II (Biorad) System. Electrophoresis was carried out in standard running buffer (250 mM glycine, 25 mM Tris, 0.1 % SDS). For estimation of protein molecular weight, a standard protein marker was used (New England Biolabs, Prestained protein marker, Broad range). Proteins were visualised in gel by Bio-Safe Coomassie (BioRad) following the manufacturer's instructions, or by the use of an adapted silver staining technique adapted from Blum et al., 1987. The gel was fixed for 1 hour in fix solution (40 % ethanol, 10 % acetic acid), washed twice in 30 % ethanol for 20 min

Table 2.7 Fly strains used in this study.

Fly strain genotype	Reference
w^{1118}	Bloomington Stock Centre
w^{1118}; *l/TM3, Δ2-3 Sb*	Lab Stock
w^{1118}; PBac*{WH}CG11120*^{F02851}	Bloomington Stock Centre
y^1 w^{67C23}; P*{EPgy}Trf4-2*^{EY05585}	Bloomington Stock Centre
w^{1118}; *Df(3R)BSC318/TM6C,* Sb^1 cu^1	Bloomington Stock Centre
w^*;*T(2;3)*ap^{xa}, ap^{xa}*/CyO;TM3,Sb[1]*	Bloomington Stock Centre
Transgenes	
pHS25[*pUASp(CG11120-GFP*)]	Made during study
pHS26[*pUASp(GFP-CG11120)]*	Made during study
yw; P{Wi^{R7}*}/TM6B, Hu*	Bloomington Stock Centre
w^{1118}; *UASpRCC1mCherry-ATG#01*, Gal4::VP16nos[Recomb07]	Lab Stock

and once in water for 20 min. The gel was then sensitized in 0.02 % $Na_2S_2O_3$ for 1 min, washed three times for 20 seconds in water and incubated in silver solution (0.2 % $AgNO_3$, 0.02% formaldehyde) for 20 min at 4 °C. After three 20 second washes in water, proteins were visualised using developing solution (3 % $NaCO_3$, 0.05 % formaldehyde). When this was sufficient, development was stopped by washing the gel in 5 % acetic acid and finally stored in 1 % acetic acid at 4 °C.

Protein samples were prepared for mass spectrometry analysis by separation on Novex NuPAGE 1.5 mm 4-12 % Tris-glycine gels (Invitrogen) using MOPS buffer (Invitrogen). To visualise protein bands, gels were fixed in 50 % methanol, 5 % acetic acid and stained using colloidal blue kit (Invitrogen) following the manufacturer's instructions.

2.7.2 Immunoblotting

For immunoblotting, proteins were transferred to nitrocellulose membrane in transfer buffer (25 mM Tris, 250 mM glycine) using the Mini-Trans Blot system (BioRad) following the manufacturer's instructions. To confirm homogenous transfer of proteins, the membrane was stained using the reversible protein stain MemCode Blue (Pierce). Nitrocellulose membranes were then blocked for up to 2 hours (minimum of 1 hour) in either PBS or TBS containing 3 % skimmed milk and 0.05 % Tween 20. After blocking, membranes were incubated with the appropriate concentration of primary antibody diluted in suitable blocking solution. Table 2.1 shows antibody dilutions used and appropriate blocking solutions. The membranes were washed for a minimum of 1 hour in either PBS or TBS containing 0.05 % Tween 20 and then

incubated for 1 hour with the secondary antibody conjugated to horseradish-peroxidase which was diluted in blocking solution. Extensive washing was again carried out. Secondary antibodies were then detected using an electrochemiluminescence (ECL) kit (Amersham) with exposure to Hyperfilm ECL (GE Healthcare).

2.7.3 Protein expression and purification

NuMAP fused to maltose binding protein (MBP) was expressed in the BL21 strain of *Escherichia coli*. Bacteria containing expression plasmids were cultured in LB medium supplemented with 50 µg/ml ampicillin at 37 ºC overnight with constant shaking. Cultures were diluted 1:100 in fresh LB medium and cultured at 37 ºC until an OD_{600} of 0.5 was achieved. Protein expression was induced by the addition of isopropyl β-D-1-thiogalactopyranoside (IPTG) to 1 mM and cells were incubated at 37 ºC for 3 hours. After this 3 hour induction, cultures were centrifugated at 4000 rpm for 15 min to pellet the cells and the supernatant was removed. The cells were either processed directly or stored at -20 ºC.

Expressed maltose binding protein (MBP) fusion protein (MBP-NuMAP) was insoluble, therefore protein was purified from gel. Cell pellets were re-suspended in inclusion body (IB) buffer (100 mM NaCl, 1 mM EDTA, 50 mM Tris (pH8), 1 mM PMSF), and lysozyme was added to a final concentration of 1 mg/ml. Suspended cells were incubated on ice for 30 min and subjected to five rounds of freeze/thaw cycles, freezing in a dry ice ethanol bath and thawing in a 37 ºC water bath. To break down DNA, the lysed suspension was sonicated on ice (1 min of

pulses of 5 s on 10 s off at 38 % amplitude using a Vibra-Cell Ultrasonic Processor, CV33 converter and 3 mm probe (Sonics)). Insoluble material was obtained by three rounds of centrifugation at 8000 rpm for 10 min followed by re-suspension in IB buffer containing 0.1 % sodium deoxycholate. The final insoluble pellet was re-suspended in 1 ml of IB buffer. The sample was boiled for 5 min after the addition of SDS sample buffer containing 5 % β-mercaptoethanol.

The insoluble material was separated by SDS-PAGE. The expressed protein band was cut from gel and divided into 8 pieces. Each piece was crushed and suspended in 700 µl of 0.2 M $NaHCO_3$, 0.02 % SDS solution and the suspension was incubated at 37 ºC overnight with constant shaking to elute the protein. The supernatant was collected and the protein concentration estimated by comparison of SDS-PAGE of sample and with a known amount of bovine serum albumin (BSA). The protein solution was then concentrated to a concentration of 1 µg/µl by evaporation using a Concentrator 5301 (Eppendorf).

2.7.4 Peptide antibody production

Peptide antibodies were produced and purified by Eurogentec. Eurogentec identified regions likely to be exposed on the protein surface and chose two peptides suitable for antibody production. These peptides were; Peptide 1, QNEETPRRSCRKSVR and Peptide 2, EVGKNSRKRGRKSKR. Both peptide sequences lie close to the N-terminus of the NuMAP (CG11120) protein. Peptides were synthesised and a mixture used to inoculate two rabbits. Antibodies were purified from crude serum using affinity purification with the above peptides. Each peptide was bound to AF-

amino TOYOPEARL 650M matrix and used to extract sequence specific antibodies from crude serum. Eurogentec purified each peptide separately producing two antibodies. The purity of the antibodies was analysed using a bioanalyser.

2.7.5 Immunoprecipitation from S2 cells

Stable cell lines expressing GFP-NuMAP and NuMAP-GFP were used to obtain cell extract for immunoprecipitation using rabbit anti-GFP antibody. Cells not expressing the GFP fusion protein were used for a control extract. 4×10^8 cells of each cell type were suspended in 4 ml of cold lysis buffer (100 mM NaCl, 20 mM Tris pH7.5, 5 mM EGTA, 1 mM DTT, 1 mM PMSF and Complete EDTA free protease inhibitor cocktail tablet (Roche)). Cells were lysed by pulse sonication on ice (1 min of pulses of 5 s on 10 s off at 38 % amplitude using a Vibra-Cell Ultrasonic Processor, CV33 converter and 3 mm probe (Sonics)). After sonication Triton X-100 was added to a final concentration of 0.3 % and the lysate incubated on ice for 10 min. To clear the lysate of insoluble material it was centrifugated at 13 krpm for 10 min. The pellet was discarded and centrifugation repeated. The cleared lysate was then added to 20 µl (solid mass) of protein A agarose beads coated in rabbit anti-GFP antibody. The beads were prepared by protein A agarose bead incubation with rabbit anti-GFP antibody (1/100 dilution) in 300 µl of PBS containing 0.5 % Triton X-100.

After immunoprecipitation reactions were incubated for 30 min at 4°C with rotation, beads were pelleted by centrifugation at 13K rpm in a bench- top centrifuge for 10 s. Protein A agarose beads were washed 3 times for 5 min in lysis buffer with

0.3 % Triton X-100. To elute the protein, immunoprecipitated beads were resuspended in SDS-PAGE protein sample buffer and analysed by SDS-PAGE followed by immunobloting with anti-GFP antibody or mass spectrometry.

2.8 Microtubule co-sedimentation from S2 cell and embryonic extracts

2.8.1 Microtubule co-sedimentation from S2 cell extract

Cells were lysed in BRB80x buffer (80 mM Pipes-KOH(pH6.8), 1 mM $MgCl_2$, 1 mM Na_3EGTA, 1 mM DTT, 1mM PMSF, Complete EDTA-free protease inhibitor cocktail tablets (Roche Applied sciences)). Cells were lysed by sonication in 1 ml of buffer for every 1 x 10^8 cells (1 min of pulses of 5 s on 10 s off at 38 % amplitude using a Vibra-Cell Ultrasonic Processor, CV33 converter and 3 mm probe (Sonics)). Following sonication, Triton X-100 was added to a concentration of 0.1 % and the lysate chilled on ice for 30 min. The extract was cleared of debris using multiple steps. Firstly the lysate was centrifuged at 55 krpm for 10 min at 4 °C using a Optima TLX personal bench top ultracentrifuge with a TLA120.20 rotor. The supernatant was removed and incubated at 30 °C in a water bath for 20 min and again centrifuged at 55 krpm for 10 min at 4 °C. The supernatant was removed and repeated centrifugation carried out until no pellet was obtained. From the final supernatant a sample of extract was taken.

In parallel to extract preparation, 7.58 µg of porcine tubulin (from Cytoskeleton inc) was polymerised for every 1 x 10^8 cells used to obtain protein extract. The appropriate quantity of tubulin was diluted to a concentration of 5 µM

with BRB80x buffer supplemented with 1 mM GTP. Stepwise addition of taxol to the final concentration of 20 µM was used to induce polymerisation and was then incubated at room temperature for 30 min. Following polymerisation, microtubules were pelleted at 13 krpm in a bench-top centrifuge for 15 min and re-suspended in 100 µl of taxol washing buffer (BRB80x supplemented with 20 µM taxol).

DTT (to 0.1 mM), GTP (to 1 mM) and latrunculin A and B (2 µg/ml) were added to cleared extract and the extract split into two; the sample and the extract. To the sample, taxol was added to a final concentration of 20 µM along with the 100 µl of washing buffer containing microtubules. To the control, colchicine was added to a final concentration of 10 µg/ml and 100 µl of colchicine washing buffer (BRB80x supplemented with colchicine to 10 µg/ml). The sample and control were then incubated at room temperature for 1 hour to allow for the binding of microtubule-associated proteins. After incubation, the sample and control were loaded on top of a 300 µl 50 % sucrose cushion (50 % sucrose in BRB80x buffer with taxol for the sample and 50 % sucrose in BRB80x buffer with colchicine for the control) and microtubules pelleted through the sucrose cushion by centrifugation at 27 krpm for 35 min at 20 °C using a TLS-55 spinning bucket rotor. Samples of the supernatants were taken, sucrose cushions removed and the pellets re-suspended in 300 µl of appropriate washing buffers (BRB80x supplemented with taxol or colchicine). Again microtubules were pelleted through a 50 % sucrose cushion. Finally, the sample and control pellets were re-suspended in 50 µl of BRB80x buffer and stored at -20 °C.

2.8.2 Microtubule co-sedimentation in Drosophila melanogaster embryonic extract

Drosophila embryos were collected and aged according to standard techniques (Ashburner, 2005). Adult flies were allowed to lay eggs on grape-juice agar plates at 25 °C for 4 hours. Embryos (0-4 hrs) were first washed with 0.1 % Triton X 100 in water 3 times and then dechorionated in 100 % bleach for 3-5 min. They were then washed thoroughly with 0.1 % Triton X 100 in water four times, followed by washing in water alone. Any residual water was removed from the embryo collection and the collection frozen at -80 °C. Approximately 5 ml of embryos were used for one microtubule co-sedimentation experiment.

For microtubule co-sedimentation, embryos were homogenised in 5 ml BRB80x buffer supplemented with 0.2 % Triton X 100 using a dounce homogenizer. The extract was incubated on ice for 30 min and then cleared of debris as follows. Firstly, large debris was removed by centrifugation at 20 krpm for 10 min at 0 °C using the Beckman Avnati J25 centrifuge with the JA-25.50 rotor. The pellet was then discarded and the supernatant was filtered through 0.2 µm MiniSart filters. Following filtration, the supernatant was centrifuged again at 20 krpm for 15 min and the pellet discarded. To remove small debris, the supernatant was next centrifuged at 55 krpm for 10 min at 4 °C, as described with S2 cell extract. The pellet was discarded and the supernatant incubated at 30 °C for 20 min in a water bath. Finally, the extract was then centrifuged repeatedly at 55 krpm for 10 min at 4 °C until minimal pellet was obtained and a sample of extract was taken at this point. Using

this cleared embryonic extract; microtubule co-sedimentation was carried out as previously described for S2 cell extract.

2.8.3 Microtubule co-sedimentation in the presence of phosphatase inhibitors.

Microtubule co-sedimentation in the presence of phosphatase inhibitors was carried out as described above, depending on cell type used. However, all buffers used were supplemented with 15 mM $NaVO_4$, 10 mM p-nitrophenyl phosphate and 1 µM okadaic acid to maintain cellular phosphorylation.

2.9 Proteomic techniques

2.9.1 Protein in gel digestion

Protein samples were electrophoresed through Novex NuPAGE 1.5 mm 4-12 % Tris-glycine gels (Invitrogen) using MOPS buffer (Invitrogen). The gels were then fixed in 50 % methanol, 5 % acetic acid and proteins visualised using the colloidal blue kit (Invitrogen). The protein lane of interest was sectioned, excised and processed following a standard trypsin digestion procedure (Shevchenko et al., 1996). Proteins present in each gel section were reduced using 100 mM DTT in 50 mM ammonium bicarbonate for 30 min at 37 °C, followed by alkylation with 55 mM iodoacetamide 50 mM ammonium bicarbonate for 30 min at room temperature in the dark. Proteins were then digested overnight at 37 °C using 12.5 ng/µl trypsin (proteomics grade, Sigma). Following digestion, the supernatant (digest) was acidified using

trifluoroacetic acid and desalted using StageTips (Rappsilber et al., 2003). For mass spectrometry analysis, peptides were eluted from StageTips using 20 µl elution buffer (80 % acetonitrile, 0.1 % trifluoroacetic acid). To ensure maximum peptide binding to the C_{18} material packed into the column needle, acetonitrile was evaporated off using a Concentrator 5301 (Eppendorf) and the volume of peptide solution adjusted to 5 µl with 0.1 % trifluoroacetic acid. Each gel section was then analysed individually, with all 5 µl being used for liquid chromatography mass spectrometry/mass spectrometry (LC-MS/MS) analysis.

2.9.2 Nano-LC-MS/MS analysis

Following protein digestion using trypsin, the resulting peptides were analysed using an Orbitrap system (Finnigan LTQ-Orbitrap, Thermo electron), 1200 series nanoflow LC system (Aligent technologies) and a HTC PAL auto sampler (CTC analytics). Peptides were loaded onto a column needle which had been prepared by packing 3 µm Reprosil C_{18} materials (Germany) into Pico Tip Emitter silica tips (8±1 µm) under the pressure of nitrogen at a flow rate of 0.7 µm/min. Mobile phases were (A) 5 % acetonitrile, 0.5 % acetic acid and (B) 99.5 % acetonitrile, 0.5 % acetic acid. A flow rate of 300 ml/min was used with a spray voltage of 1.8 kV. Analysis was performed using either a two-step linear gradient of 0-20 % B in 35 min, 20-80 % B in 4 min and 80 % for 2 min or a two-step linear gradient of 0-20 % B in 75 min, 20-80 % B in 13 min and 80 % B for 10 min. The gradient used was determined by protein sample quantity and complexity estimated by colloidal blue staining. Each

MS cycle consisted of one full MS scan acquired on the Orbitrap, followed by MS/MS scans of the six most abundant peptides in the ion trap.

2.9.3 Database searching

Peak lists were extracted from MS raw files using the MaxQuant Quant module (Cox and Mann 2008) or DTAsupercharge (V1.18). Peaks lists extracted using DTAsupercharge were used in Mascot daemon (V2.2.0) to conduct an automated database search against the UniProt/SwissProt *Drosophila melanogaster* database. Search parameters were precursor mass tolerance of 10 ppm, fragmentation ion mass tolerance to 0.8 Da enzyme trypsin and allowance of 3 missed cleavages. Peptide charge was set to 1+, 2+ and 3+. Carboamidomethylation of cysteine was set as a fixed modification, with oxidation of methionines as a variable modification. For SILAC sample analysis, arginine ^{13}C (C^6) and lysine ^{13}C (C^6) were also set as variable modifications. Quantification of SILAC samples processed by DTAsupercharge and Mascot daemon were obtained using MSQuant followed by manual verification.

Peaks lists extracted using the MaxQuant Quant module, were also submitted to the Mascot search engine for an MS/MS ion search. The search engine results were next processed using the MaxQuant Identify module which integrates and statistically validates peptides, assembling them into proteins. The proteins were then quantified for a second time and results tables produced (Cox et al., 2009).

2.10 Drosophila techniques

2.10.1 Imprecise excision of P-element

The remobilisation of a P-element was used to create a NuMAP deletion mutant as described in the crossing scheme in Figure 2.1. The P{*EPgy2*}*Trf4-2*^{EY05585} line was crossed to the Δ2-3 fly strain carrying the transposase gene and individual jump-starter males where identified by their mosaic eye colour and the stubble (Sb) marker. These jump-starter males from F1 were crossed with virgin females from the P{w^+}*/TM6B,Hu* line (a source of balancer chromosome). In F2, individual males showing P-element loss (eye colour revertant; white eye) were crossed to females with a deficiency in which the NuMAP gene is deleted, *Df(3R)BSC318/TM6C, Sb*^{1} *cu*^{1}. Male F3 flies carrying the excised P-element chromosome and deficiency chromosome were identified by their lack of Sb and humeral (Hu) marker chromosomes and were analysed by PCR for imprecise P-element excision removing the NuMAP coding sequence. The primer pair oHS90/oHS92 (shown in Table 2.8) was used to amplify a region of the NuMAP coding sequence. The lack of amplification of this region indicated removal of the 3' end of the NuMAP coding sequence. Further PCR analysis was carried out to determine the full extent of NuMAP coding sequence removal. All primers used to determine the extent of P-element excision are shown in Table 2.8 and Figure 2.2. From 115 successful crosses, 8 events removing part of the NuMAP coding sequence were recovered with only one of these deleting the entire NuMAP gene (Δ52).

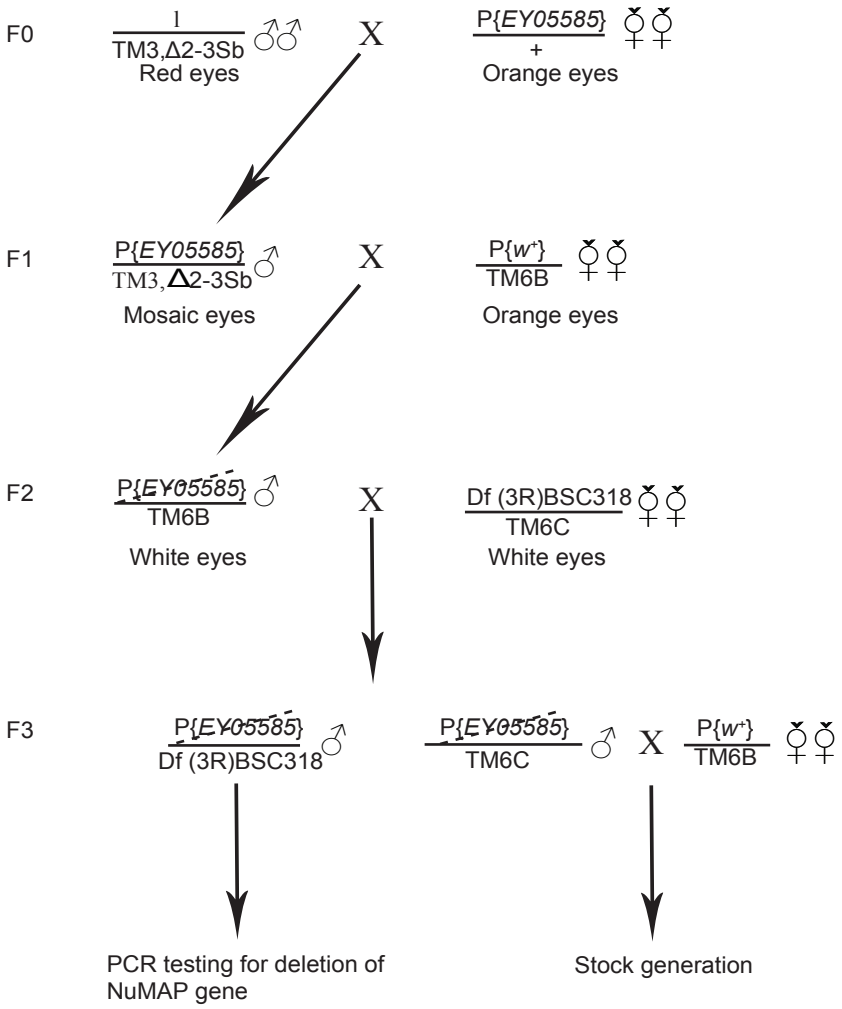

Figure 2.1 Crossing scheme for NuMAP deletion by P-element excision. The diagram shows the crossing scheme used to generate a *NuMAP* deletion by P element excision. The transposase gene was introduced into the fly strain *P{EPgy2}Trf4-2*^{EY05585} containing the P element *P{EY05585}.* Males containing both transposase (*Δ2-3*) and *P{EY05585}* were crossed with virgin females containing a balancer chromosome (*P{w*$^{+}$*}/TM6B*). Male flies which had lost *P{EY05585}* and contained the balancer chromosome (TM6B) were crossed with virgin females of a fly strain with a deficiency in which the *NuMAP* gene is deleted. Males containing the deficiency chromosome and P-element excision chromosome were analysed by PCR for deletion of the *NuMAP* gene.

Table 2.8 Primers used to detect P-element imprecise excision events.

Primer number	
Forwards	
oHS24	ACGGAGTTGGAGGTCCCA
oHS26	ATAGAGGTGTTATACCGC
oHS31	TACCACATACGATGCAGA
oHS63	AACGATGTCGGCGTCTTG
oHS75	ATGCAGAGCACCACGTCT
oHS89	AATCGCCCAAACGATGTCGG
oHS90	CGAGTGCAGCCGATACGGAT
oHS91	CACGACAACAAGCTGGCTGA
oHS99	GCGCTGGGCAGGACTTCAAA
oHS107	CTGCAAGGAACCCTTTCCACT
Reverse	
oHS40	CTTCGTGGATAGTGCCAC
oHS64	TTCTTCCTCTGCTTGCTC
oHS65	CTCAATAGGACTCTGAAA
oHS66	CACTCCGCGGATAAACTC
oHS76	CTAATCCTCCTCCAGGTG
oHS92	CTAATCCTCCTCCAGGTGTC
oHS100	CTTCAAAGGCAAACGTGATGA
oHS101	CTGCATTTTCTTCGCCGCCGA
oHS102	CTTATTCACCTTGCTGGGTGT
oHS108	TTAGCACTCTTCGTTGAGGGA
oHS109	GCAAGCATATGACGTTCACTA

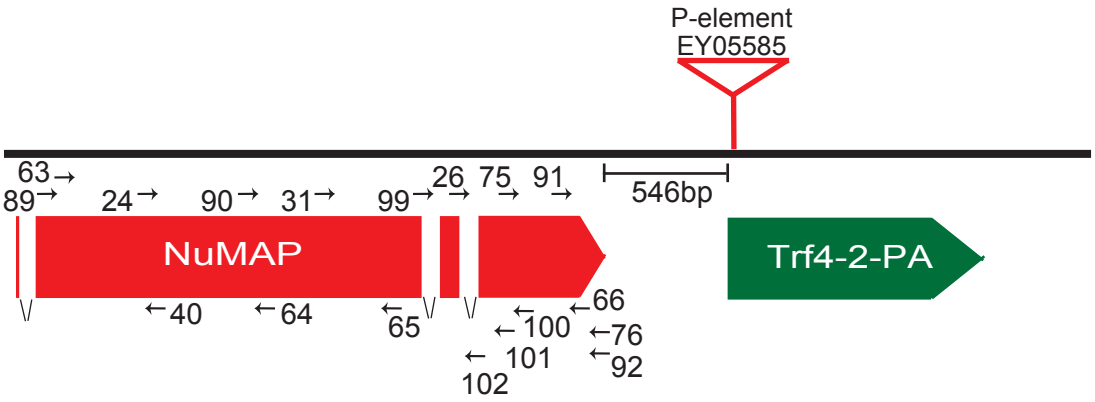

Figure 2.2 Characterisation of imprecise excision events.
Genomic localisation of primers used for imprecise excision events. Primers oHS90 and oHS92 were used to screen for deletion of NuMAP coding sequence. Other primers were used to assess the size of NuMAP deletion. These are not shown for simplicity.Further analysis is needed to ensure no deletion of gene upstream of NuMAP.

2.10.2 Fly transformation

Transgenic flies carrying GFP-NuMAP or NuMAP-GFP were generated by the company Genetic Services Inc using P-element transformation. w^- pre-blastoderm embryos were injected with plasmids containing GFP-NuMAP and NuMAP-GFP along with a helper plasmid which encodes transposase and enables P-element insertion into the genome. Both transgenes were cloned in the pUASp vector which carries the mini-w^+ marker and therefore transformants were identified by their orange eye colour.G0 adults were crossed with w^{1118} flies.

The insertion sites of the transgenes were mapped to specific chromosomes by each transgeneic fly line being crossed with a fly line carrying a marked chromosome II balancer (*CyO*) and a marked chromosome III balancer (*TM6C, Sb*). Flies from F1 carrying the transgene and both markers were then crossed with w^{1118} virgin females and chromosome segregation followed using chromosome markers. The chromosomal locations of the transgenes were identified by the chromosomal segregation patterns observed. For example, if the transgene was inserted on the II chromosome, no flies with orange eyes would be seen to carry the chromosome 2nd marker (*CyO*).

2.10.3 Live imaging of NuMAP in Drosophila embryos

Drosophila embryos were collected and aged according to standard techniques (Ashburner, 1989). To obtain early embryonic stages, transgenic flies (GFP-NuMAP and NuMAP-GFP) were allowed to lay eggs on grape-agar plates for 1 hour at 25 °C

and aged for another hour at 25 °C. To enable clear visualisation, embryos were dechorionated by dissection, adhered to the coverslip surface and covered with halocarbon oil (700). Mitotic division in the syncytial embryo was then observed using an Axiovert (Ziess) microscope with a spinning disc confocal head (Yokogawa) with an Apochromat 63x lens and movies were acquired using the Volocity software. A series of z-sections (15 x 0.5µm slices) which covered an entire spindle were acquired. Due to the rapid progression of mitosis in the embryo, no delay between acquiring Z stacks was used.

2.10.4 Live imaging of NuMAP in Drosophila meiosis I spindle

Oocytes from homozygote transgenic matured adult females were dissected in halocarbon oil (700). The meiotic I spindle was observed by using the Axiovert microscope with spinning disc confocal head. A series of z-sections (separated by 0.5 µm) which covered the entire spindle were taken every 20-35 s.

2.11 Bioinformatics techniques

Homology analysis of the NuMAP protein sequence was carried out using the Basic Local Alignment Search Tool (BLAST) at http://blast.ncbi.nlm.nih.gov/Blast.cgi. Further domain analysis was carried out using protein sequence analysis tools at http://bioweb.pasteur.fr/protein/intro-en.html and http://www.ch.embnet.org/software/COILS_form.html to predict coiled-coil protein regions.

3. Identification of microtubule associated proteins which associate with microtubules specifically during mitosis

3.1 Background

Microtubules are key components of all eukaryotic cells and play a major role in the segregation of chromosomes during mitosis. The organisation and dynamics of microtubules change dramatically from interphase to mitosis and it is thought that these changes are regulated by a number of proteins which bind microtubules. These proteins are collectively called microtubule-associated proteins (MAPs). I hypothesised that there are a set of MAPs which associate with microtubules solely in mitosis, and play crucial roles in regulating the mitotic spindle. Prior to this study a number of MAPs had been identified through different screening methods (Gatti and Baker, 1989; Kellogg et al., 1989), but few have been shown to exclusively associate with microtubules only in mitosis.

In order to better understand the formation and regulation of the mitotic spindle, I decided to identify MAPs which show association to microtubules specifically during mitosis (mitotic-specific MAPs). This chapter describes the development of a method for the identification of mitotic-specific MAPs. It also discusses the subsequent identification of a mitotic-specific MAP, Nuclear microtubule associated protein (NuMAP), which is described further in chapter 4.

3.2 Development of a method for the identification mitotic-specific MAPs

To identify mitotic-specific MAPs, a comparison of MAPs associated to microtubules during interphase and in mitosis was needed. To accomplish this I isolated, identified and quantified MAPs from both cellular states.

3.2.1 Optimisation of microtubule co-sedimentation in Schneider 2 cells

As the first step, microtubule binding proteins from interphase and mitotic extracts needed to be purified and identified. Microtubule co-sedimentation using *Drosophila* embryonic extract is a common and effective method for the isolation of MAPs (Hughes et al., 2008; Kellogg et al., 1989). Embryonic extract has a high tubulin content and enables the polymerisation of endogenous tubulin in the presence of taxol. However, *Drosophila* embryos were not suitable for obtaining a synchronised population for stable isotope labelling by amino acids in cell culture (SILAC, described in 3.2.2) and therefore I chose to perform microtubule co-sedimentation using the *Drosophila* Schneider 2 (S2) cell line.

For the identification of isolated MAPs, I decided to use mass spectrometry. Mass spectrometry is both a fast and sensitive method for the identification of proteins and also allows their relative quantification when in combination with SILAC (Bauer and Kuster, 2003). As there was only one previous publication describing the purification of MAPs from S2 cells (Goldstein et al., 1986), my first aim was the optimisation of microtubule co-sedimentation in S2 cells.

S2 cell extract has a significantly lower quantity of tubulin compared to embryonic extract. This lower tubulin content is supposed to be below the critical level for microtubule polymerisation, even in the presence of taxol. Therefore microtubule co-sedimentation was first tried using the addition of microtubules polymerised from purified porcine tubulin. This approach is illustrated in Figure 3.1. Briefly, S2 cell extract was obtained by sonication of S2 cells in BRB80, a buffer previously used for microtubule co-sedimentation. This extract was cleared of insoluble material by repeated high speed centrifugation. The cleared extract was divided into two, the sample and negative control. Porcine tubulin was separately polymerised in BRB80 using GTP and taxol and added to the sample extract. BRB80 buffer containing colchicine was then added to the control. Colchicine is a microtubule depolymerising drug and therefore was used to ensure the control would contain no microtubules. Both the sample and control extract were then incubated at room temperature for 1 hour. The incubation time allowed for proteins from the extract to bind microtubules. The microtubules were then twice pelleted through a sucrose cushion, pulling down any associated proteins (Figure 3.1).

Sample and control protein pellets were analysed by SDS-polyacrylamide gel electrophoresis (SDS-PAGE) and silver staining. Silver staining showed a number of proteins in the sample pellet. In contrast, the control pellet contained no microtubules and showed less protein, but still contained a significant amount. This result demonstrated that the use of exogenous microtubules could co-sediment MAPs. However, this procedure also sedimented non-specific proteins which is most likely due to protein aggregation during co-sedimentation (Figure 3.2a).

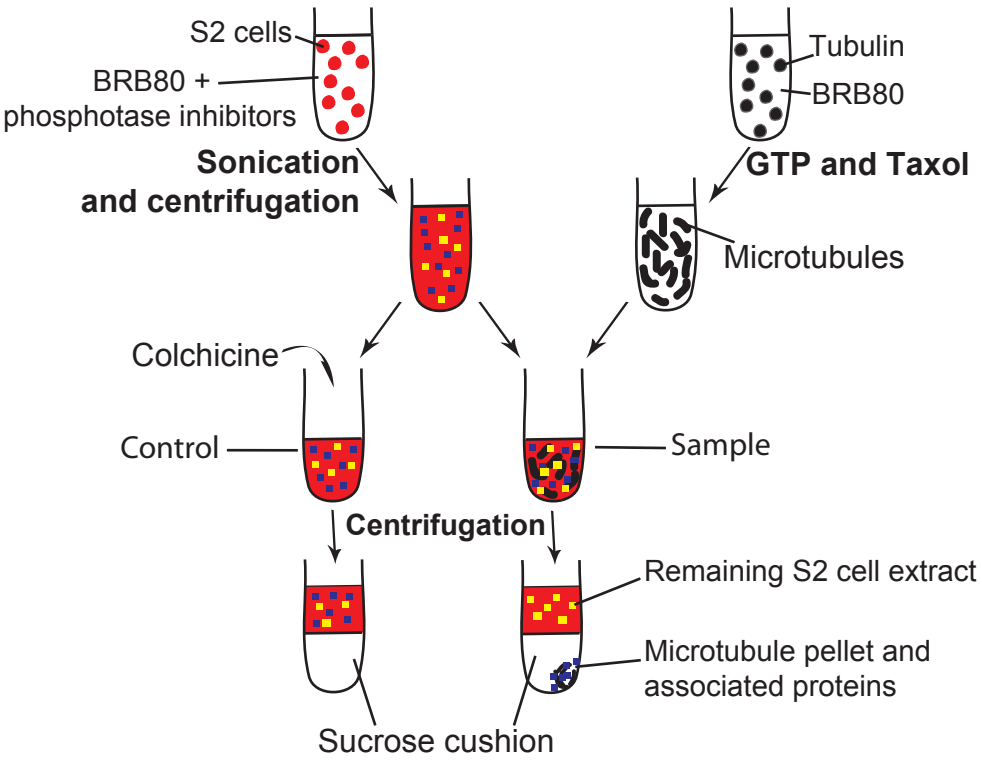

Figure 3.1 Microtubule co-sedimentation protocol. Schematic representation of microtubule co-sedimentation from *Drosophila* S2 cells**.** Cell extract is incubated with microtubules and then centrifuged through a 50% sucrose cushion. Only microtubules and their associated proteins are able to pellet; all other proteins remain in the supernatant. Sedimentation with colchicine is performed in parallel as a control.

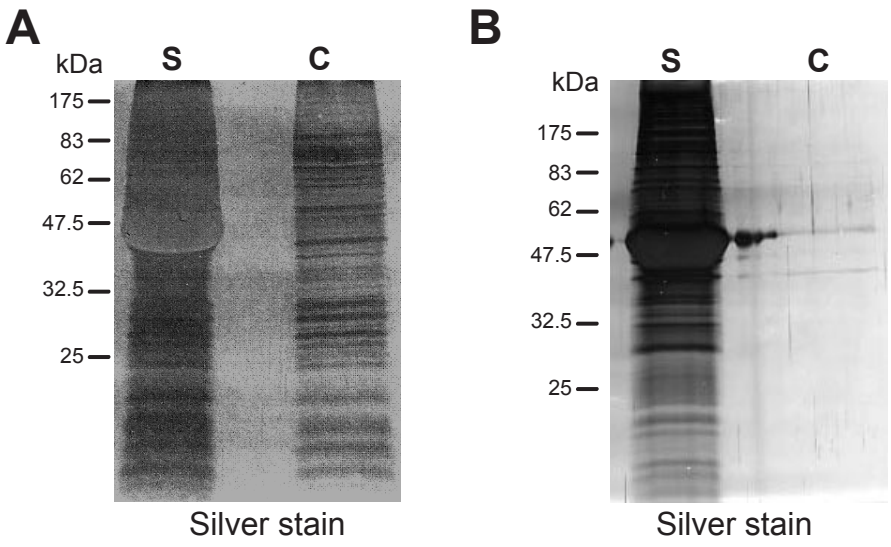

Figure 3.2 Microtubule co-sedimentation in *Drosophila* S2 cells. **(A)** Silver stain analysis of sample (S) and control (C) protein pellets. The control pellet, without microtubules, contains a significant number of aggregating proteins. **(B)** Silver stain analysis of sample and control protein pellets. Cell extract was prepared differently than that used to obtain pellets in (A). During extract preparation, extract was warmed at 30 °C for 20 min. The extract was then repeatedly centrifuged to remove all aggregating proteins. The control pellet showed that few proteins aggregate during co-sedimentation under these extract preparation conditions.

To remove all aggregating proteins before co-sedimentation, the S2 extract was warmed during extract clearance. The extract was first centrifuged to remove insoluble material and then was next warmed to 30 °C for 20 min. This allowed for any protein aggregates to form rapidly. The extract was then centrifuged repeatedly until no pellet was visible and this cleared extract used for microtubule co-sedimentation. Silver staining of the control pellet showed minimal protein content, indicating that after warming, few proteins aggregated during co-sedimentation (Figure 3.2b). Therefore the remaining proteins in the sample pellet were most likely microtubule binding proteins.

If proteins associate with microtubules at precise times during the cell cycle, they are most likely regulated by a post-translational modification. Therefore to identify proteins whose microtubule associations are regulated, it is crucial to maintain major post-translational modifications during MAP purification. Phosphorylation is a key post-translational modification and is known to play a significant role in cell cycle regulation of multiple proteins (Suryadinata et al., 2010). Therefore it is likely that phosphorylation will play a role in regulating MAPs and must be maintained during MAP purification.

To maintain phosphorylation, phosphatase inhibitors can be used. However when adding phosphatase inhibitors there were a number of factors which I needed to consider. Firstly the phosphatase inhibitors used needed to maintain phosphorylation in S2 cell extract. They also needed to be compatible with microtubule co-sedimentation. Phosphatase inhibitors are often highly charged molecules and salt containing chemicals and therefore may affect the polymerisation of microtubules and the association of proteins. Therefore I needed to identify a combination of

phosphatase inhibitors which maintained polymerised microtubules and did not affect the co-sedimentation of microtubule-associated proteins.

Firstly, a mixture of common phosphatase inhibitors was assessed for their ability to maintain phosphorylation. S2 cells were lysed in the presence of $NaVO_4$, NaF, p-nitrophenyl phosphate and β-glycerophosphate (Mixture 1, Table 3.1). The level of phosphorylation was assayed by western blot using MPM2, a monoclonal antibody identified to detect many mitosis-specific phosphorylations (Davis et al., 1983) at serine and threonine (Zhao et al., 1989) Western blotting analysis showed significantly more MPM2 signal from cells lysed in the presence of phosphatase inhibitors than those lysed without. This indicated phosphorylation within the S2 cell extract was maintained by this mixture of phosphatase inhibitors (Figure 3.3).

Next, the compatibility of this phosphatase inhibitor mixture with MAP purification was examined. Microtubule co-sedimentation was carried out in the presence of the above phosphatase inhibitor mixture. SDS-PAGE analysis followed by coomassie blue staining showed a lower amount of tubulin in the pellet when phosphatase inhibitors were used. This suggested that microtubules were depolymerised under these conditions (Figure 3.4a).

To overcome this problem, various combinations of phosphatase inhibitors were tested for the maintenance of phosphorylation and polymerised microtubules (Table 3.1). One additional phosphatase inhibitor, Okadaic acid was introduced to the mixture. Okadaic acid is a potent phosphatase inhibitor and thus enabled the use of lower concentrations of other phosphatase inhibitors. Phosphatase inhibitor combinations were first tested for their capability to maintain phosphorylation by

Phosphatase inhibitor	Mixture							
	1	2	3	4	5	6	7	8
$NaVO_4$ (mM)	20	20	20	20		20	15	10
NaF (mM)	100	100	100		100			
p-nitrophenyl phosphate (mM)	15	15		15	15	10	10	10
β-glycerophosphate (mM)	100		100	100	100			
Okadiac acid (as shown)		2 µM	2µM	2µM	2µM	1 µM	1µM	1µM
Maintain phosphorylation	YES	YES	NO	YES	YES	YES	YES	NO
Maintained polymerised microtubules	NO	YES	YES	NO	YES	NOT TESTED	YES	NOT TESTED
Compatible with co-sedimentation	Reduced MAPs	Reduced MAPs	Reduced MAPs	Reduced MAPs	Reduced MAPs	Reduced MAPs	Normal MAPs	Normal MAPs

Table 3.1 Table of phosphatase inhibitor combinations. This table shows the mixtures and concentrations of phosphatase inhibitors tested for the maintenance of phosphorylation and compatibility with microtubule (MT) co-sedimentation. Some mixtures are omitted for simplicity. The final combination of phosphatase inhibitors chosen is in red.

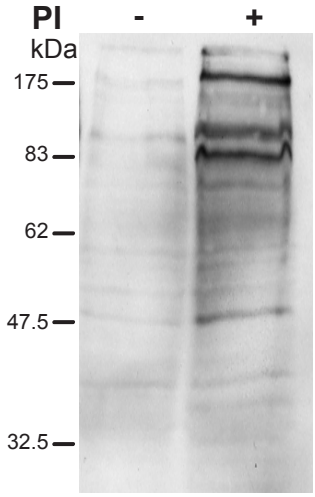

Figure 3.3 Maintenance of phosphorylation by phophatase inhibitor mixture (PI). *Drosophila* S2 cells were lysed in the presence of a phosphatase inhibitor mixture 1 containing, $NaVO_4$, NaF, p-nitrophenyl phosphate and β-glycerophosphate. Maintenance of phosphorylation was assayed using MPM2, an anti-phosphoserine/threonine antibody. Phosphorylation was maintained by this phosphatase inhibitor mixture.

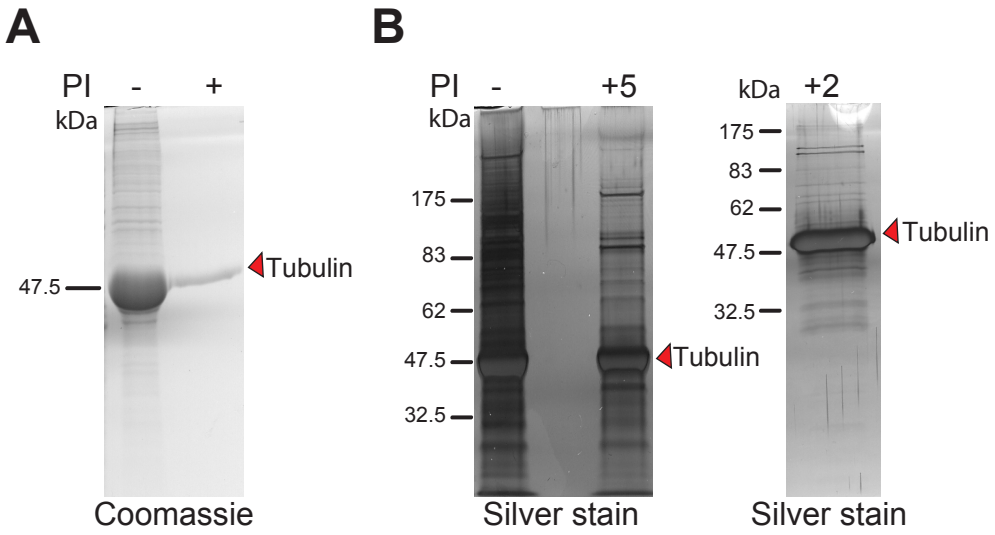

Figure 3.4 Microtubule co-sedimentation with various phosphatase inhibitor mixtures (PI). (A) Microtubule co-sedimentation sample pellet with mixture 1 ($NaVO_4$, p-nitrophenyl phosphate, β-glycerophosphate and NaF). Microtubules depolymerise in these conditions.
(B) Microtubule pellets with and without phosphatase inhibitor mixtures 5 and 2. Mixture 5: NaF, p-Nitorphenyl phosphate, β-glycerophosphate and Okadiac acid (OA). Mixture 2: $NaVO_4$, NaF, OA and p-Nitorphenyl phosphate. Microtubules remained intact in both phosphatase inhibitor mixtures. The number of proteins which bound microtubules was higher in mixture 5. However, the number of proteins co-sedimented when no phosphatase inhibitors were used was still significantly higher.

western blot using MPM2. Each combination which maintained phosphorylation was then further assessed for the maintenance of polymerised microtubules and co-sedimentation. Microtubule co-sedimentation was performed with the various combinations. Each microtubule pellet was analysed using SDS-PAGE and silver staining (Figure 3.4b). The pellet obtained in the presence of mixture 5 (NaF, p-nitrophenyl phosphate, β-glycerophosphate and Okadaic acid) contained a significant quantity of tubulin and the largest number and quantity of other proteins.

In addition to microtubule depolymerisation I also noticed that the presence of phosphatase inhibitors did reduce the quantity and number of proteins which co-sedimented with microtubules (Figure 3.4b). There were two possible reasons for this reduction. Firstly, phosphorylation significantly reduces the number of proteins which bind microtubules. Alternatively, independently of maintaining phosphorylation, phosphatase inhibitors chemically affect the binding of proteins to microtubules. To distinguish between these two possibilities, microtubule co-sedimentation was carried out in the absence of phosphorylation but in the presence of phosphatase inhibitors. S2 cell extract was prepared in the absence of phosphatase inhibitors, allowing phosphorylation to be removed by active phosphatases. Phosphatase inhibitors were then added to the extract and co-sedimentation carried out. In parallel co-sedimentation was carried out without the addition of phosphatase inhibitors. Analysis of microtubule pellets by silver stain showed the pellet containing phosphatase inhibitors had fewer associated proteins (Figure 3.5a). This result showed that the reduction in the binding of proteins to microtubules is due to the presence of phosphatase inhibitors during co-sedimentation, not the maintenance of phosphorylation.

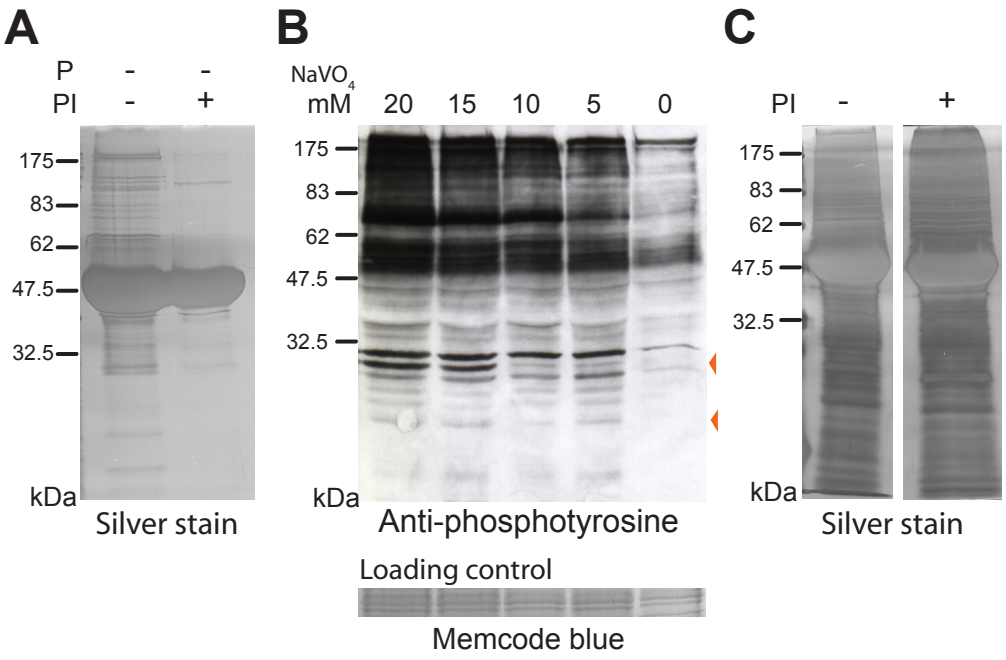

Figure 3.5 Optimisation of phosphatase inhibitor mixture for microtubule co-sedimentation. (A) The presence of phosphatase inhibitors reduces the number of proteins which bind microtubules. Microtubule co-sedimentation in the absence of phosphorylation but in the presence of phosphatase inhibitors, mixture 5 (NaF, p-nitrophenyl phosphate, β-glycerophosphate and okadaic acid). Microtubule pellets were analysed by silver stain. **(B)** *Drosophila* S2 cells were lysed in the presence of decreasing concentrations of $NaVO_4$. The maintenance of tyrosine phosphorylation was assessed by immunoblot with anti-phosphotyrosine. Two bands (indicated by arrowheads) showed reduced signal in extract obtained with a $NaVO_4$ concentration of 10 mM and 5 mM. **(C)** Microtubule pellets obtained in the presence and absence of final concentration of phosphatase inibitor mixture 7; 15 mM $NaVO_4$, 10 mM p-nitrophenyl phosphate and 1 uM okadaic acid. Co-sedimentation with this phosphatase inhibitor combination purified a comparable number of MAPs to those purified in the absence of phosphatase inhibitors. P = Phosphorylation, PI = Phosphatase inhibitors

As I mentioned earlier phosphatase inhibitors are often salt based chemicals. Three of the phosphatase inhibitors used here were sodium salts, β-glycerophosphate, p-nitrophenyl phosphate and NaF. Therefore, the phosphatase inhibitor mixture probably contained a high concentration of sodium ions (Na^+). High sodium ion concentrations can disrupt protein-protein interactions, suggesting that high Na^+ was the reason for the reduction in protein binding to microtubules. I also observed that the phosphatase inhibitor that inhibits tyrosine phosphatase ($NaVO_4$) had been inadvertently omitted for the mixture. Although tyrosine phosphorylation is less common than serine and threonine phosphorylation, $NaVO_4$ was reintroduced to maintain tyrosine phosphorylation. This raised the Na^+ concentration of the mixture even further. Therefore, to reduce the Na^+ concentration, both β-glycerophosphate and NaF were removed from the mixture.

To reduce the Na^+ concentration further, the concentration of $NaVO_4$ was decreased. S2 cell extracts were obtained using gradually reducing concentrations of $NaVO_4$ in combination with other phosphatase inhibitors (Table 3.1). The lowest concentration to maintain tyrosine phosphorylation was assessed by western blot using an anti-phosphotyrosine antibody (Figure 3.5b). Cell extract obtained using 15 mM $NaVO_4$ showed significant signal with anti-phospho tyrosine antibody. However, the signal was reduced when a concentration of 10 mM was used (Figure 3.5b). This result showed that 15 mM was the minimum concentration of $NaVO_4$ needed to maintain tyrosine phosphorylation.

This final combination of phosphatase inhibitors, shown to maintain phosphorylation (15 mM $NaVO_4$ 10 mM p-nitrophenyl phosphate and 1µM Okadaic acid), was next tested further for its compatibility with co-sedimentation.

Microtubule co-sedimentation was performed with and without the phosphatase inhibitors and the pellets analysed by SDS-PAGE and silver stain. Both microtubule pellets showed a similar amount of protein and band pattern. This result showed that co-sedimentation with this phosphatase inhibitor mixture purified a comparable number and quantity of MAPs to co-sedimentation in the absence of phosphatase inhibitors (Figure 3.5c). From this work the final phosphatase inhibitor mixture chosen for further use was: 15 mM $NaVO_4$, 10 mM p-nitrophenyl phosphate and 1 µM okadaic acid.

3.2.2 Optimisation of Stable isotope labelling by amino acids in cell culture in Schneider 2 cells

To identify mitotic-specific MAPs isolated from interphase and mitosis needed to be quantitatively compared. As mass spectrometry was the chosen method of MAP identification, it was decided to couple this method with stable isotope labelling by amino acids in cell culture (SILAC). SILAC was chosen as it is a simple and accurate procedure which has been used in a variety of cell types to obtain relative protein quantities (Ong et al., 2002; Ong et al., 2003).

SILAC relies on the incorporation of a 'heavy' (^{13}C) or 'light' (^{12}C) form of certain amino acids into cellular proteins. Two populations of cells are cultured in identical media, with the exception that one contains 'heavy' and the other contains 'light' (normal) forms of certain amino acids. For example, cells can be cultured with arginine labelled with six ^{13}C atoms, instead of the normal ^{12}C. The 'heavy' amino acid isotopes are incorporated into all newly synthesised proteins. After a

number of cell divisions all instances of the amino acid, are replaced by their analogue. Next, the two cell populations are mixed in an equal ratio and after protease digestion are analysed by mass spectrometry. Chemically identical peptides containing different isotopes can be differentiated in the mass spectrometer by their mass shift. For example, those peptides containing a single arginine ^{13}C will have a mass shift of 6 Da compared to the ^{12}C counterpart. The ratio of peak intensities of such peptides reflects the relative quantities of the protein in the two cell populations (Figure 3.6). Although SILAC is a powerful and widely used method, at this stage its use in S2 cells had not been published. Therefore the establishment of SILAC in S2 cells was necessary for this study.

To gain full incorporation of the isotope labelled amino acid, all other sources of amino acids must be removed from the culture media. As standard S2 cells are cultured with 10 % foetal bovine serum (FBS), this is an alternative source of amino acids in the media. Therefore, SILAC cells were cultured in media containing dialysed FBS. S2 cells grew in these conditions however their doubling time increased two-fold.

Trypsin digestion is commonly used to create peptides for mass spectrometry analysis. Trypsin is a protease which cleaves polypeptide sequences after arginine and lysine. By using arginine and lysine for isotope-labelled culture coupled with trypsin digestion all peptides will be labelled. I therefore decided isotope labelled arginine and lysine were most suitable for use in this experiment.

However, arginine can be converted to proline in the cell. This conversion results in 'heavy' proline in cells cultured in isotope labelled arginine media. The

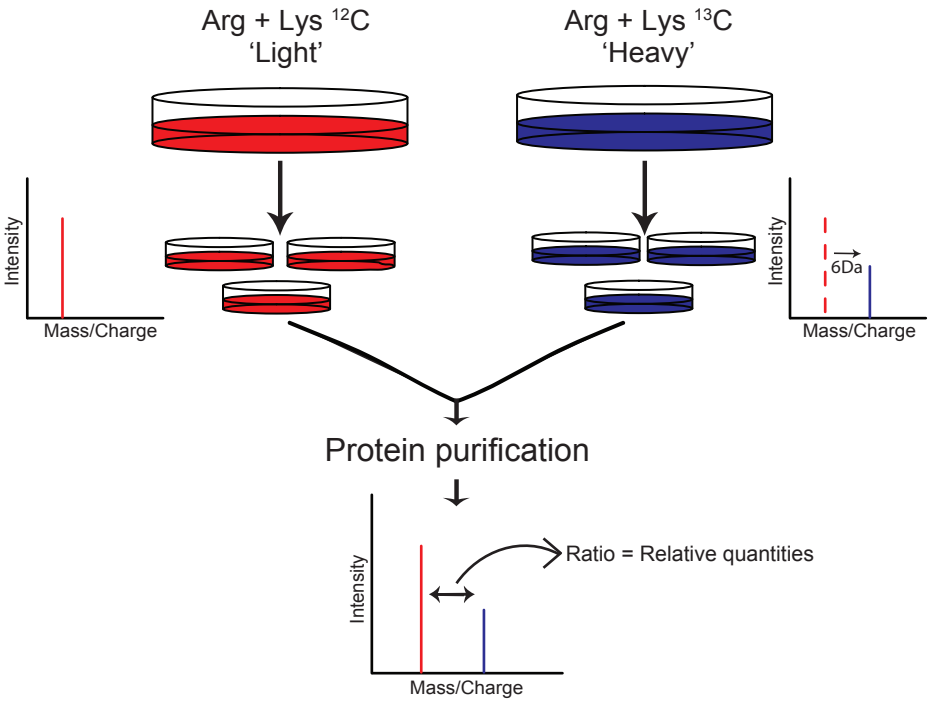

Figure 3.6 Schematic representation of Stable isotope labelling by amino acids in cell culture (SILAC). Cells are cultured in 'Heavy' or 'Light' arginine media. Cells are mixed and protein purification carried out. Chemically identical peptides containing different isotopes are differentiated by the their mass shift in the mass spectrometer. The ratio of peak intensities reflects the relative quantities of the protein in the two orginial cell populations.

production of ‘heavy’ proline creates an additional peptide signal affecting the ability to quantify peptides containing proline. To prevent this conversion the arginine concentrations in the media needs to be optimised. By reducing the concentration of arginine, the conversion and the quantity of ‘heavy’ proline is reduced, however this must be balanced with cell growth. In order to optimise the arginine concentration, cells were cultured in media with 3.4 mM (standard media concentration), 1.7 mM, 1.1 mM and 0.84 mM arginine. Lysine concentrations were also reduced to enable minimal use of isotope-labelled amino acids. S2 cells grew normally in all culture conditions. To measure the degree of conversion to proline, extracts from each culture condition were analysed by mass spectrometry. The spectrum of proline containing peptides showed a minimal intensity of ‘heavy’ proline labelled peaks at all arginine concentrations (Figure 3.7a). I therefore concluded that the conversion of arginine to proline was negligible in S2 cells and decided to continue with SILAC culture using standard amino acid concentrations.

When analysing the spectrum I noticed that there was still an 8.9 % ‘light’ peak for each peptide, indicating that full incorporation of the ‘heavy’ isotope was not obtained (Figure 3.7a). This was likely due to the one remaining source of ‘light’ arginine and lysine in the media, which was yeast extract. To overcome this, I first tried to culture cells without any yeast extract, however S2 cells failed to grow in these conditions. The yeast extract was therefore dialysed overnight and added to SILAC media. These conditions supported cell growth and to assess for full incorporation, the cell extract was analysed by mass spectrometry. Although a 2.9 % ‘light’ peptide signal was still present, it was not significant and was acceptable to work with (Figure 3.7b). Under these SILAC culture conditions, containing the

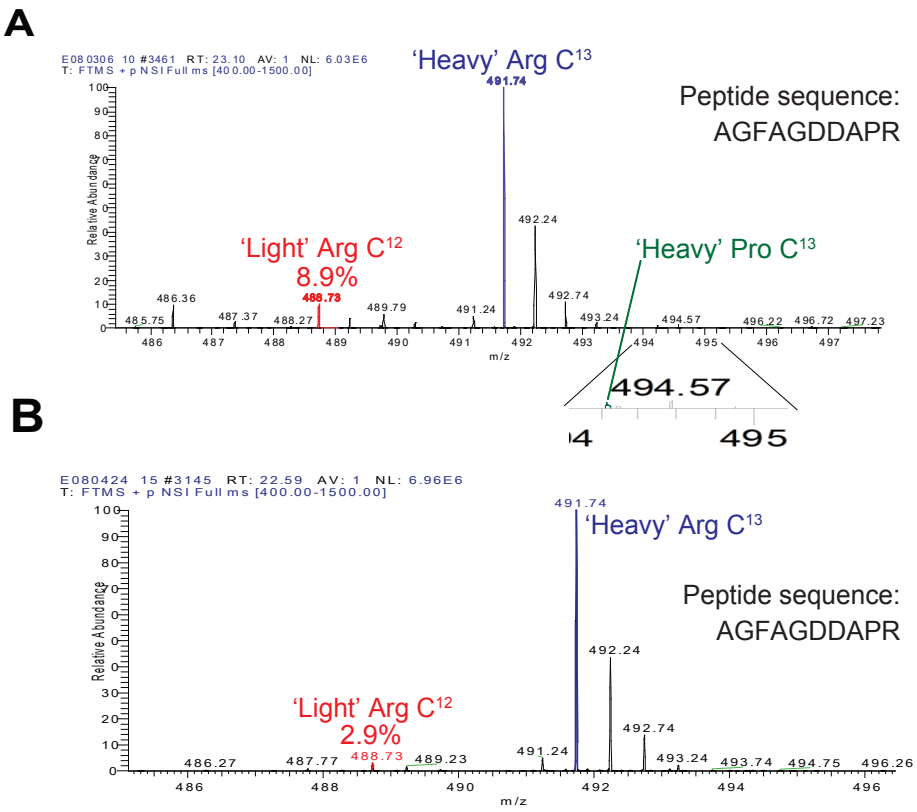

Figure 3.7 Analysis of isotope incorporation and conversion. Cell extract from cells cultured with 3.4 mM 'heavy' arginine were analysed by mass spectrometry. **(A)** MS spectrum showing mass/charge ratio for pepide of interest. A 'heavy' peptide peak was identified at 491.74 (blue), with the charge state of the peptide determined to be 2+. There is a minimal peak (green) for the peptide containing 'heavy' proline. A 'light' peptide peak was also identified at 488.73 (red). **(B)** MS spectrum obtained when cells cultured with dialysed yeast extract. The 'heavy' peptide peak was present, with a smaller 'light' peptide peak.

dialysed FBS and yeast extract, S2 cells showed normal microtubule arrays. I could therefore assume cells cultured in these conditions to be wild-type.

3.2.3 Optimisation of SILAC and microtubule co-sedimentation for MAP quantification

The next step was to test the protocol for the quantification of MAPs. Although from previous analysis of co-sedimentation from S2 cells I had identified multiple MAPs, it was still unknown if the protocol was able to quantify a sufficient number of MAPs by mass spectrometry. The population of cells cultured within 'light' media were enriched in mitosis by treatment with colchicine, a microtubule depolymerising drug. Those cultured in 'heavy' media were left untreated and taken to be 'interphase' cells.

To identify those proteins that bind microtubules specifically in mitosis, I needed to ensure that the two cell populations had significantly different mitotic indices. *Drosophila* culture cells, including S2 cells, do not arrest efficiently in mitosis in the presence of microtubule poisons, including colchicine. Therefore for each experiment, the mitotic index of both the interphase and mitotic enriched cells needed to be confirmed. To measure the mitotic index, a sample of cells was taken and adhered to concanavalin A coated coverslips. The cells were then fixed and immunostained with anti phospho-H3. Histone H3 is phosphorylated at serine 10 (H3P) during mitosis (Hans and Dimitrov, 2001) and therefore was used to identify mitotic cells. The mitotic index was calculated by dividing the number of anti phospho-H3 positive cells by the total number of cells counted. The mitotic indices

were 0.5 % and 22 % for the interphase and mitotic cells respectively. Although the mitotic index of the arrested cells was not very high, the difference between the interphase and mitotic enriched population was significant. This difference was sufficient for the identification of mitotic-specific MAPs, although it was not possible to identify any interphase specific MAPs from this experiment. The two cell populations were then mixed in equal numbers and used for co-sedimentation with phosphatase inhibitors.

Next, each element of co-sedimentation was analysed individually. Firstly, the sample and control pellets were analysed by silver staining after SDS-PAGE. The sample pellet contained a significant number of proteins and in contrast the control pellet contained minimal, if any proteins (Figure 3.8a). This result showed that those proteins within the sample pellet were proteins that bound specifically to the microtubules.

Secondly, the maintenance of phosphorylation was assessed by western blot using MPM2 antibody. To monitor the level of phosphorylation throughout the experiment, samples were obtained during co-sedimentation. A sample of the total extract was taken before it was split into experimental sample and control. Samples of the supernatants after microtubules had been pelleted, were taken from both the experimental sample and control. All three samples were then analysed by western blot using MPM2 and the signal obtained was compared to that of an S2 cell extract obtained by cell lysis in SDS sample buffer. Direct denaturation of proteins by SDS sample buffer should have maintained cellular phosphorylation in this extract. Supernatants showed significant signal, confirming that phosphorylation was maintained during co-sedimentation (Figure 3.8b).

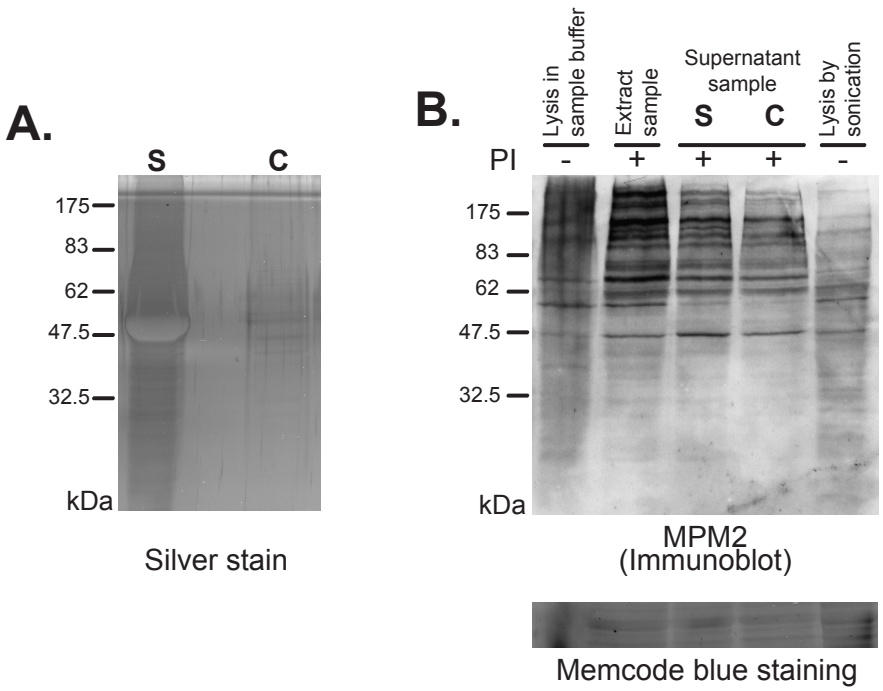

Figure 3.8 Microtubule co-sedimentation analysis. Analysis of first quantification of MAPs **(A)** Silver stain analysis of microtubule pellets from sample (S) and control (C) using SILAC cultured cells. Sample pellet contains tubulin and MAPs. The control pellet contains minimal protein.
(B) Immunoblot with MPM2 of samples during microtubule co-sedimentation in the presence of phosphatase inhibitors (PI). Phosphorylation was maintained throughout the microtubule co-sedimentation.

After experimental parameters had been confirmed as above, samples were analysed by mass spectrometry. The microtubule pellet was run on SDS-PAGE and the gel was cut into sections. In-gel digestion by trypsin was then carried out on each section. Each digest was desalted and concentrated using a C_{18} stage tip (Rappsilber et al., 2003) and run on an liquid chromatograpghy mass spectrometry/mass spectrometry (LC MS/MS) Orbitrap. The spectrum was then processed using DTAsupercharge and Mascot. DTAsupercharge processes the spectrum into peak lists which are then used by Mascot (Mortensen et al., 2010). Mascot searches this peak list for a match to theoretical peptide masses calculated from a sequence database, identifying those proteins present in the sample (Perkins et al., 1999). Finally the data was processed using MSQuant, a program which extracts corresponding mass spectrum peaks and subsequently calculates each protein ratio (Mortensen et al., 2010). From the data obtained, in total only 59 proteins were identified. Moreover, of these, only 10 proteins were identified by three or more peptides and could be reliably quantified. This indicated that the method needed to be improved in order to quantitate a significant number of MAPs.

Large quantities of a single peptides can mask other proteins in the mass spectrometer. The co-sedimentation microtubule pellet contained a large amount of tubulin which will result in a large number of single peptides. The high concentration of tubulin is therefore the likely cause of the low number of quantified MAPs. To overcome this, I needed to identify the lowest quantity of exogenous tubulin that would co-sediment the maximum quantity of MAPs.

Microtubule co-sedimentation was performed with varying quantities of polymerised tubulin. For each co-sedimentation experiment, 1×10^8 cells were used.

The quantity of MAPs pulled down was monitored by silver stain and western blot after SDS-PAGE. Silver staining showed that the quantity of MAPs which co-sedimented decreased between the use of 7.5 µg and 5 µg of tubulin. This was also confirmed by western blot using an antibody against the protein Mini spindles (Msps), a previously studied MAP (Figure 3.9). The quantity of Msps present in the microtubule pellet was also reduced between the use of 7.5 µg and 5 µg of tubulin. The results showed collectively that the optimum ratio between the number of S2 cells and the quantity of tubulin used was 1×10^8 cells for 7.5 µg of tubulin. This ratio was roughly comparable to that seen naturally in embryonic extract, further supporting the use of these proportions.

The protocol using reduced amounts of tubulin was next tested to determine the number of quantifiable MAPs. The sample was processed as above. For details of results see 3.3.1. However, this time the resulting spectra were processed using the newer, more sophisticated MaxQuant. MaxQuant is a quantitative software package designed for the quantitation of high resolution SILAC mass spectrometry data (Cox and Mann, 2008; Cox et al., 2009) and incorporates all the steps needed for computational proteomics processing. However, it does use Mascot to generate peptide candidates for each peptide spectrum. MaxQuant first identifies peaks by fitting a Gaussian curve to raw data points in each mass spectrum scan. These are then assembled into 3D peak hills over the mass/charge-retention time plane. SILAC pairs are identified by grouping those peaks at the correct distance for isotope labelling with correlated Gaussian curves. Peptides are next identified by a database search using Mascot. Peptide hits are assembled into proteins and the ratio median calculated, minimizing the effect of outlying peptides. Ratios are calculated and

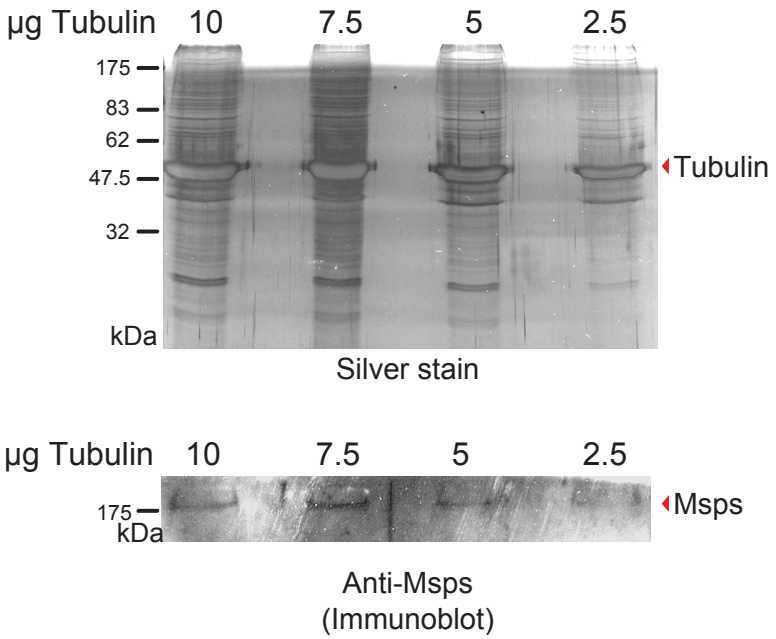

Figure 3.9 Optimisation of tubulin:cell extract ratio. Microtubule co-sedimentation was carried out with various quantities of tubulin using 1 x 10^8 cells. The quantity of MAPs purified was monitored by silver stain and immunoblot. An antibody against the MAP Mini spindles (Msps) was used for immunoblot. The number of purified MAPs decreased with the use of 5 µg tubulin. The optimum ratio between cell number and tubulin was identified to be 7.5 µg tubulin : 1 x 10^8 cells.

normalised, correcting for any unequal protein loading assuming the majority of proteins show no difference. From the data obtained, 271 proteins were quantified (see 3.3.1 for more details). Using the minimum amount of tubulin to reduce masking of MAPs in the mass spectrometer and the use of a new data analysis procedure, the number of MAPs quantified was dramatically increased.

3.3 Identification of mitotic-specific microtubule associated proteins

To identify mitotic-specific MAPs relative quantification of MAPs from interphase and mitosis was carried out in duplicate. Each experiment was analysed individually for mitotic arrest, the specificity of microtubule co-sedimentation and the maintenance of phosphorylation. As each experiment had different mitotic enrichment levels, they were treated independently to identify mitotic-specific MAPs. The final MAPs list was obtained by comparison of the results from both experiments.

For the first of the duplicate experiments as mentioned previously in 3.2.3, co-sedimentation using reduced amounts of tubulin was carried out and the sample processed. The analysis showed that the percentages of H3P positive cells were 22 % and 1.8 % of the mitotic enriched and interphase cells respectively. The sample pellet contained a large number of proteins and the control pellet no detectable proteins (Figure 3.10a). Western blot using MPM2 showed the supernatant to have a reduced but clear signal for phosphorylation (Figure 3.10b). Together these results confirmed that MAPs had successfully been purified from a mixture of interphase and mitotic extracts in the presence of phosphorylation. The proteins in the

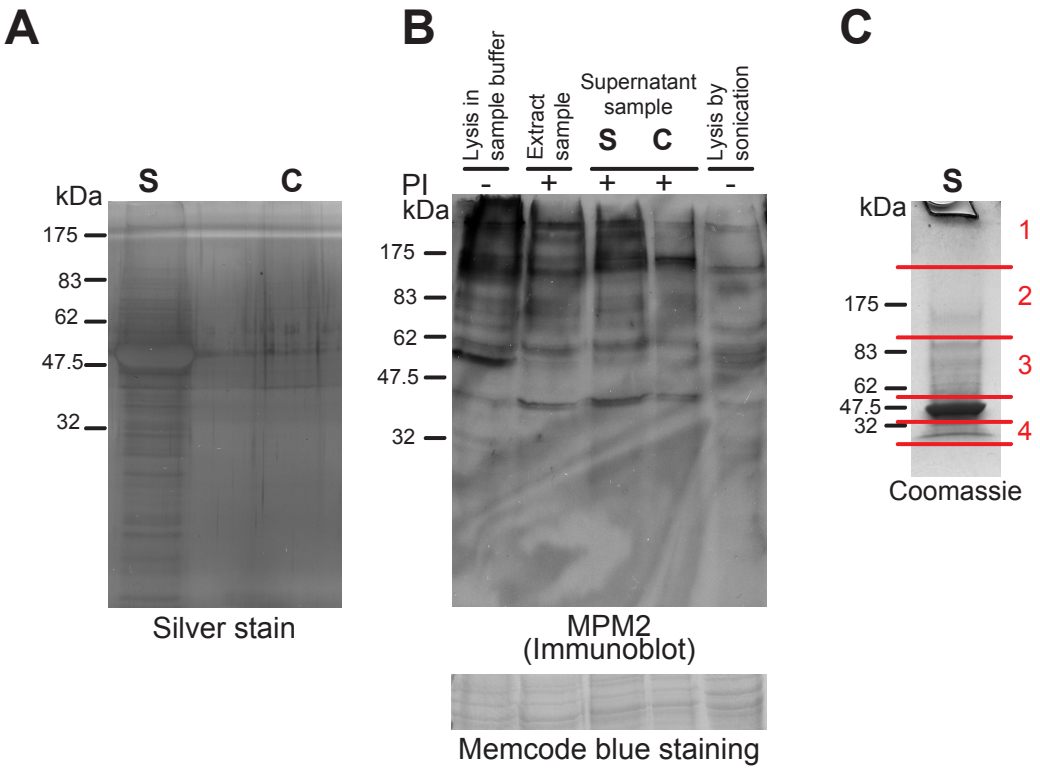

Figure 3.10 Microtubule co-sedimentation with SILAC exp 1. (A) Microtubule co-sedimentation was carried out using cells cultured in SILAC conditions. Silver stain analysis showed no detectable proteins in the control (C) pellet identifying those in sample (S) pellet to be microtubule-associated proteins. **(B)** Maintenance of phosphorylation in the presence of phosphatase inhibitors (PI) was assessed by immunoblot using MPM2. Sample of supernantants were taken after microtubule co-sedimentation and used for immunoblot. Phosphorylation was reduced but maintained. **(C)** The sample microtubule pellet was fractioned by SDS-PAGE and sectioned for trypsin digestion.

microtubule pellet were next fractioned by SDS-PAGE and sectioned for trypsin in gel protein digestion (Figure 3.10c). The peptide mixtures were analysed by mass spectrometry and the resulting data was processed using MaxQuant.

In total 467 proteins were identified and 'heavy' / 'light' protein ratios were calculated for 271 of these (Table A2). Figure 3.11 shows a functional classification of these 271 quantified proteins. Protein ratios were then plotted against relative intensities and also the number of unique peptides (Figure 3.12). If a protein associates with microtubules throughout the cell cycle, then 'heavy' / 'light' ratio will be equal to one. Due to the use of the 'light' population as mitotic extract, any protein which binds to microtubules specifically in mitosis will show a small ratio, close to zero. Taking into account the level of mitotic arrest, I calculated that if a protein bound exclusively to microtubules during mitosis its 'heavy' / 'light' ratio would be around 0.1. I therefore applied a stringent cut off of 0.2 'heavy' / 'light' protein ratio to the data (Table 3.2 and Figure 3.12). This gave a shortlist of 15 proteins whose ratio was below 0.2. This list includes all exogenous proteins used during sample preparation as expected: tubulin, trypsin and bovine serum albumin (BSA). Porcine tubulin was used during co-sedimentation. Trypsin was used as the protease during in gel protein digestion and BSA was used as a standard protein for the assessment of the mass spectrometer performance. Due to these proteins being exogenous, they were all composed of 'light' amino acids. This results in them obtaining a low protein ratio during quantification. These exogenous proteins were therefore removed from the 'hit' list. This first experiment therefore results in a list of seven proteins which appear to associate with microtubules specifically in mitosis. Of these three are uncharacterised (Table 3.2 and Figure 3.12).

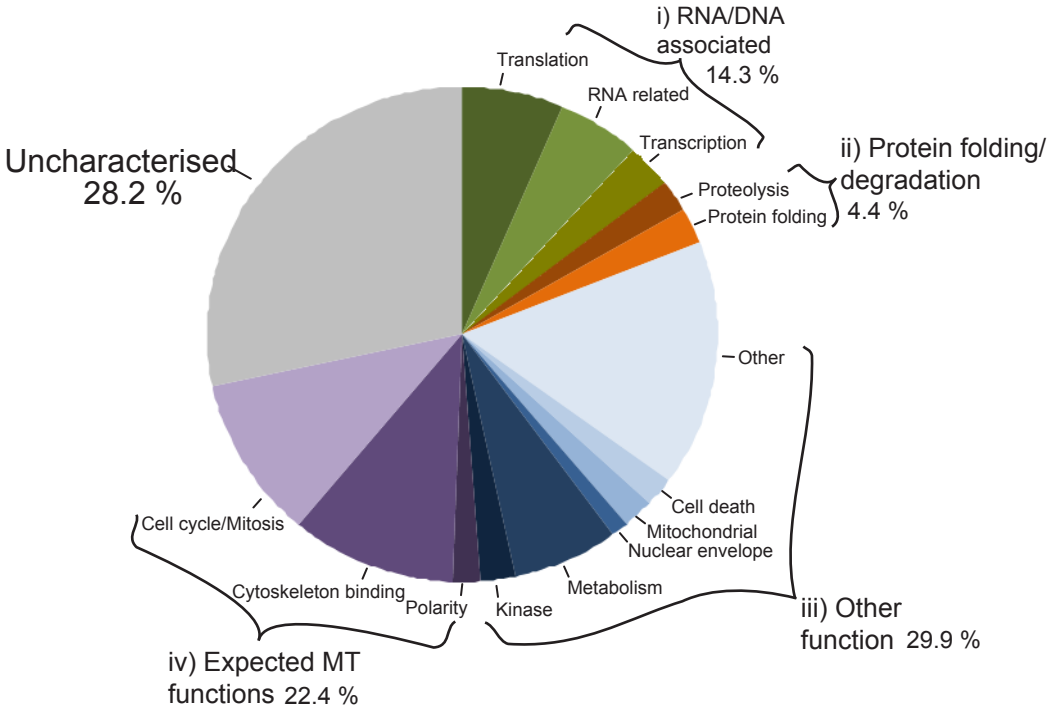

Figure 3.11 Functional classification of 271 quantified proteins. Pie chart representing the classification of quantified MAPs from experiment 1. Classification was determined according to Gene ontology, supported by manual data mining using Flybase. This classification was carried out in April 2010. All proteins were grouped into five main categories i) RNA/DNA associated, ii) Protein folding/degradation, iii) Other, iv) Expected MT functions and v) Uncharcterised.

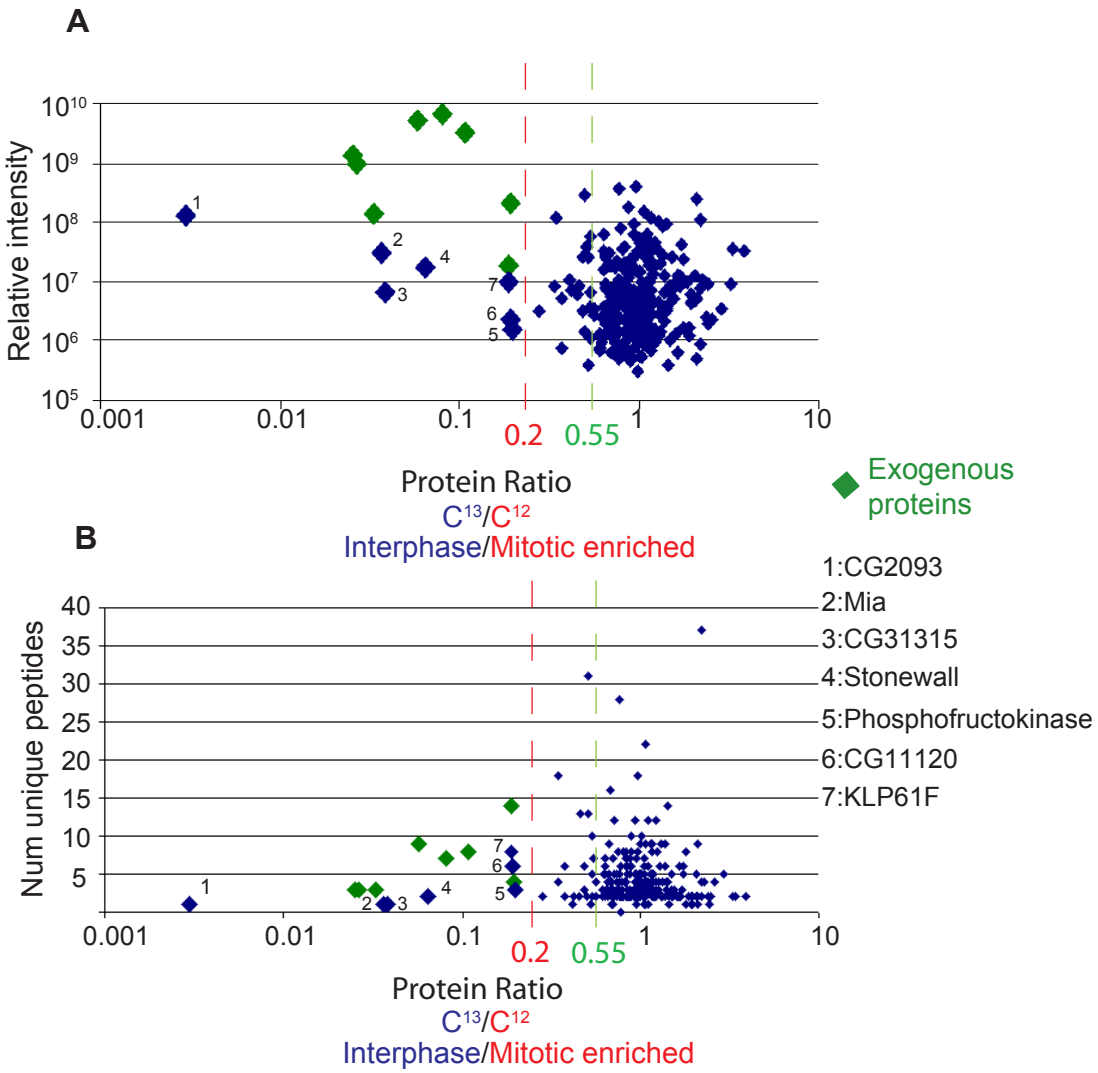

Figure 3.12 Graphic representation of SILAC data. Protein ratios were calculated by dividing peptide relative intensities, 'heavy'/'light'. **(A)** The protein ratio was plotted on a log scale against the relative intensity. **(B)** The protein ratio was plotted on a log scale against the number of unique peptides. A stringent cut off of 0.2 was applied to the data. Those proteins to the left of this cut-off show increased binding to microtubules during mitosis. A second less stringent cut-off of 0.55 was also applied to the data.

Table 3.2 Table of identified mitotic-specific MAPs. Microtubule co-sedimentation was used, with SILAC, to identify mitotic-specific MAPs. The table shows those MAPs identified from experiment one with a H/L ratio below 0.55. It also shows their protein ratios from experiment two if they were identified/quantified. Those in red have protein ratios below the stringent cut-off of 0.2. Those in blue have protein ratios below the less stringent cut-off of 0.55.

CG Number	Synonym	Number of unique peptides		Ratio 'heavy' / 'light'		Identified but not quantified in Exp 2
		Exp 1	Exp 2	Exp 1	Exp 2	
CG2093	Vacuolar protein sorting 13	1		0.0029		Not identified
CG9359	β-Tubulin at 85D	16	14	0.0252	0.14124	
CG9476	α-Tubulin at 85E	13		0.0268		Not identified
CG3401	β-Tubulin at 60D	13	11	0.0331	0.0113	
CG10390	Meiosis I arrest	1		0.0369		Not identified
CG31315		1		0.0385		
CG2512	α-Tubulin at 84D	19		0.0578		Not identified
CG3836	Stonewall	2		0.0651		Not Quantified
CG9277	β-Tubulin at 56D	24	19	0.0809	0.0365	
	Porcine Trypsin	8	6	0.1070	0.224	
	Bovine Albumin	14		0.1883		Not identified
CG9191	Kinesin-like protein at 61F	8	12	0.1886	0.2492	
CG11120		6	5	0.1927	0.3030	
CG4869	β-Tubulin at 97EF	12	10	0.1949	0.1787	
CG4001	Phosphofructokinase	3		0.1981		Not Quantified
CG13345	Tumbleweed	2	3	0.2796	0.8132	
CG10641		4		0.3419		Not identified
CG1258	Pavarotti	18	9	0.3438	0.7808	

Table continues over page

CG Number	Synonym	Number of unique peptides		Ratio 'heavy' / 'light'		Identified but not quantified
		Exp 1	Exp 2	Exp 1	Exp 2	Exp 2
CG11207	Fascetto	6	2	0.3771	0.9258	
CG9193	Mutagen-sensitive 209	2		0.4216		Not identified
CG10160	Ecdysone-inducible gene L3	2		0.4531		Not identified
CG1977	α Spectrin	13	8	0.4625	1.345	
CG3902		6	3	0.4867	0.6139	
CG5099	Musashi	2	2	0.4958	0.8571	
CG7831	Non-claret disjunctional	13	17	0.5048	0.9512	
CG18076	Short stop	31	42	0.5081	0.9902	
CG10236	Laminin A	1	4	0.5210	0.5632	
CG2238	Elongation factor 2b	10		0.5297		Not identified
CG12165	Inner centromere protein	5	2	0.5370	0.8567	
CG3415		2		0.53766		Not identified
CG6647	Porin	7	5	0.5429	0.7525	
CG1782	Ubiquitin activating enzyme 1	7		0.5434		Not identified

These seven proteins included KLP61F, also known as Kinesin-5, a kinesin like protein whose microtubule association is known to be cell cycle-regulated. During interphase, KLP61F is diffuse within the cytoplasm. As the cell progresses through mitosis, KLP61F becomes phosphorylated. Upon phosphorylation the protein associates with spindle microtubules and is essential for the formation of a bipolar spindle (Goshima and Vale, 2005). The identification of a protein already known to associate with microtubules specifically during mitosis, gave confidence in my identification of the other proteins.

On looking at the intensity graph (Figure 3.12), it appeared that there were a number of proteins which lay outside the main group, but did not make it through my stringent cut-off. The very stringent cut-off took into account the level of mitotic arrest, but it did not take into account that microtubule association of proteins may not be a switch, an 'all or nothing' association, between interphase and mitosis. For example, a protein may bind with 90 % and 10 % affinity in mitosis and interphase respectively and its ratio would therefore be 0.4. This would be missed by the more stringent cut off and therefore to ensure no interesting protein had been missed, a less stringent cut off of 0.55 was also used. It allowed the identification of an additional 20 proteins whose binding potentially 'increases' in mitosis compared to interphase (Table 3.2 and Figure 3.12). A number of these proteins have already been shown to play a role in microtubule regulation and spindle formation.

For the second of the duplicate experiments, the mitotic index of mitotic and interphase extracts were 23 % and 2.8 % respectively. The specificity of microtubule co-sedimentation and the maintenance of phosphorylation are shown in Figure 3.13. A total of 322 proteins were identified, with 156 being quantified (Table A3). The

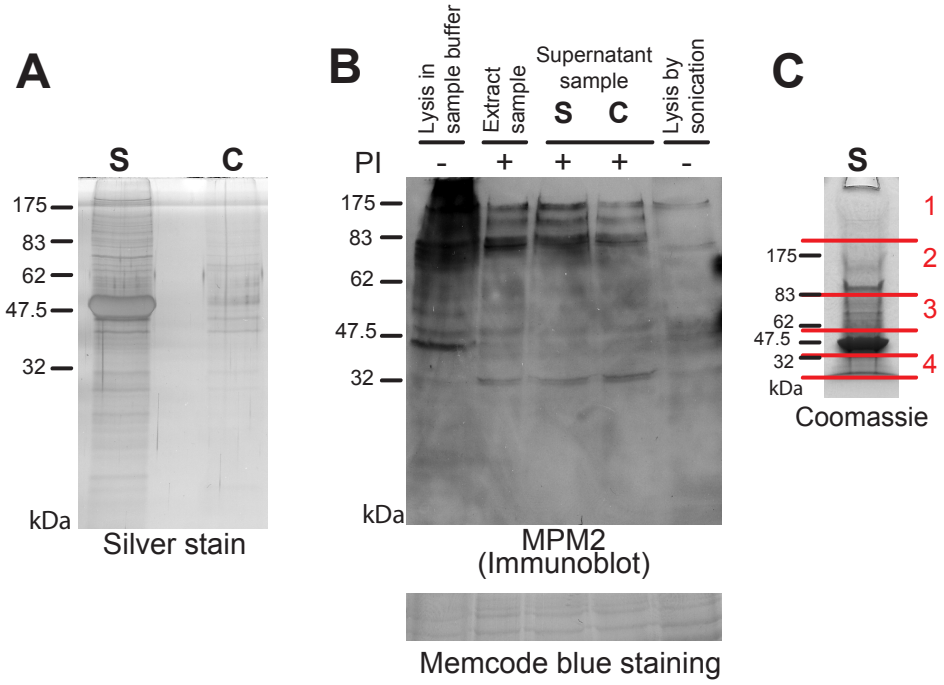

Figure 3.13 Microtubule co-sedimentation with SILAC exp 2. (A) Microtubule co-sedimentation was carried out using cells cultured in SILAC conditions. Silver stain analysis showed little protein in the control (C) pellet identifying those in sample (S) pellet to be microtubule associating protiens. **(B)** Maintenance of phosphorylation was assessed by immunoblot using MPM2. Phosphorylation was reduced but maintained. **(C)** The sample microtububule pellet was fractioned by SDS-PAGE and sectioned for trypsin digestion.

number of proteins identified in this duplicate experiment was significantly lower than the previous experiment, with a number of proteins having considerable changes in their ratio. Protein ratios were again plotted against intensities and also the number of unique peptides (Figure 3.14).

To obtain the final list of mitotic-specific MAPs, those identified in the duplicate experiments were compared. In total 326 individual proteins were quantified, however only four proteins were identified as mitotic-specific MAPs in both experiments. Figure 3.15 shows a functional classification of these 326 proteins. These four proteins were KLP61F, Laminin A and two uncharacterised proteins, CG11120 and CG3902. Laminin A is a non-essential protein which has been suggested to be involved in cell adhesion, migration and rearrangement during organogenesis. It is extracellular and highly studied. Therefore I chose not to pursue it further.

Of the two uncharacterised proteins, CG11120 had a ratio of most significance. It consistently gained a low ratio and in both experiments lay close to that of KLP61F. I therefore decided to study it more closely.

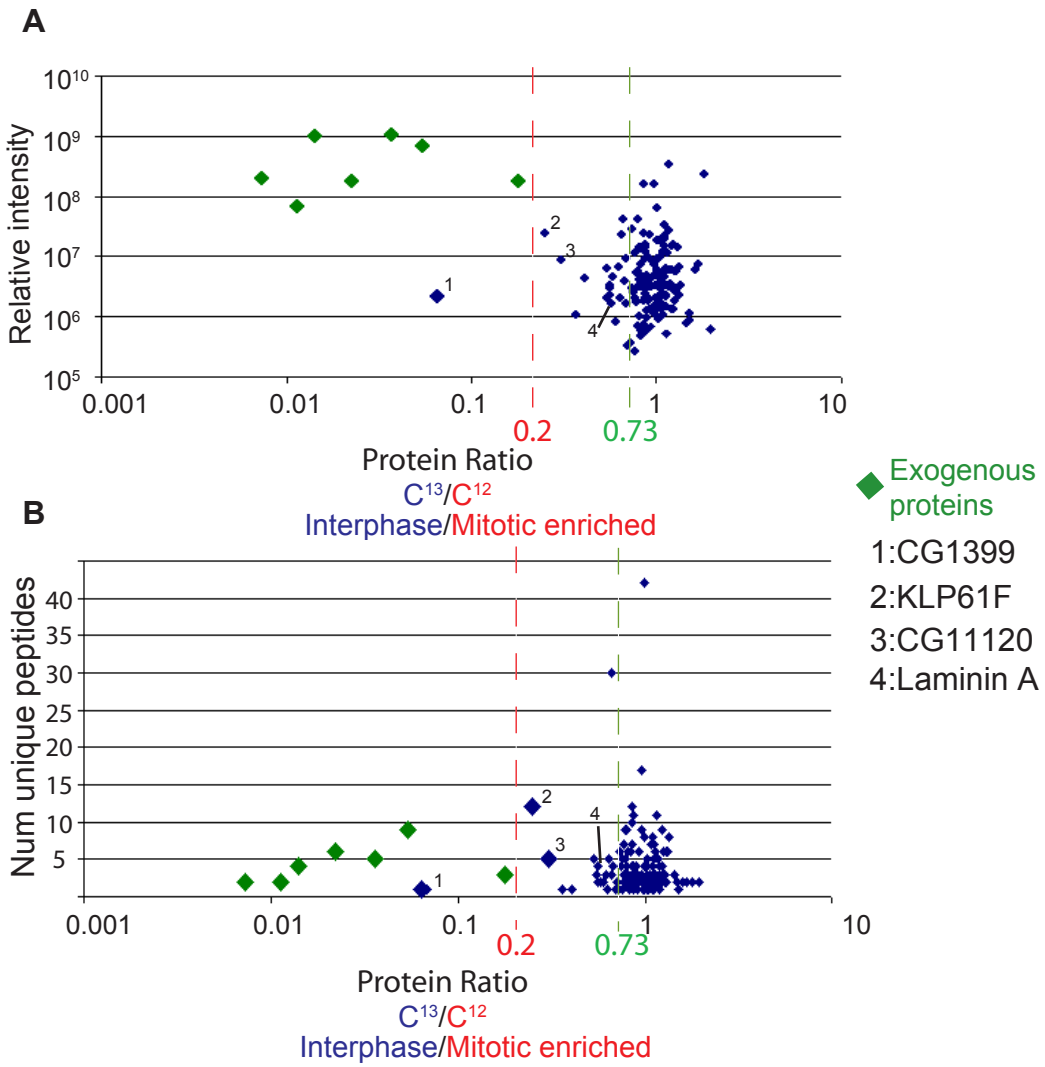

Figure 3.14 Graphic representation of SILAC data. Protein ratios were calculated by dividing peptide relative intensities, 'heavy'/'light'. **(A)** The protein ratio was plotted on log scale against the relative intensity. **(B)** The protein ratio was also plotted on a log scale against the number of unique peptides. A stringent cut-off of 0.2 was applied to the data. Those proteins to the left of this cut-off show increased binding to microtubules during mitosis. A second less stringent cut-off of 0.73 was also applied to the data.

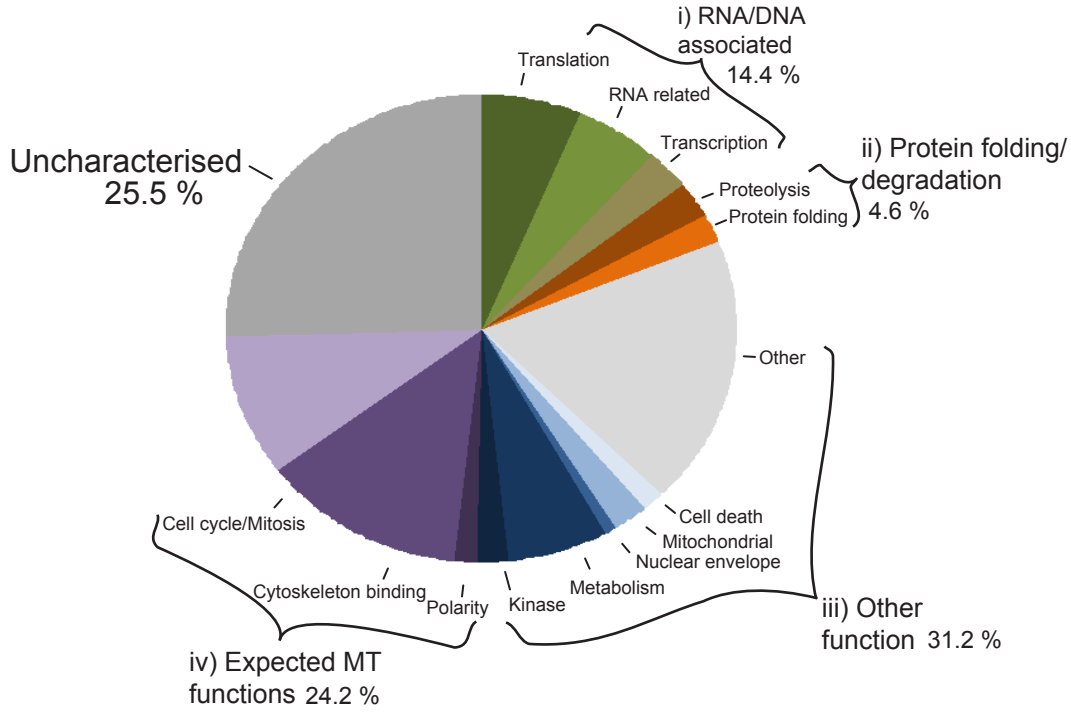

Figure 3.15 Functional classification of 326 quantified proteins. Pie chart representing the classification of quantified MAPs of combined experiments. Classification was determined according to Gene ontology, supported by manual data mining using Flybase. This classification was carried out in November 2010. All proteins were grouped into five main categories i) RNA/DNA associated, ii) Protein folding/degradation, iii) Other, iv) Expected MT functions and v) Uncharcterised. (December 2010)

3.4 Analysis and discussion of the developed protocol's ability to identify mitotic-specific MAPs

3.4.1 Possible reasons behind the small number of identified mitotic-specific MAPs

In this chapter, I have described the development of a method for the systematic identification of proteins that bind to microtubules specifically during mitosis. Using this method I have identified a new microtubule-associated protein which shows binding to microtubules specifically during mitosis which is discussed in detail in chapter 4.

However, the number of proteins identified to associate with microtubules specifically in mitosis was smaller than expected. Although I hypothesised that only a small proportion of MAPs would bind microtubules specifically in mitosis, I had expected that more than four proteins would be replicated between the two experiments. There are various reasons why a reduced number may have been identified and how this could be improved.

Firstly, there may only be four MAPs that associate with microtubules specifically during mitosis in S2 cells. However, the mitotic spindle is a complex structure and it is unlikely that only four proteins are needed to regulate is function during chromosome segregation. I therefore suspect this study has not identified all potential mitotic-specific MAPs.

Secondly, the amount of protein analysed may be insufficient for effective protein quantification. The larger the quantity of protein injected into the mass spectrometer, the better the quality of the spectrum. A better quality of spectrum

enables the sequencing of more peptides and therefore the identification and quantification of more proteins. Consequently, if I had used a larger number of S2 cells, and purified greater quantities of MAPs, I may have identified more mitotic-specific MAPs.

Not only the quantity but also the quality of the sample used may affect the identification of mitotic-specific MAPs. To increase the number of identified MAPs, the method of their purification could also be improved. The method of microtubule co-sedimentation is most often used, identifying abundant proteins which bind to the entire length of the microtubule. In 1989, Kellogg *et al* developed a new method to identify less abundant MAPs. Fifty *Drosophila* embryonic proteins which bind microtubules were identified using a microtubule affinity column (Kellogg et al., 1989). Embryonic extract was passed over columns containing taxol stabilised microtubules coupled to an agarose matrix, the column washed and MAPs eluted. In parallel to affinity chromatography, Kellogg *et al* (1989) also performed microtubule co-sedimentation. A comparison of the two sets of proteins identified in both experiments showed a greater variety of proteins identified by microtubule affinity chromatography (Kellogg et al., 1989). With the use of identical buffers in both procedures, more similarities between the two sets of results were seen, although some differences still remained.

Although microtubule co-sedimentation was faster and more convenient, affinity chromatography allowed better control of elution conditions (Kellogg 1989). Here I have used only microtubule co-sedimentation for the purification of MAPs. To further identify those proteins that associated with microtubules specifically

during mitosis, it would be advantageous to use multiple methods of purification. Affinity chromatography purification may uncover less abundant MAPs.

A further possibility that may play a role in reducing the number of mitotic-specific MAPs identified was the partial loss of phosphorylation. Throughout the experiments I aimed to maintain phosphorylation, however in both experiments, although phosphorylation was still present it was not fully maintained. This reduction in phosphorylation may result in the loss of cell-cycle regulation of some microtubule associated proteins. The loss of regulation will most likely result in the equal association of proteins with microtubules from interphase and mitotic extracts. This then leads to the failure to identify proteins which are cell cycle regulated. To prevent a reduction in phosphorylation, the phosphatase inhibitor mixture needs to be improved further. However, simply increasing the concentration of phosphatase inhibitors poses a problem in the purification of MAPs. I found that a high concentration of phosphatase inhibitors reduces the binding ability of MAPs. The reason for the reduction in binding appeared to be from a high concentration of sodium ions present within the phosphatase inhibitor mixture. Increasing the concentration of phosphatase inhibitors would result in an increase of the sodium ion concentration, and a reduction in MAP purification. Therefore there is a fine balance between the maintenance of phosphorylation and the purification of MAPs and therefore further testing of various combinations of phosphatase inhibitors will maximise the number of quantifiable MAPs.

Another aspect that may impair the identification of mitotic-specific MAPs is a failure to maintain other cellular post-translational modifications. I hypothesised that phosphorylation was the major post-translational modification used to regulate

protein association with microtubules. However, there are other post-translational modifications which may also be used, such as methylation and acetylation. These reversible post-translational modifications are more commonly known to act on nuclear proteins. Acetylation however, has been shown to be present on cytoplasmic proteins such as tubulin. The acetylation of tubulin at lysine 40, located on the luminal side of the microtubule, is thought to direct the formation of a docking site for motor proteins (Yang and Seto, 2008). Stabilisation of microtubules is also thought to be affected by this acetylation (Matthias et al., 2008). Interestingly however, acetylation has also been shown to be involved in the polymerisation and branching of actin filaments. The protein cortactin interacts with F-actin to promote polymerisation and branching. The acetylation of cortactin prevents actin binding, affecting the formation of the actin cytoskeleton, resulting in a reduction in cell mobility (Zhang et al., 2007). It is therefore a possibility that this form of cytoskeletal regulation is also used within the microtubule network. Therefore, the maintenance of other post-translational modifications may aid the identification of mitotic-specific MAPs.

The protocol used here only identifies those proteins regulated by phosphorylation or by cell-cycle degradation. Other post-translational modifications were not maintained during co-sedimentation. Proteins regulated by these modifications would therefore not have differentiated binding when purified from interphase and mitotic extract. To address this further and identify more MAPs which specifically bind microtubules during mitosis, it would be advantageous to perform multiple experiments, each maintaining a set of major post-translational modifications.

There are also a number of proteomic aspects that could be altered to increase the number of quantifiable proteins. The first aspect is the preparation of the sample. To fractionate the proteins, I ran a short 1D denaturing gel. This primarily separated tubulin from MAPs. However, had a larger quantity of MAPs been purified, it would have been advantageous to fractionate the proteins further. Different fractionation methods are used to prepare samples for mass spectrometric analysis. Predominantly proteins are fractioned using 1D and 2D PAGE. 2D PAGE creates single protein spots, which can then be individually analysed by mass spectrometry for protein identification. Mass spectrometry from 1D and 2D PAGE has been shown to identify significantly different set of MAPs (Hughes et al., 2008). However, 2D PAGE needs significant protein quantities and proteins can be 'lost' within the gel. Therefore had a larger quantity of MAPs been purified, 2D PAGE may have been of benefit.

Mass exclusion is another aspect that could be introduced during data collection. The mass spectrometer can be programmed to exclude specific masses from peptide fragmentation analysis, which provides the information for protein identification. Excluding specific masses leaves the mass spectrometer available to fragment other peptides. Microtubule co-sedimentation samples contain large quantities of tubulin and although I have optimised the protocol to use the minimal amount of tubulin, mass exclusion could reduce masking further. A sample of tubulin would first need to be analysed alone, resulting in a list of peptide masses being produced. Those peptides which are high in intensity could be put together to formulate an exclusion list. The mass spectrometer could be programmed to exclude peptides within narrow ranges surrounding these high intensity peptides. This would

result in the mass spectrometer no longer continuously sequencing tubulin peptides but only peptides resulting from MAPs within the sample. This would increase the number of proteins able to be identified. However, although this excludes specific peptides, it may also be excluding other interesting peptides whose masses lie within the exclusion zones. Therefore it is a fine balance between selecting the number of mass regions to exclude and the masking of high intensity peptides.

Another aspect of mass spectrometry that could be adapted is that of charge exclusion. Similar to mass exclusion, it excludes specific peptides from fragmentation analysis. Most protein peptides become doubly charged in the mass spectrometer, they can however be more highly charged. Noise within the mass spectrometer is more commonly singly charged, unlike protein peptides. It could therefore be advantageous to exclude singly charged proteins from fragmentation analysis thus mainly noise would be excluded. A drawback however is that as phosphopeptides are often singly charged, charge exclusion will exclude many phosphopeptides from analysis. However, as phosphopeptides are in the minority, single charge exclusion could increase the number of quantifiable MAPs.

3.4.2 Identification of MAPs that bind microtubules specifically in interphase

Although I set out to identify those proteins that showed association with microtubules specifically during mitosis, the experimental design should have also allowed the identification of interphase-specific proteins. However, the cell cycle arrest of S2 cells limited protein identification to mitotic specific binders. *Drosophila* culture cells, including S2 cells, do not efficiently arrest in mitosis when

using microtubule poisons. The majority of cells in both populations were therefore interphase cells. Any increase in protein microtubule affinity in interphase would not be detectable at peptide level in the mass spectrometer. This therefore prevented the identification of proteins whose affinity for microtubules increased during interphase.

To improve this, various cell cycle arrests could be used alone or in combination thus eliminating the dependence on arrest using microtubule poisons. For example, RNA interference (RNAi) could be used to deplete proteins such as cdc27, which has previously been shown to increase the mitotic index. The extent to which the RNAi of these proteins enriches for mitotic cells is still low (cdc27 ≈ 10 %) (Goshima et al., 2007) but in combination with microtubule poisons an effective arrest could be obtained. However, the depletion of such proteins can have knock-on effects on the cell. Directly depleting known MAPs may affect other protein regulation and therefore cause changes to their microtubule association. The use of RNAi arrest-based methods alone or in combination with microtubule poisons would therefore need to be monitored closely for secondary effects.

Another way to address the issue of cell cycle arrest may be to change model organism. Cell cycle arrest in other organisms such as yeast and human cell lines can be achieved close to 100%. Ozlu *et al* (2010) were able to obtain synchronies of more than 90 % for mitosis in HeLa S3 cells. An arrest of this extent would enable the identification of more MAPs that associated with microtubules specifically during interphase or mitosis (Ozlu et al., 2010).

The use of Hela cell types however has its limitations compared to S2 cells. *Drosophila melanogaster* has been used in laboratories for more than a hundred years, with the availability of working with a complex, multi cellular organism with a short generation time being taken advantage of. There are a large array of genetic and molecular tools, which have evolved to enable the analysis of genes. The creation of mutants, using tools such as P elements, has allowed the investigation of gene function within the multicellular organism. Aspects of *Drosophila* development and behaviour have been shown to parallel that of the human, and therefore the creation of mutants within *Drosophila* allows the study of these complex processes. A wide base of knowledge and communication within the field gives *Drosophila* an advantage over other model organisms. There are numerous available resources, such as Flybase, for sharing information and reagents. Working with S2 cells gives the advantage to move directly into the multicellular organism and investigate the function of identified genes.

However, the use of alternative model organisms may be useful within the screening process. For example, HeLa cells have previously been used with SILAC and therefore are suitable for the experiment. Due to a relatively high level of homology between *Drosophila* and human, the use of HeLa cells for screening MAP cell cycle binding may be advantageous. A high cell-cycle synchronisation would enable the identification of not only mitotic specific MAPs but also interphase specific ones. Once key proteins have been recognized, using homology, individual genes could be studied more closely in *Drosophila*, taking advantage of its multi-disciplinary tools.

In summary, I have developed a method for the systematic identification of MAPs that associate with microtubules specifically during mitosis and using this method I identified a new MAP, CG11120.

4. Characterisation of CG11120 – A new mitotic microtubule associated protein

Using microtubule co-sedimentation coupled with SILAC and mass spectrometry, I identified CG11120 to bind microtubules specifically during mitosis. I next wanted to confirm this cell cycle related microtubule association and investigate the mechanism of its regulation, as well as uncover the function of CG11120.

4.1 Analysis of protein localisation

To confirm the association of CG11120 with microtubules specifically during mitosis, I decided to analyse the localisation of the protein in S2 cells and developing flies. For this purpose, I created green fluorescent protein (GFP) tagged CG11120 and peptide antibodies.

4.1.1 Localisation analysis of CG11120 protein in S2 cells

I first used green GFP-tagged CG11120 to visualise its localisation in S2 cells. To create GFP-tagged protein, CG11120 cDNA was used in the Gateway cloning system to create N- and C-terminal GFP-tagged protein under the control of the actin promoter. S2 cells were transfected with N- or C-terminal GFP-tagged CG11120 using a non-liposomal lipid formulation with DNA-condensing enhancer. A sample of transfected cells was fixed and immunostained for GFP, DNA and α-tubulin.

Both the N- and C-terminal GFP-tagged protein showed identical localisation. During mitosis, GFP immunostaining showed a uniform signal which localised along the entire length of all spindle microtubules. In interphase a distinct GFP immunostaining signal was distributed evenly throughout the nucleus, with no obvious specific point of localisation. This indicated that the localisation of CG11120 is regulated through the cell cycle (Figure 4.1). Interestingly, in interphase cells expressing high levels of GFP-tagged protein, the GFP signal was often associated with bundled microtubules (Figure 4.1). As seen in mitosis, this localisation of CG11120 was uniform and associated with the full length of the bundled microtubules.

To confirm the localisation of endogenous protein, peptide antibodies were used in immunostaining of S2 cells. Peptide antibodies were generated by Eurogentec using peptides corresponding to regions which are likely to lie on the exterior of the protein. The peptides chosen by Eurogentec were as follows: Peptide 1 (QNTETPRRSCRKSVR) and Peptide 2 (EVGKNSRKRGRKSKR). Both of these sequences are close to the N-terminus of the protein. Both peptides were synthesised and a mixture of the two peptides was used to inoculate two rabbits. Peptide antibodies were then purified from rabbit serum using affinity chromatography with the above peptides. Each peptide was used separately resulting in two individual peptide antibodies, peptide antibody 1 and 2.

A sample of wild-type S2 cells was taken and cells adhered to Concanavalin-A coated coverslips. Cells were fixed using -20 °C methanol and immunostained with peptide antibody 1 or 2, anti α-tubulin antibody and DAPI. Peptide antibody 1 showed no clear signal throughout the cell cycle. Peptide antibody 2 showed a signal

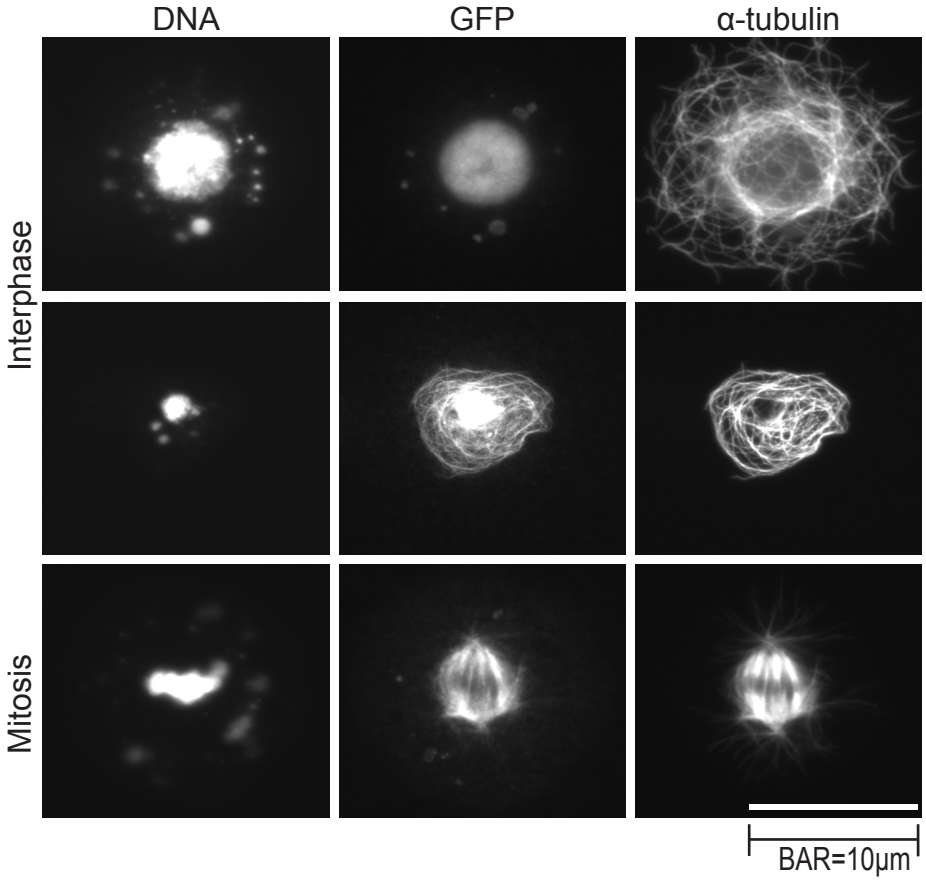

Figure 4.1 CG11120 localisation is cell cycle regulated. S2 cells were fixed with cold methanol 48 hours after transfection with GFP-CG11120. Fixed cells were immunostained using antibodies specific for GFP (to visualise CG11120 localisation) and α-tubulin (to visualise microtubules). DNA was stained using DAPI. GFP-CG11120 localised to the nucleus during interphase and spindle microtubules during mitosis. Some interphase cells showed GFP-CG11120 localisation to microtubules. Exposures of these cells are roughly equivalent and therefore images can be compared.

uniformly associated with the mitotic spindle (Figure 4.2), but did not show any distinct signal in interphase cells.

To test whether the fixation method affected staining, cells were fixed using paraformaldehyde at room temperature. Peptide antibody 1 again showed no significant signal. Although the staining was less prominent with paraformaldehyde fix, peptide antibody 2 did show staining of the mitotic spindle, with a lack of distinct staining in interphase. This indicated that staining of the spindle is independent of fixation method. For the following experiments, peptide antibody 2 with methanol fixation was used.

Although antibody 2 gave staining on the mitotic spindle, I needed to confirm this staining was derived from CG11120 protein and not from other proteins which the antibody cross-reacts with. To address this I performed RNA interference (RNAi) in S2 cells followed by immunostaining. Cells were treated for 5 days with double-stranded RNA (dsRNA) against CG11120. As a control, a culture was treated in parallel with dsRNA against β-lactamase (a bacterial enzyme which is not found in the S2 cell genome). A sample of each RNAi culture was adhered and fixed to Concanavalin A coverslips. Both CG11120 and control knock-down cells were stained with peptide antibody 2, anti α-tubulin antibody and DAPI. Control cells showed a signal uniformly associated with the mitotic spindle. CG11120 RNAi cells, those lacking CG11120 protein, showed no localised signal in interphase or mitosis (Figure 4.2). These results confirmed that the staining seen in control RNAi cells was specific to CG11120. I therefore concluded that endogenous CG11120 protein co-localises to spindle microtubules during mitosis.

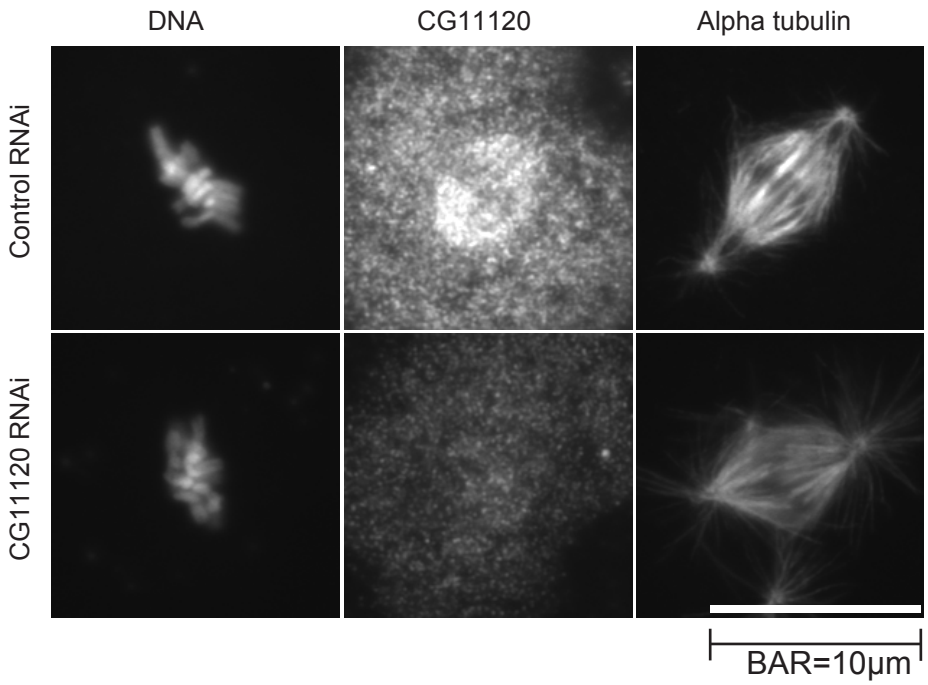

Figure 4.2 CG11120 localisation in Schneider 2 cells. Cells were fixed with cold methanol 5 days after treatment with dsRNA corresponding to β-lactamase (control) or CG11120. Fixed cells were immunostained with peptide antibody 2 for CG11120 and an antibody specific for α-tubulin (to visualise microtubules). DNA was stained with DAPI. CG11120 localises to spindle microtubules. Exposure lengths are roughly equivalent and therefore these images can be fairly compared.

From localisation analysis in S2 cells, I determined that CG11120 was localised to the nucleus during interphase and as cells progress into mitosis CG11120 associates with spindle microtubules. From these results I named CG11120 Nuclear microtubule associated protein (NuMAP).

4.1.2 Localisation analysis of NuMAP in Drosophila melanogaster

To analyse the localisation of NuMAP in the fly, I decided to make use of the Gal4-UAS system to express GFP-NuMAP in *Drosophila* oocytes. The Gal4-UAS system is a commonly used method of ectopic expression of genes within *Drosophila* (Brand and Perrimon, 1993). There are two elements to this system: the Gal4 gene, which encodes the Gal4 transcriptional activator protein and the upstream activation sequence (UAS), to which Gal4 protein binds and activates gene transcription. The gene of interest is placed downstream of a UAS and when crossed with a Gal4 containing line, the gene of interest is therefore expressed. Expression can be restricted to specific cell types by placing the expression of Gal4 protein under an endogenous tissue-specific promoter.

I first generated transgenic flies in which GFP-NuMAP or NuMAP-GFP was downstream of a Gal4-UAS. To do this I used the gateway system to clone NuMAP cDNA into a vector containing N- or C-terminal GFP tags and a UASp promoter. The UASp promoter and 3' UTR allows Gal4 driven expression of a transgene in the *Drosophila* germline (Rorth, 1998). Transgenic flies were then created by the injection of UASp-GFP-NuMAP or UASp-NuMAP-GFP into pre-blastoderm embryos with a helper plasmid containing the transposase coding sequence. The

helper plasmid enables the insertion of the construct into the *Drosophila* genome in a P-element mediated manner. The injection and selection of transgenic flies was performed by the Genetic services Inc, Cambridge. The insertion sites of transgenes were genetically mapped to specific chromosomes. GFP-NuMAP and NuMAP-GFP were expressed by crossing transgenic fly lines with a line containing the maternal Gal4 driver, driven by the nanos promoter (nanosGal4:VP16). This fly strain also carried the transgene RCC1-mCherry, a chromatin associated protein, enabling the visualisation of chromosomes as well as NuMAP. The nanos-Gal4:VP16 gives high levels of transgene expression in the germline from the germarium to the mature egg with products loaded into the embryo (Rorth, 1998).

To analyse the localisation of GFP-NuMAP and NuMAP-GFP in oocytes, live imaging analysis was carried out using confocal spinning disc microscopy. Oocytes were dissected in halocarbon oil from female flies expressing the transgenes and the metaphase-I meiotic spindle was examined. Preliminary results showed that both constructs, GFP-NuMAP and NuMAP-GFP, appeared to localise to spindle microtubules with higher accumulation to the central spindle (Figure 4.3a). Dissection of oocytes also allowed examination of NuMAP localisation in the karyosome. The karyosome is a discrete mass of chromosomes which forms during prophase of meiosis I. NuMAP localised in the nucleoplasm, but was excluded from the karyosome (Figure 4.3b).

To analyse the localisation of NuMAP during mitosis in early development, I examined syncytial embryos. At cycle 8 of embryonic development, multiplying nuclei migrate to the surface of the embryo and divide in synchrony through cycle 9 and 10. I examined embryos at these stages to enable the visualisation of multiple

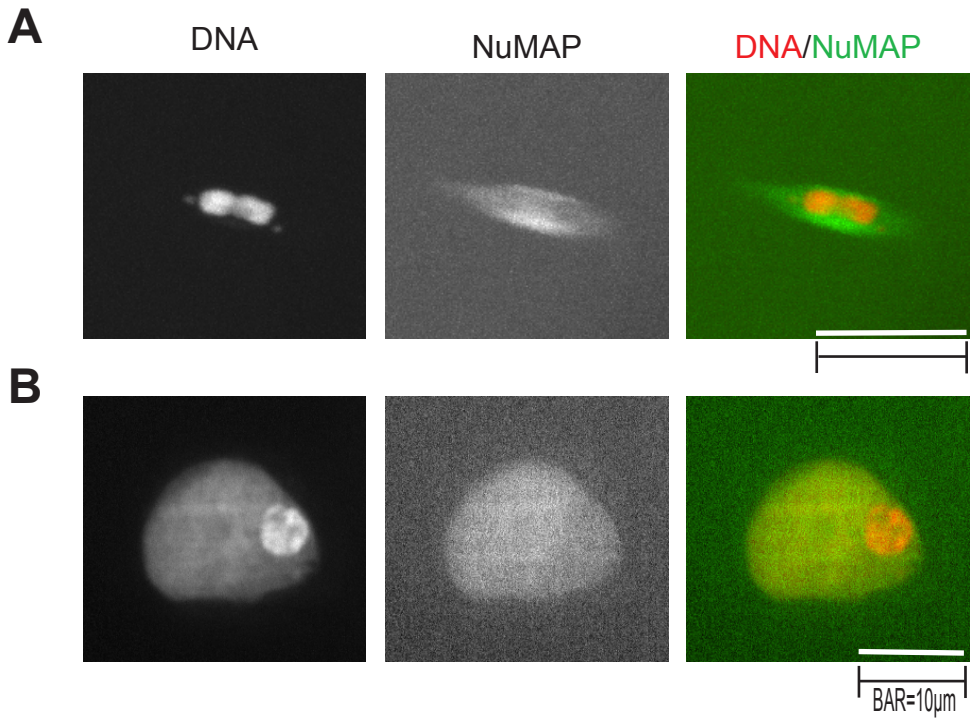

Figure 4.3 NuMAP localisation in *Drosophila* oocytes. Oocytes from GFP-NuMAP (green) and RCC1-cherry (to mark DNA, red) expressing females were analysed by confocal microscopy. **(A)** NuMAP localises to the meiotic spindle, with enrichment at the central spindle. **(B)** NuMAP localises to the nucleoplasm of *Drosophila* oocytes.

dividing nuclei, which lay at the periphery of the embryo. Embryos (0-4 hrs old) were collected from flies expressing GFP-NuMAP or NuMAP-GFP on grape juice/agar plates. Embryos were dechorionated by dissection, mounted onto coverslips and covered with halocarbon oil. Mitotic spindles were then examined using confocal spinning disc microscopy. Imaging of the mitotic spindle was difficult due to the embryo depth and spindle movement, resulting in blurred images. However, a general localisation of NuMAP could be distinguished. During prophase NuMAP is localised to centrosomes. As the mitotic spindle is formed, NuMAP becomes localised to spindle microtubules and remains localised to spindle microtubules through anaphase and into telophase. During telophase NuMAP is localised to a structure that appears to be the central spindle, though it is restricted to specific parts of this structure (Figure 4.4).

The above preliminary analysis of NuMAP localisation in *Drosophila melanogaster* shows NuMAP localises to spindle microtubules in female meiosis I and during mitotic divisions in the embryo. At early stages of oogenesis, NuMAP appears to localise in the nucleoplasm with exclusion from chromatin. From this I concluded that NuMAP can associate with spindle microtubules at different developmental stages.

4.2 Domain structure of NuMAP

To investigate NuMAP protein structure and function, I first used a basic local alignment search tool to identify any closely related proteins or possible homologues. The results showed a range of proteins with different levels of homology. The most

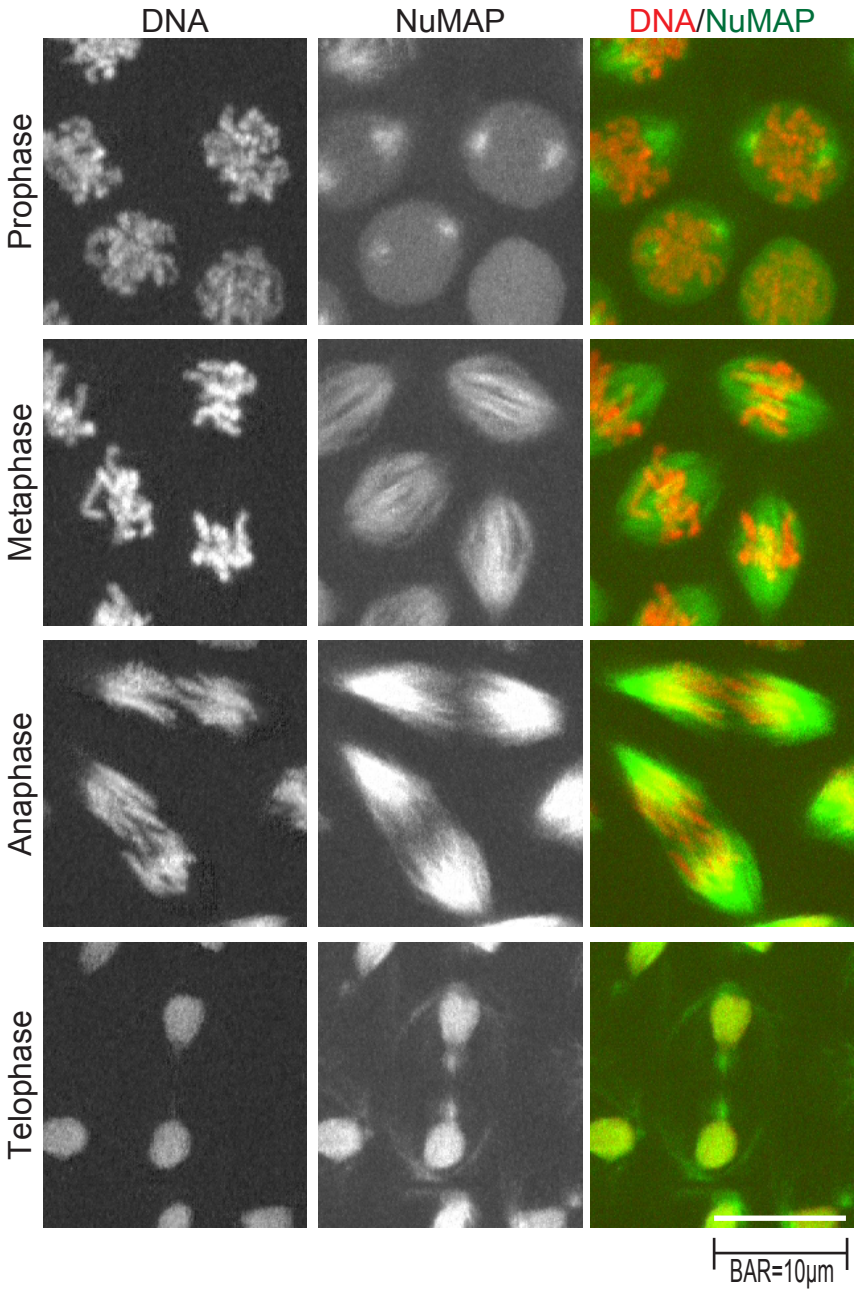

Figure 4.4 NuMAP localisation in embryonic mitosis. 0-4 hour old embryos laid by females expressing GFP-NuMAP (green) and RCC1-cherry (red) at 25 °C and analysed with confocal microscopy. NuMAP localises to centrosomes in prophase and the mitotic spindle in metaphase and anaphase. In telophase NuMAP appears to localise to remaining spindle microtubules and central spindle, though is excluded from the central midbody region.

closely related proteins were from other *Drosophila* species. More limited similarities are found with *Aedes aegypti* and *Anopheles gambiae* (mosquito) proteins (Figure 4.5a). Interestingly, the region (573-750) showed similarity to the *Lepeophtheirus salmonisi* protein nucleolar and spindle associated protein 1. By reducing the region of protein alignment to this area, 40 % homology with the human protein Nucleolar and spindle-associated protein (NuSAP) was identified for a 50aa region (Figure 4.5b). NuSAP is a 55 kDa protein with selective expression in proliferating cells. Its localisation is predominantly nucleolar during interphase and on the central spindle during mitosis (Raemaekers et al., 2003).

Due to the localisation of NuMAP to the nucleus, I analysed the NuMAP protein sequence for the presence of a nuclear localisation signal (NLS). The NLS has been identified on multiple nuclear proteins. It has been shown that a short amino acid sequence can alone determine the localisation of a protein to the nucleus (Kalderon et al., 1984). NLSs are usually rich in positively charged amino acids such as lysine and arginine (Alberts, 2002), although other signals have been identified but not yet characterised. Automated tools have been developed for the analysis and determination of NLS sequences. Using PredictNLS, no NLS was identified in the NuMAP protein. Two coiled-coil structures were predicted using Coils, a program which calculates the probability that the sequence will adopt a coiled-coil conformation (Lupas et al., 1991) shown in Figure 4.5c.

Further sequence analysis using an internet based motif prediction tool (http://bioweb.pasteur.fr/protein/intro-en.html) predicted three potential PEST motifs at (324-364), (154-172) and (154-172). PEST motifs are hydrophilic polypeptide sequences enriched in proline (P), glutamic acid (E), serine (S) and threonine (T)

A

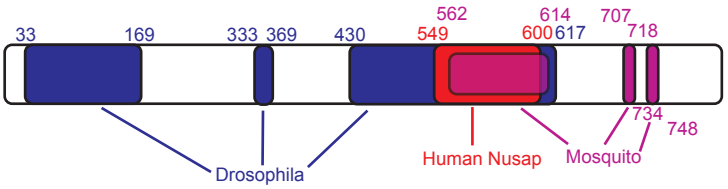

B

```
NuMAP   549    SRIPKPNRGVIPLNKTITPSKVNKRTKM--PNFAAMHERQFAKMESLVDHVERK  600
               S++P   +  +  +++  P K NKRT +  PNF  +HE  F +MES+  ++ERK
NuSAP   154    SKVPSEGKKSLYTDESSKPGK-NKRTAITTPNFKKLHEAHFKEMESIDQYIERK  206
```

C

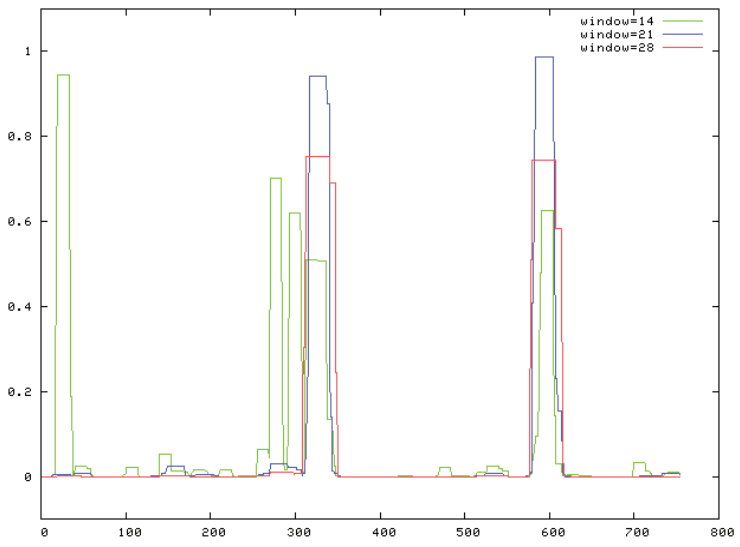

Figure 4.5 NuMAP homology and predicted secondary structure.
(A) Schematic representation of homology regions in NuMAP identified using the basic local alignment search tool. **(B)** Identified region of homolgy to human NuSAP using NuMAP amino acid sequence 541-754 and a basic local alignment search tool. Substitutions are marked by (+). Identical matches are displayed in letter code. **(C)** Prediction of coiled-coil secondary structures in NuMAP. Coloured lines show different window sizes used for coil prediction by prediction software Coils.

which targets proteins for rapid degradation. Proteins containing PEST motifs often have a half life of less than 2 hours, suggesting that NuMAP may also have a short half life.

4.3 Identification of localisation domains

Localisation analysis in S2 cells showed that NuMAP localises to the nucleus during interphase and spindle microtubules during mitosis. The nuclear localisation of NuMAP precludes its interaction with microtubules and therefore prevents analysis the microtubule binding capabilities during interphase in cells. The identification and separation of the microtubule binding and nuclear localisation domains will enable us to mis-localise NuMAP protein to the interphase cytoplasm and analyse the microtubules binding of NuMAP during interphase.

To identify the regions of the protein responsible for nuclear and microtubule localisation of NuMAP, I created several GFP-NuMAP truncations and examined their localisation by immunostaining after transfection. As described earlier, there are 4 main regions of homology with *Drosophila* and mosquito proteins. I therefore first created C-terminal truncations, removing each major region of homology. These truncations were created by introducing premature stops into the NuMAP coding sequence by site-directed mutagenesis. All truncations created no longer associated with microtubules during mitosis. All except the smallest protein fragment, NuMAP(0-44), localised to the nucleus (Figure 4.6a). These results indicated that the C-terminus is required for microtubule binding and a nuclear localisation signal lies to the N-terminus of the protein. I also identified a region of

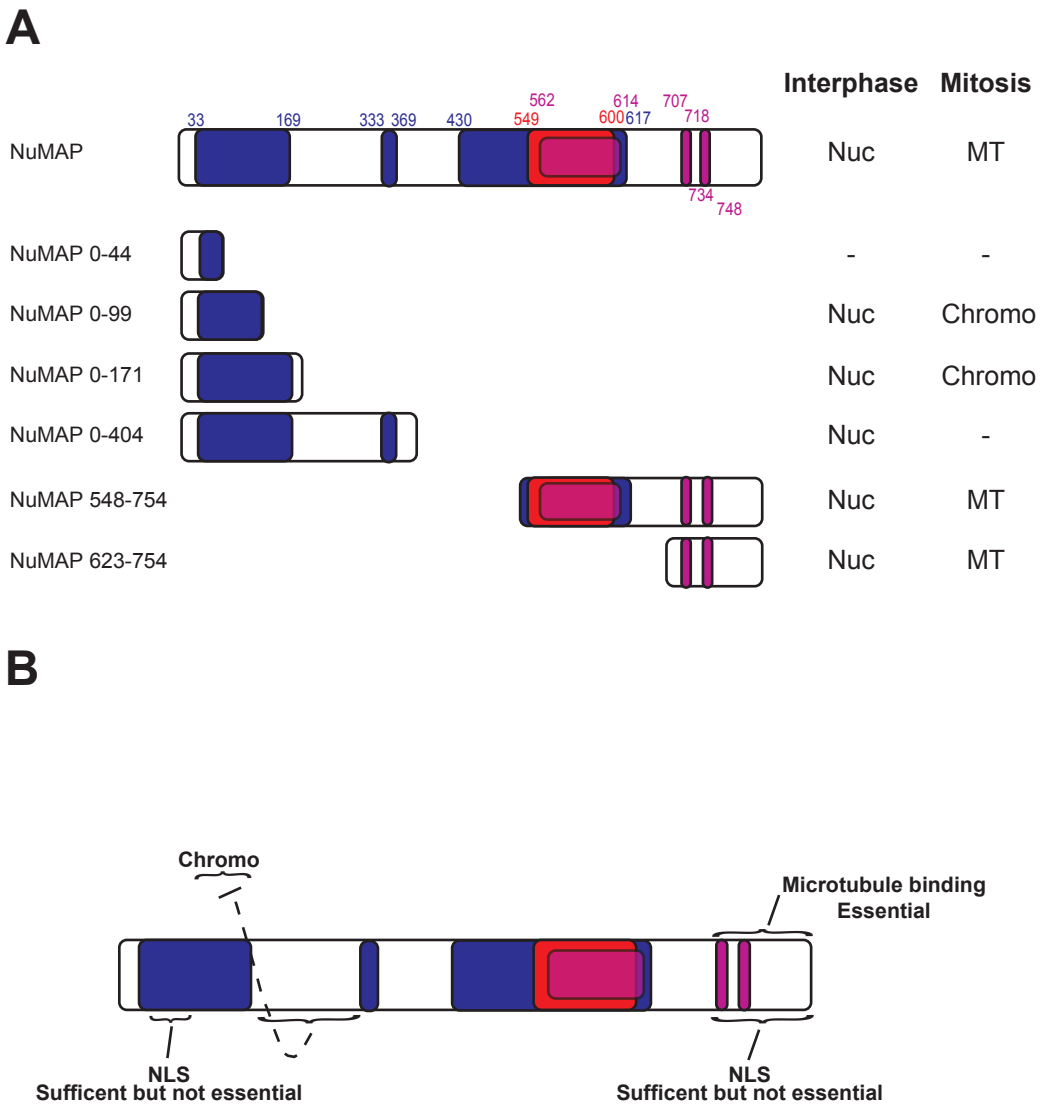

Figure 4.6 NuMAP truncation analysis. (A) Schematic represenation of created truncations and their localisation in interphase and mitosis. (Nuc) indicates protein localisation to the nucleus. (MT) indicates protein localisation to microtubules. (Chromo) indicates localisation to mitotic chromosomes. (-) indicates diffuse protein, no localisation. **(B)** Schematic representation of regions identified for NuMAP localisation. NuMAP contains 2 NLS sequences, a microtubule binding region and a region that shows localisation to mitotic chromosomes.

NuMAP with affinity for chromosomes. NuMAP(0-171) showed association to the chromosomes during mitosis, as NuMAP(0-404) did not. These results suggest that there is a region of NuMAP capable of chromosome association which is negatively regulated by an adjacent region (Figure 4.6b).

To confirm that the microtubule binding domain is at the C-terminal and to narrow down the protein region, I created N-terminal truncations (Figure 4.6a). All C-terminal fragments including the smallest, NuMAP(623-754), showed nuclear localisation during interphase and localisation to microtubules during mitosis. This confirmed that the microtubule binding region and a nuclear localisation signal lies at the C-terminal end of the protein. It also indicated that NuMAP contains two nuclear localisation signals, both sufficient but not essential to localise NuMAP to the interphase nucleus (Figure 4.6b). To further focus in on the microtubule binding domain, I truncated NuMAP(623-754) further. NuMAP(623-693) and NuMAP(623-718) were diffuse and did not localise to microtubules (Figure 4.7a). Truncations (623-729) and (623-632/713-754) showed nuclear and mitotic microtubule localisation (Figure 4.7a). These results indicate the C-terminal nuclear and microtubule localisation domains are very close together, if not overlapping, in the protein region of 713-729 (Figure 4.7c). However, NuMAP(623-729) and NuMAP(623-630/713-754) localisation was not as pronounced as full length NuMAP (Figure 4.7b). There are two regions of homology in this section of NuMAP. NuMAP(623-729) and NuMAP(623-630/713-754) each disrupt one of these regions suggesting they may collaborate to ensure effective localisation to the microtubules and the nucleus (Figure 4.7c). Table 4.1 shows quantified localisation analysis of created truncations.

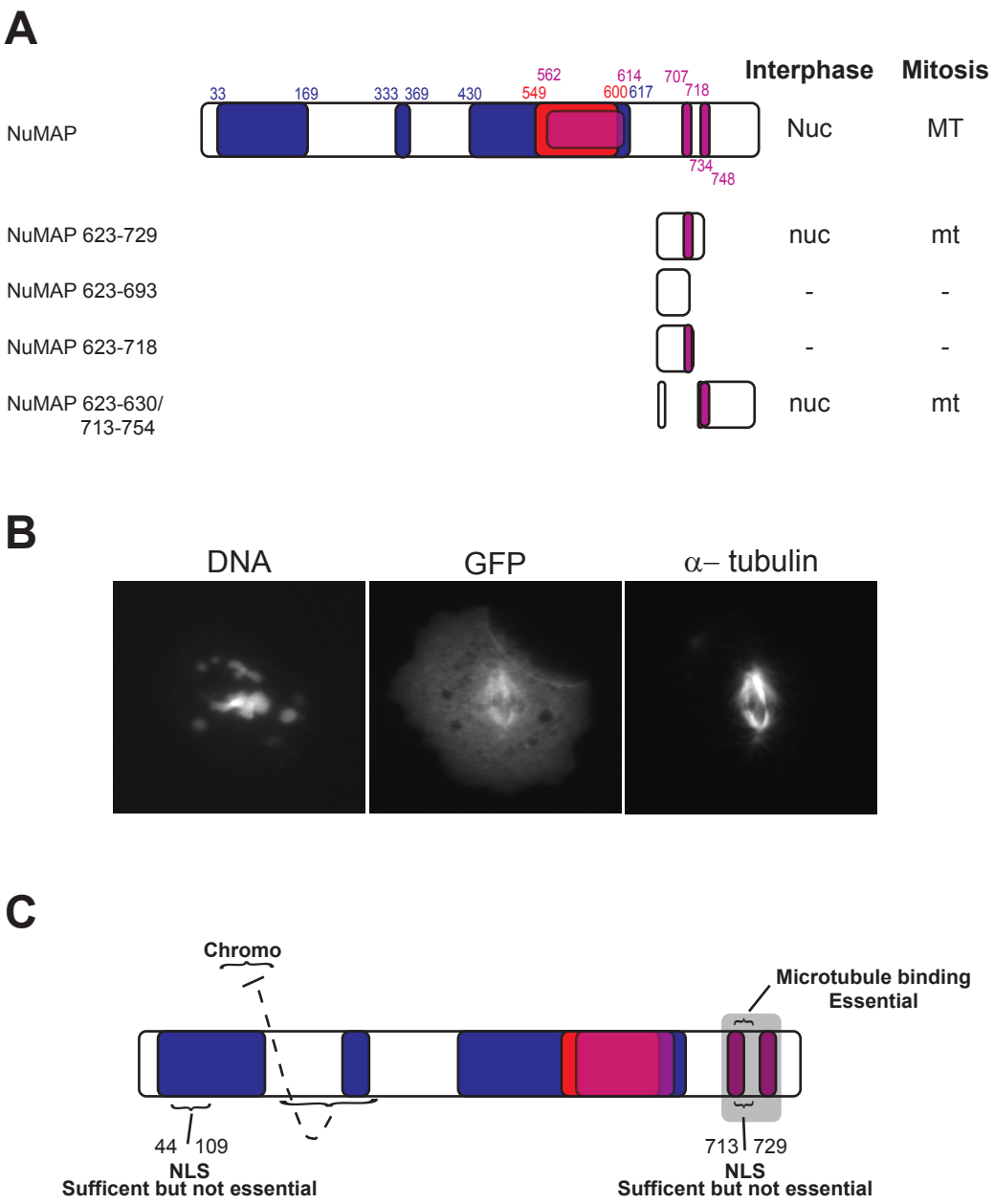

Figure 4.7 Identification of NuMAP nuclear and microtubule localisation domains. (A) Schematic representation of truncations created and their protein localisation in interphase and mitosis. (Nuc) indicates localisastion to the nucleus. (MT) indicates localisation to microtubules. (nuc) indicates reduced localisation to the nucleus. (mt) indicates reduced localisation to microtubules. (-) indicates diffuse protein, no localisation. **(B)** S2 cell images showing observed decrease in localisation of NuMAP(623-729) and NuMAP (623-630/713-754) . Exposure times of tuncations were similar enabling their comparison. **(C)** Schematic representation of regions identified for NuMAP localisation. Grey box represents two homology regions which may come together to regulate microtubule binding.

Table 4.1 Analysis of the localisation of NuMAP truncations in S2 cells. S2 cells were transfected with various NuMAP truncations and cultured for 48 hours. Protein localisation was observed in immunostained fixed samples. A total of 500 transfected cells were counted to assess the mitotic indices. 100 transfected interphase cells were assessed for protein localisation.

		Interphase					Mitosis			
Construct	Mitotic index (%)	Nucleus	Nucleus and cytoplasm	Bundled microtubules	Emanating microtubule array	Cytoplasm	Chromosomes	Spindle microtubules	Spindle poles	Cytoplasm
0-754 (Full length)	1.4	100					1	26	3	
0-44	0.79					100				9
0-109	0.99	106								7
0-171	1.4	97	2				8			5
0-404	0.9	99	1				4			11
548-754	0.6	80		19	1			3		
623-754	2.4	74		23	2			19		
623-729	1.2	4	71			38		6 + cytoplasm		1
623-693	2.3			1		99	4			17
623-718	1.8					100				19
623-630/ 713-754	2.2		77	28		4		3		

4.4 Analysis of NuMAP microtubule binding in interphase

Although I had narrowed down the regions of NuMAP which regulate its localisation, I had not managed to separate nuclear and microtubule localisation. This prevented me from investigating whether NuMAP can bind to microtubules during interphase by mutating the NLSs. To overcome nuclear localisation of NuMAP during interphase, I decided to generate NuMAP fused to a nuclear export signal (NES). The short hydrophobic signal of PKI, a heat stable inhibitor of the catalytic subunit of cAMP-dependent protein kinase, is sufficient to induce nuclear export (Roth et al., 2003; Wen et al., 1995). Therefore to create an interphase cytoplasmic pool of NuMAP, I fused the PKI NES to GFP-NuMAP. PKI NES was inserted at either side of NuMAP to create GFP-NES-NuMAP and GFP-NuMAP-NES (Figure 4.8a). After transfection in S2 cells, the microtubule binding of NuMAP in interphase was analysed by immunostaining. Both constructs showed increased localisation to the cytoplasm, though the nucleus remained the predominant region of localisation. The pool of NuMAP in the cytoplasm did not associate with interphase microtubules (Figure 4.8b). In mitosis both constructs still showed association with spindle microtubules, confirming the ability of fusion proteins to associate with microtubules. This confirms that the interphase form of NuMAP has low affinity to microtubules.

I also fused an NES to the microtubule binding domain of NuMAP to create GFP-NES-NuMAP(623-754) (Figure 4.8a). This construct showed greater localisation to the cytoplasm during interphase than full length NES fused protein. In contrast to the full length protein construct, it showed association with interphase microtubules (Figure 4.8b). However, microtubules associated with NuMAP were

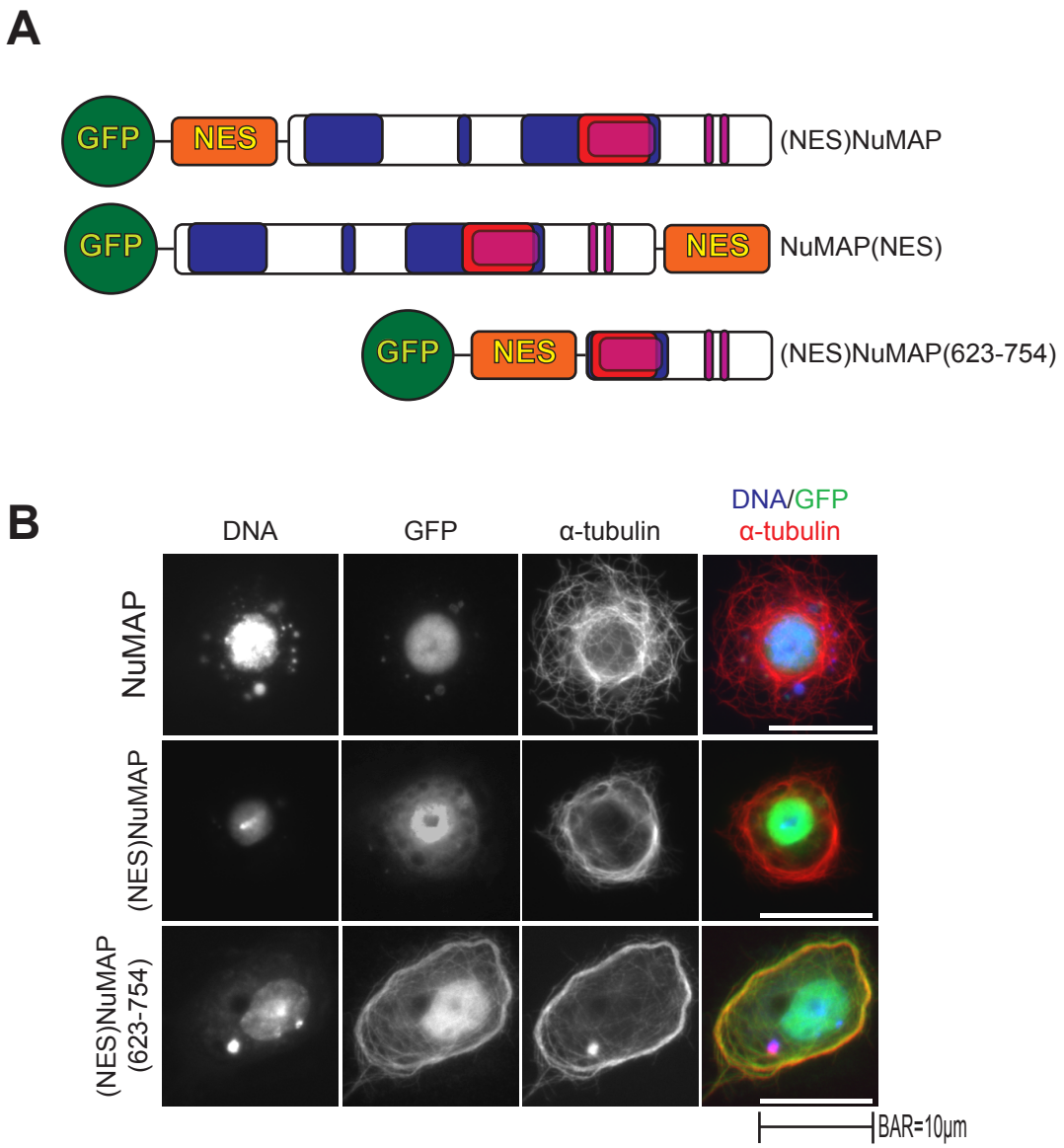

Figure 4.8 Localisation of NuMAP fused with an NES **(A)** Schematic representation of NuMAP constructs containing an NES. **(B)** Images representing localisation observed of NuMAP containing an NES. S2 cells were fixed with cold methanol 48 hours after transfection with plasmid for expression of specific NuMAP constructs, NuMAP (no NES), (NES)NuMAP and (NES)NuMAP(623-754). Fixed cells were immunostained with antibodies for GFP (to visualise NuMAP) and α-tubulin (to visualise microtubules). DNA was stained with DAPI. (NES)NuMAP showed an increased cytoplasmic pool that did not co-localise with microtubules. (NES)NuMAP(623-754) showed an increased cytoplasmic pool and co-localised with microtubules and induces their bundling. Exposure times of images in this figure are comparable and therefore images can be compared.

bundled and showed a circular interphase microtubule array. These results show the microtubule binding domain alone has a high affinity to microtubules even in interphase, indicating that the cell cycle regulation is mediated by a region other than this domain. This also suggests that the nuclear localisation of NuMAP and the regulation of its microtubule binding ability are crucial to prevent bundling of interphase microtubules.

4.5 Analysis of NuMAP function

Although I had identified the localisation of NuMAP, no clear function had been determined. Next I therefore decided to address the function of NuMAP using two approaches, in cultured cells and developing flies.

4.5.1 Analysis of NuMAP function in S2 cells using RNAi

To analyse NuMAP function in S2 cells during mitosis, I used RNAi to deplete NuMAP protein and analysed spindle morphology by immunofluorescence. As previously described, S2 cells were treated for 5 days with either dsRNA against NuMAP or β-lactamase. Cells were adhered to Concanavalin A coverslips and immunostained for α-tubulin, DNA and phospho-H3 (to identify mitotic cells) and examined for microtubule organisation in mitosis. Spindle abnormalities were classified into the following categories: monopolar, bipolar with no asters, bipolar with one aster, tripolar, multipolar and other abnormalities. Chromosome alignment was also examined and categorised as follows: misaligned, lagging and chromosome

bridges. A minimum of 100 mitotic cells were examined from both NuMAP and control RNAi samples. There was an increase in the number of bipolar spindles with only one aster after NuMAP RNAi compared with the control (Table 4.2). There was also an increase in other abnormalities in the NuMAP knock down cells.

As a lack of aster is likely to be caused by a lack of centrosome at spindle poles, I co-stained for γ-tubulin. In addition, to enhance any defects I decided to perform 8-day RNAi. Again 100 mitotic spindles were examined. Spindles were classified to be bipolar with one centrosome if γ-tubulin staining was absent from one pole (Figure 4.9a). Compared to the control, NuMAP RNAi showed an increase in the number of bipolar spindles with one centrosome. The Fisher exact test showed this to be a statistically significant difference, with a p-value of 0.02 (Figure 4.9b).

4.5.2 Analysis of NuMAP function in Drosophila melanogaster

I took advantage of a fly strain that has a transposable element, the P-element, which is close to the NuMAP gene. P-elements are transposable elements which tend to insert into the genome 5' to the transcriptional start regions of genes and can be stimulated to 'jump' when a source of transposase is provided. When excision occurs, it is not always precise and often removes surrounding chromosomal regions. In the strain *EY05585*, there is a P-element approximately 550 bp downstream of the NuMAP stop codon. I therefore decided to mobilise this P-element to create a deletion mutant of NuMAP. The P-element, however, is within the downstream gene, Trf4-2. Previous analysis of a Trf4-2 disruption resulted in viable flies (Nakamura et al., 2008). However, analysis of any phenotype caused by the

RNAi target	Number Mitotic/Interphase	Mitotic index (%)
5 Day		
β-lactamase	18/482	3.6
NuMAP	14/486	2.8
8 Day		
β-lactamase	31/971	3.1
NuMAP	12/993	1.2

RNAi target			Mitotic spindle phenotypes						Mitotic chromosome phenotypes	
	Mitotic cells counted	Normal spindles	Monopolar	Bipolar		Tripolar	Multipolar	Other	Lagging	Mis-aligned
				No asters	Mono aster					
5 Day										
β-lactamase	103	54	1	1	9	17	12	6		3
NuMAP	102	37	1	2	14	16	6	19	1	6
8 Day										
β-lactamase	207	145	3		4	18	16	20		1
NuMAP	200	117	4		14	36	13	15		1

Table 4.2 Table of RNAi phenotypes in S2 cells. S2 cells were treated with dsRNA targeting NuMAP for a period of 5 or 8 days. Mitotic phenotypes observed in fixed samples are shown, with mitotic indices.

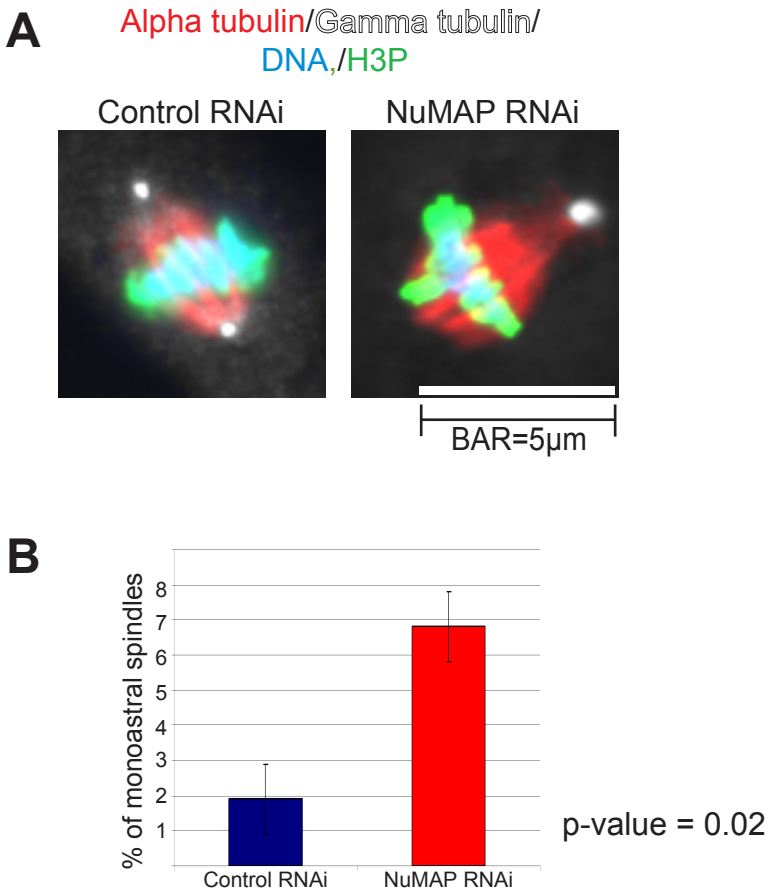

Figure 4.9 NuMAP RNAi induces monoastral spindles. (A) Typical spindle morphologies of control and NuMAP depleted S2 cells. S2 cells were fixed with cold methanol 8 days after treatment with dsRNA against β-lactase (control) or NuMAP. Fixed cells were immunostained with antibodies for gamma tubulin (to identify spindle poles, white), α-tubulin (to visualise spindle microtubules, red) and H3P (to identify mitotic cells, green). DNA was stained using DAPI (blue). Depletion of NuMAP increased the number of cells lacking gamma tubulin staining at one end of the spindle.
(B) Increase in the number of cells lacking gamma tubulin staining at pole of mitotic spindle.

remobilisation of the P-element must be tested with reference to the disruption of Trf4-2.

Following P-element mobilisation, flies which had lost the P-element were selected by eye colour and chromosome marker and were then analysed by PCR to determine if the P-element remobilisation had deleted any region of the NuMAP coding sequence. Among 115 successful crosses, 7 strains had between 10-800 bp of NuMAP coding sequence excised. In one strain the entire NuMAP coding region was deleted. This strain is viable and indicates that the NuMAP gene is not essential for viability. Although preliminary results show the gene upstream from NuMAP, CG11168, is disrupted, the extent of the deletion is not yet fully determined. Initial analysis of the homozygotes of this deletion shows them to have reduced viability and to be female sterile. Of seven female homozygotes analysed, only two of many embryos laid by them developed to third instar lava but no further. Further analysis is required to test whether these phenotypes are due to the deletion of NuMAP.

4.6 Analysis of NuMAP binding proteins

I next wanted to identify NuMAP-interacting proteins. The identification of NuMAP binding proteins may uncover regulating proteins and give further insight into the function of NuMAP in the cell.

To identify interacting proteins, I first made a stable cell line expressing GFP tagged NuMAP. S2 cells were transfected with two plasmids; the first containing GFP-NuMAP sequence under the actin promoter, the second plasmid contained a gene conferring blasticidin resistance. The concentration of this plasmid was lower

than that encoding GFP-NuMAP to ensure the majority of cells which took up the resistance plasmid also obtained GFP-NuMAP. After transfection, cells were treated with blasticidin for six weeks, this resulted in a blasticidin resistant population in which most cells expressed GFP-NuMAP.

The stable cell line was next used for the purification of GFP-NuMAP and interacting proteins. Cell lysate was incubated with beads coated with an anti-GFP antibody, allowing GFP-NuMAP and interacting proteins to bind. Beads were then repeatedly washed using lysis buffer and finally boiled in SDS-PAGE sample buffer, dissociating all proteins. As a control, the pull down was performed in parallel using cells that did not contain any GFP construct. Protein samples were analysed by western blot using anti-GFP and silver staining after SDS-PAGE. Western blot showed a 175 kDa band in the pull down sample from cells expressing GFP-NuMAP. This band was absent from the control, which confirmed GFP-NuMAP had been successfully pulled down. Silver staining showed a number of proteins had been pulled down from both cells with and without GFP-NuMAP. There was no significant difference between the two samples, showing that although GFP-NuMAP was specifically pulled down, the majority of proteins were not specifically bound to NuMAP.

I next decided to analyse the sample by mass spectrometry. Although GFP-NuMAP had been pulled down, I wanted to determine if the total quantity purified protein was sufficient to identify interacting proteins. I therefore first analysed the section of the gel containing GFP-NuMAP, to assess if NuMAP could be identified by mass spectrometry. Following in-gel trypsin digestion and peptide analysis, mass spectrometry data was processed using DTAsupercharge and Mascot. However,

NuMAP was not identified, nor was the GFP tag. This indicated that a significantly larger quantity of NuMAP needed to be purified before the sample could be used to identify interacting proteins.

4.7 Discussion

4.7.1 Regulation of NuMAP during interphase

To investigate the microtubule binding ability of NuMAP during interphase, I mis-localised NuMAP to the cytoplasm by fusing it with the PKI NES motif. Analysis of this construct in S2 cells showed increased protein localisation to the cytoplasm though its localisation to the nucleus remained predominant. This cytoplasmic pool of NuMAP did not associate with interphase microtubules indicating that the interphase form of NuMAP has low affinity for microtubules. In contrast to the NES fused full length protein, the NES fused microtubule binding domain showed a more pronounced cytoplasmic localisation which associated with bundled interphase microtubules.

Although the fusion of an NES increases the interphase cytoplasmic pool of full length NuMAP, the immunofluorescent signal is weak. Therefore to confirm no microtubule association of NuMAP during interphase, the cytoplasmic pool of NuMAP needs to be increased.

As described previously, the NES microtubule binding domain construct showed a greater localisation to the cytoplasm than the NES full length protein. Interestingly, full length protein contains two NLS sequences as the NES

microtubule binding domain only contains one. Wen *et al* (1995) observed that the NLS is slightly stronger than an NES. Therefore the weaker cytoplasmic signal of NES full length protein may result from the presence of two NLS and only one NES. To increase the interphase cytoplasmic pool of NuMAP further, multiple NES motifs could be fused to NuMAP. This may enhance the export of protein from the nucleus and result in a more prominent cytoplasmic localisation of NuMAP.

4.7.2 NuMAP: a potential Drosophila homologue of human NuSAP

From BLAST similarity search, I identified that NuMAP has a small region of homology with human nucleolar spindle associated protein (NuSAP). Similar cell-cycle localisation of NuSAP and NuMAP, interphase nuclear localisation and mitotic spindle localisation, raises the possibility that these proteins are functional homologues. NuSAP was originally identified in proliferating and differentiating mouse MCSTSE1 oseteoblasts. Gene expression patterns identified a cDNA which was enhanced during proliferation and the protein product was later called NuSAP (Raemaekers et al., 2003). It was shown to be highly conserved in vertebrates, with little homology found to invertebrate proteins. This current study may have uncovered a new invertebrate homologue.

There are a number of similarities between human NuSAP and *Drosophila* NuMAP. Firstly, both proteins have similar domain and secondary structures. NuSAP contains potential PEST and SAP motifs. PEST motifs are hydrophilic sequences which target proteins for rapid degradation and SAP motifs are putative DNA-binding motifs involved in chromosomal organisation (Aravind and Koonin,

2000). NuMAP contains three potential PEST sequences at (324-364), (154-172) and (154-172), with no SAP motif being identified at present. NuSAP has two domains which are sufficient for its nuclear targeting during interphase, a bipartite NLS sequence and a charged helical domain. Although no NLS sequence has been predicted in NuMAP, it too has two domains which can direct its localisation to the nucleus during interphase. Both NuSAP and NuMAP have domains at their C-terminus which enables their association with microtubules. The interaction of NuSAP with microtubules has been shown to be direct, however this is yet to be confirmed with NuMAP. However, a significant difference between the protein structures is their size. NuMAP is almost double the size of NuSAP, with NuMAP's 754 amino acids to NuSAP's 427 amino acids.

Another similarity is that both NuSAP and NuMAP behave in a similar manner when analysed by SDS-PAGE. The mouse NuSAP cDNA was predicted to encode a protein of 427 amino acids with a molecular mass of 48.6 kDa. However, during SDS-PAGE analysis NuSAP shows a significant band shift which suggests its apparent molecular mass is slightly higher at 55 kDa. This decrease in protein mobilisation can be partially accounted for by protein phosphorylation, but appears to be primarily due to the protein's high basic amino acid content (Raemaekers et al., 2003). NuMAP also shows a decrease in protein mobilisation when analysed by SDS-PAGE. NuMAP cDNA encodes a 754 kDa amino acid protein with a predicted molecular weight of 84.5 kDa. When NuMAP is tagged with GFP, the predicted molecular weight is 112 kDa. However, SDS-PAGE followed by western blot showed an apparent molecular weight of approximately 175 kDa. Multiple phosphorylation sites have previously been identified throughout NuMAP protein by

genome wide phosphoproteomics in *Drosophila melanogaster* Kc167 cells (Bodenmiller et al., 2007).

A further similarity between NuSAP and NuMAP is their ability to bundle microtubules. Over-expression of NuSAP in Cos1 cells resulted in the localisation of NuSAP to long, curved, thick microtubule bundles in the cytoplasm. These bundles were characterised to be extremely stable and remained polymerised in the presence of high doses of nocodazole (Raemaekers et al., 2003). The expression of GFP-NuMAP showed a population of cells with GFP-NuMAP localised to bundled microtubules. This population of cells appeared to be those where GFP-NuMAP was heavily over-expressed. When the cytoplasmic pool of NuMAP(623-754) is increased by the expression of NuMAP(623-754)+NES, interphase microtubules are bundled. These comparable phenotypes suggest NuMAP and NuSAP may have similar functions in the cell.

Another common feature of NuSAP and NuMAP is that they both show localisation to mitotic chromosomes. Immunostaining revealed that NuSAP localised to microtubules in the vicinity of chromosomes during metaphase and early anaphase. In later anaphase, the intensity of this staining increases (Raemaekers et al., 2003). Interestingly, Raemakers *et al* (2003) showed that the localisation of NuSAP to the vicinity of the chromosomes is independent of microtubule integrity. Furthermore, NuSAP has been shown to have the ability to bind DNA directly (Ribbeck et al., 2007). This localisation and direct binding to both DNA and microtubules, has led to the hypothesis that NuSAP may play a role in linking microtubules to the mitotic chromosomes (Ribbeck et al., 2007). In this study immunostaining and expression of GFP-NuMAP showed NuMAP localisation to the

entire mitotic spindle in S2 cells and *Drosophila* syncyial embryos. Interestingly, two NuMAP truncations, NuMAP(0-171) and NuMAP(0-404), showed chromosomal localisation during mitosis.

Although NuSAP and NuMAP have similar protein structure, possible function and potential chromosome binding, they do not localise to the exact same region of the mitotic spindle. Yet NuSAP and NuMAP localisation in meiotic spindles is comparable. By indirect immunofluorescence in *Xenopus laevis*, NuSAP was detected on the entire metaphase I spindle, showing enrichment at microtubules in the immediate vicinity of chromosomes (Ribbeck et al., 2006). Preliminary live imaging results of GFP-NuMAP suggest that NuMAP also localises to the entire meiotic spindle with enrichment at microtubules surrounding the chromosomes.

There are a number of similarities between NuSAP and NuMAP and there are also some significant differences. The phenotypes seen after protein knockdown are notably different. Depletion of NuSAP using siRNA in HeLa cells showed a number of different mitotic phenotypes. Microtubule organisation of the prometaphase spindle was abnormal and frequently coupled with an abnormal chromosome condensation pattern. Metaphase cells also show disorganised microtubules, with less dense arrays of spindle microtubules and misaligned chromosomes (Raemaekers et al., 2003). However, depletion of NuMAP by RNAi in S2 cells does not result in disorganisation of microtubules, but an increase in the number of monoastral spindles. Monoastral spindles are generally created by the lack of centrosome duplication/separation during S phase (Wilson et al., 1997). The increase in monoastral spindles in cells treated with dsRNA against NuMAP is not consistent with protein localisation. As I have said previously, NuMAP is localised in the

nucleus during interphase and no localisation in the cytoplasm is seen. Localisation of NuMAP to the centrosomes was seen in the embryo. However this occurs after centrosomes have been duplicated/separated. The increase in the number of monoastral spindles in cells treated with dsRNA against NuMAP is statistically significant, but not dramatic. The phenotype was not penetrant and the loss of asters is common in S2 cells. I therefore do not think this result reflects the primary function of NuMAP and further study of NuMAP function in the null mutant should be carried out to assess its central function.

Another aspect of NuMAP and NuSAP which differs is their behaviour when present in the cytoplasm during interphase. By permeabilizing the nuclear envelope of MC3T3E1 cells with detergent, NuSAP was seen to pass into the cytoplasm and localise to the perinuclear microtubule network during interphase. Raemakers *et al* (2003) showed that this localisation was dependent on microtubule integrity. However, when an NES sequence is coupled to NuMAP, thereby increasing its cytoplasmic pool during interphase, no localisation to the microtubule network is seen. These results suggest that NuMAP may undergo a post-translational modification which NuSAP does not, preventing its association with microtubules during interphase.

4.7.3 Mechanism of NuMAP cell cycle regulation

I identified NuMAP biochemically by its ability to associate with microtubules specifically during mitosis. NuMAP localises to the nucleus during interphase but when it is mis-localised to the cytoplasm by fusion to an NES, it does not associate

with the microtubule network. Both biochemical and cytological studies show that NuMAP has a mechanism present during interphase that prevents its association with microtubules. There are multiple ways of protein regulation which may control NuMAP function independently or together.

Firstly, a post-translational modification might be present during interphase. This modification may be on the NuMAP protein itself, but it could equally be likely present on a NuMAP-binding protein. Phosphorylation is a key post-translational modification and has been shown to play a role in the regulation of multiple proteins through the cell cycle. Thus it is likely that phosphorylation plays a role in the regulation of MAPs through the cell cycle. In addition, in this study phosphorylation was maintained during MAP purification from interphase and mitotic cell extracts. This supports the possibility that the regulation of NuMAP may be through phosphorylation.

Secondly, NuMAP may undergo rapid protein degradation in a cell cycle dependent manner. NuMAP is predicted to contain a PEST sequence. PEST sequences are hydrophobic stretches involved in the rapid degradation of proteins. These sequences are often conditional proteolytic sites, but it has also been suggested that phosphorylation of PEST sequences may direct the attachment of multiple ubiquitin chains (Rechsteiner and Rogers, 1996). SDS-PAGE followed by western blot of GFP-NuMAP showed reduced mobility of NuMAP. Ubiquitination of potential PEST sequences in NuMAP may contribute to this decrease in protein mobility during SDS-PAGE. This could be investigated by western blot using an anti-ubiquitination antibody.

Protein and mRNA levels of NuSAP peak at G2 to mitosis and decline rapidly after cytokinesis, reducing the quantity of NuSAP during interphase. NuSAP degradation is proposed to be carried out by the ubiquitin/proteasome pathway using its KEN box and PEST sequences and is important for accurate spindle formation (Song and Rape, 2010). During this study, high over-expression of GFP-NuMAP resulted in the bundling of interphase microtubules. Therefore to remove excess protein during interphase, endogenous NuMAP may be regulated using its potential PEST sequence. It would be interesting to monitor the degradation of NuMAP protein through the cell cycle to observe if it is degraded at specific stages similar to its potential homologue NuSAP.

Lastly, a number of MAPs which localise to the nucleus during interphase and to the spindle during mitosis have been shown to be regulated by the RanGTP pathway. NuMAP may fall within this group. Ran is a member of the Ras GTPase family which regulates intracellular processes such as spindle assembly at the start of mitosis and nuclear envelope reassembly after mitosis. The activity of Ran is activated by the GTPase activating protein RanGAP1, which stimulates the hydrolysis of Ran bound GTP to GDP. The non-catalytic protein Ran binding protein 1 (RanBP1) also plays a role in this process. In isolation RanBP1 stabilises RanGTP and in the presence of regulators increases the activity of the RanGAP1 protein. GDP bound to Ran is next exchanged for GTP. This exchange is instigated by the nucleotide exchange factor RCC1 (regulator of chromosome condensation 1). RCC1 is chromosomal associated, binding to chromatin through an interaction with histones H2A and H2B. Therefore a pool of RanGTP is created in the vicinity of chromatin. During interphase RCC1 associates with chromatin within the nucleus

and RanGAP1 is located in the cytoplasm. Therefore a high concentration of RanGTP is present in the nucleus and RanGDP in the cytoplasm.

The Importin (Imp) β family of proteins, known to be transport receptors, are effectors of the RanGTP pathway. The Imp family are normally classified as the importins and the exportins. Importins bind their cargo in low RanGTP environments and release this cargo upon the binding of RanGTP. Exportins work in the opposite way; they bind their cargo in a high RanGTP environment and unload their cargo upon the hydrolysis of GTP. The binding of importins and exportins not only regulates the localisation of their cargo but also the cargo's activity.

The RanGTP pathway has been shown to regulate the key proteins involved in the formation of the mitotic spindle such as TPX2, NuMA and also NuSAP. The binding of importin-α and -β to NuSAP was shown to inhibit protein activity, preventing its binding to microtubules. Data also suggested that the importin-α and importin-β heterodimers may mediate NuSAP localisation to the nucleus (Ribbeck et al., 2006). The RanGTP pathway regulation of spindle factors, specifically NuSAP, suggests that NuMAP might be regulated in a similar way. Two features of NuMAP which also hint that NuMAP might be a component of the RanGTP network are NuMAP is imported into the nucleus during interphase and NuMAP localises to the mitotic spindle. I therefore believe that NuMAP is regulated in the same manner as NuSAP, by the RanGTP pathway.

I hypothesise that during interphase the importin proteins, importin-α and importin-β, associate with NuMAP and mediate its localisation to the nucleus. As cells progress into mitosis the nuclear envelope is broken down and NuMAP is

released into the cytoplasm. Importin-α and importin-β proteins are likely to remain associated with NuMAP restricting its activity. However, in the vicinity of the spindle, NuMAP is released from the importin proteins by RanGTP and is able to associate with microtubules. This proposed model is illustrated in Figure 4.10.

If Ran and the importin proteins only regulated NuMAP association with microtubules then the protein would be localised to microtubules in the vicinity of the chromosomes. However, NuMAP is distributed evenly over the entire spindle. Therefore I propose that though Ran regulation may play a role in determining NuMAP association with microtubules, it may more importantly regulate the activity of NuMAP and therefore its function thus restricting NuMAP activity to the vicinity of the chromosomes. Two truncations of NuMAP showed it to have the ability to associate with the chromosomes during mitosis. It is therefore possible that like NuSAP, NuMAP may function near the chromosomes to link them to microtubules.

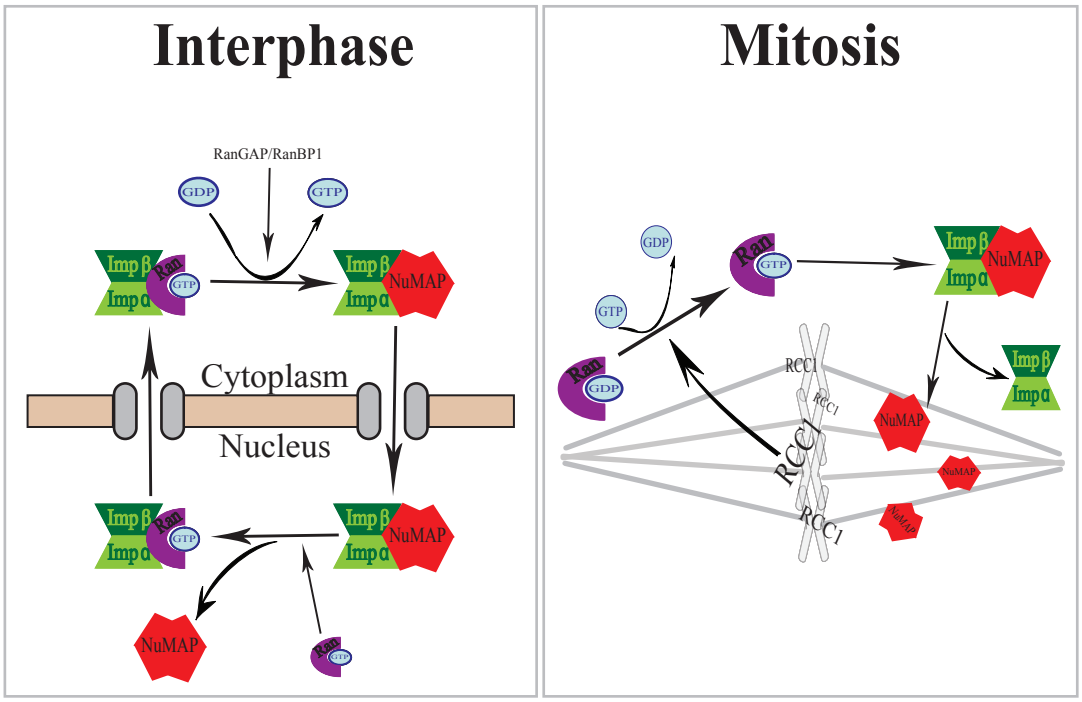

Figure 4.10 Proposed model of NuMAP cell cycle regulation. Schematic representation of proposed mechanism of the cell-cycle regulation of NuMAP. During interphase, cytoplasmic NuMAP is bound by the importin proteins (α and β), and imported into the nucleus. The high concentration of RanGTP in the nucleus releases this binding, leaving NuMAP free in the nucleus. During mitosis, the importin proteins are likely to remain associated with NuMAP restricting its activity. However, in the vicinity of the chromosomes, NuMAP is released from the importin proteins by a high concentration of RanGTP and is able to associate with microtubules.

5 Summary and future direction

5.1 Background

The microtubule cytoskeletal network functions as a central framework of diverse cellular processes such as cell division, migration and morphogenesis (Valiron et al., 2001). One of the most remarkable structures formed by microtubules is the mitotic spindle, which is crucial for correct chromosome segregation during cell division. As cells progress through the cell cycle, the microtubule array changes dramatically from interphase to mitosis. During interphase, microtubules emanate from the microtubule organising centres located at the centre of the cell towards the cell periphery. At the onset of mitosis, the interphase array is reorganised into the dynamic mitotic spindle.

This crucial re-organisation of microtubules is dependent on an abundance of proteins that interact with microtubules. This group of proteins are called microtubule-associated proteins (MAPs). Together these proteins use diverse mechanisms to regulate the organisation and function of microtubules through the cell cycle.

As MAPs play a central role in the regulation of microtubule organisation, I hypothesised that there are distinct groups of MAPs which associate and regulate microtubules at specific times during the cell cycle. Specifically, I proposed that as a cell progresses from interphase to mitosis, an interphase group of MAPs will dissociate and a mitotic-specific group of MAPs will associate with microtubules.

This group of mitotic MAPs will be important for the formation and function of the mitotic spindle.

Although MAPs play an essential role in the regulation of microtubules and the formation of the mitotic spindle, only a handful of proteins are known to associate with microtubules specifically during mitosis. The aim of this study was to identify more of those MAPs that associate with microtubules specifically during mitosis and to understand their regulation and function. To fulfil this aim, I developed a method to determine the profiles and relative quantities of MAPs purified from mitotic and interphase *Drosophila* culture cells.

5.2 A new method for the identification of MAPs

The developed method utilises mass spectrometry combined with stable isotope labelling by amino acids in cell culture (SILAC) for protein quantification. In brief, two populations of Schneider 2 (S2) cells were cultured, one in media containing 'heavy'(^{13}C) amino acids and the other in media containing 'light' (^{12}C) amino acids. Using these cultures as sources of interphase and mitotic proteins, MAPs were purified by microtubule co-sedimentation from mixed extracts ('heavy' interphase and 'light' mitotic) and analysed by mass spectrometry to determine their protein ratios. These ratios represent the microtubule affinity of individual MAPs in interphase and mitosis, allowing the identification of those MAPs whose microtubule affinity increases in mitosis. The advantage of using SILAC is that the proteins from both cell populations can be combined and analysed together by microtubule binding

assay and mass spectrometry. This reduces the possibility of experimental variance and enables an accurate comparison of interphase and mitotic MAPs.

Three major aspects of the method were optimised during this study. Firstly, microtubule co-sedimentation in S2 cells was established. For microtubule co-sedimentation in S2 cells the addition of exogenous tubulin is required for microtubule polymerisation. I identified that 7.5µg of exogenous tubulin to 1 x 10^8 cells was the optimal ratio of tubulin to cell number in order to quantitate a significant number of MAPs using mass spectrometry.

Secondly, to identify MAPs which are cell cycle regulated, major post-translational modifications were maintained. Phosphorylation is a key post-translational modification and regulates multiple proteins through the cell cycle and is probably significant in MAP regulation. I therefore identified a combination of phosphatase inhibitors which was compatible with microtubule co-sedimentation and maintained cellular phosphorylation. Using the MPM2 antibody to monitor extract phosphorylation, I identified the combination of 15 mM $NaVO_4$, 10 mM p-nitrophenyl phosphate and 1 µM okadaic acid to be suitable.

Lastly, previous to this study SILAC had not been carried out using S2 cells, I therefore identified suitable SILAC culture conditions for S2 cell growth. Although cell morphology was normal, S2 cell doubling time increased two-fold in dialysed FBS and yeast extract. Mass spectrometry analysis revealed minimal arginine conversion in S2 cells, allowing the use of standard media concentrations (3.4 mM) of arginine.

The use of the optimised protocol identified 4 proteins (KLP61F, laminin A and two uncharacterised proteins CG11120 and CG3902) which showed increased microtubule affinity during mitosis. CG11120 consistently gained a significant ratio which in both experiments lay close to that of KLP61F, a previously characterised cell cycle-regulated MAP. I therefore studied CG11120 more closely, naming it nuclear microtubule associated protein (NuMAP).

The identification of KLP61F confirms that the developed method is effective and appropriate for the identification of mitotic specific MAPs. However, the number of proteins identified to associate with microtubules in mitosis was smaller than expected. In the future, the sensitivity of the screen and hence its application on a larger scale may be improved by the measures discussed in chapter 3 in order to further dissect and identify the molecular mechanism of spindle formation in mitosis.

The design of the method also allows for its application to a large range of microtubule processes other than its use in this present study. Although microtubule reorganisation from interphase to mitosis is crucial, other changes in microtubule organisation occur during the cell cycle and development. This described method could therefore be utilised as a tool for the rapid identification of MAPs regulating these other transitions in future studies.

The method described here can be broken down into individual, specific tools which can be used separately. Importantly, I have developed the use of SILAC in S2 cells, a strategy which makes it possible to monitor quantitative differences at the protein level between different cell conditions. Although the *Drosophila melanogaster* genome is among the best annotated, proteomic studies in *Drosophila*

are uncommon, with quantitative proteomics being very few. In parallel to this study, was demonstrated that SILAC in *Drosophila* cells in combination with RNAi can be used to study gene function at the protein level (Bonaldi et al., 2008). On the other hand, I have demonstrated that using SILAC in S2 cells can identify genes involved in specific cellular processes. Therefore the developed tool when applied to future studies can give greater insight and understanding into the cellular mechanisms of *Drosophila* in top down and bottom up approaches.

5.3 NuMAP: A new mitotic-specific MAP

5.3.1 Localisation of NuMAP

I next characterised the localisation of the identified protein NuMAP. In S2 cells and early embryonic divisions, GFP-tagged NuMAP localised to the nucleus during interphase and to microtubules only during mitosis, confirming NuMAP to be a cell cycle regulated MAP. The localisation to the spindle was confirmed for endogenous NuMAP by immunostaining with anti-NuMAP peptide antibodies coupled with RNAi. Live imaging analysis in the syncytial embryo shows that NuMAP localises to duplicated centrosomes during prophase and as the mitotic spindle is formed, localises uniformly to the length of spindle microtubules. NuMAP protein remains localised to spindle microtubules through anaphase and into telophase where it appears to localise to discrete regions of the central spindle.

Due to the distinctive cell cycle localisation of NuMAP, I identified its localisation domains and investigated the ability of NuMAP to associate with interphase microtubules. Truncation analysis of NuMAP protein revealed that it

contains two domains that are sufficient but not essential for nuclear localisation and one C-terminal domain which is essential for microtubule association. To overcome nuclear localisation of NuMAP during interphase and study its microtubule binding activity during interphase, I generated NuMAP protein fused to a nuclear export signal (NES). Though nuclear localisation remained predominant, an increased cytoplasmic pool of NuMAP was generated. This cytoplasmic pool of NuMAP fused NES protein did not associate with interphase microtubules, indicating that the interphase form of NuMAP has low affinity for microtubules. In contrast, expression of the microtubule binding domain alone fused with an NES showed association with interphase microtubules. Interestingly, microtubules were bundled and showed a circular interphase microtubule array. This indicated that the microtubule binding domain of NuMAP alone has high affinity for microtubules even in interphase and that the cell cycle regulation of NuMAP is mediated by another region of the protein. The nuclear localisation and regulation of the microtubule binding ability of NuMAP is therefore critical to prevent the bundling of interphase microtubules.

The characterisation of NuMAP localisation and its regulation was carried out in S2 cells. S2 cells are a non-clonal population which were originally derived from the *Drosophila* embryo and have been adapted for growth in suspension. As a model system, cells are diverse and the cell population is not homogeneous. Therefore work in this model system must take this into consideration and quantitative analysis of phenotypes is essential. During transfection cells can take up single copies of the plasmid construct resulting in average levels of over-expression. In contrast however, cells in the same transfected population can take up multiple copies of the plasmid. This results in high levels of over-expression which may

affect protein localisation. Therefore due to the variation in expression in S2 cells, the protein localisation of NuMAP constructs were counted and categorised. However, this was done by eye and therefore human error and opinion will have an effect on the results. On drawing conclusion on NuMAP function and regulation this must be taken into consideration.

5.3.2 NuMAP function

To study the function of NuMAP, I used two approaches; the depletion of NuMAP in cultured cells and its deletion in developing flies. The use of RNAi to deplete NuMAP protein in S2 cells resulted in an increase in the number of bipolar spindles with only one aster compared to control RNAi cells. The lack of an aster at a spindle pole generally occurs due to the lack of centrosome duplication/separation during S phase. This therefore suggests that NuMAP may somehow play a role in centrosome duplication. However, this is not consistent with NuMAP localisation and therefore may not represent the primary function of NuMAP. In parallel, the deletion of the NuMAP gene in flies, generated by P-element excision, indicated that NuMAP is not essential for fly viability. However, preliminary results show that homozygotes of the NuMAP deletion mutant have reduced viability. Also, only two of the many embryos laid by seven homozygote females developed to third instar larva but no further, suggesting the mutant to be female sterile. Further analysis is needed to test whether these phenotypes are due to the deletion of NuMAP, as the extent of the deletion is yet to be determined.

5.4 Future directions

The work summarised here advances our understanding of microtubule regulation through the cell cycle, proving my hypothesis that a group of MAPs associate with microtubules specifically during mitosis to be correct. This study identified a new MAP which associates with microtubules specifically during mitosis, I named this protein NuMAP. Although NuMAP has been shown to co-localise with microtubules, all microtubule association of NuMAP has been demonstrated in cell extract. Therefore an *in vitro* microtubule binding assay is needed to distinguish if the association of NuMAP with microtubules is direct or if its association is dependent on a binding partner. To determine this, I will incubate bacterially produced NuMAP protein with microtubules and then sediment the microtubules by centrifugation. If NuMAP directly interacts with the microtubules, it will co-sediment and be present in the microtubule pellet.

Although NuMAP localisation and microtubule binding domains have been identified, little is known about its function. To investigate the function of NuMAP in the developing fly, I will first examine the expression pattern of NuMAP during development by western blot. Through development, proteins are often expressed at their time of function, therefore examination of their expression profile during development can suggest their role in development. Due to the method used for the discovery of NuMAP, I propose that it plays a role in spindle formation and it would therefore be interesting to know if the expression of NuMAP is specific to developmental stages of increased cell division, such as the early embryo.

To understand the function of NuMAP in *Drosophila* development further, it is invaluable to analyse the NuMAP deletion mutant generated in this study. Firstly I would like to define the region of genomic sequence removed during P-element excision. Further analysis is therefore required to test whether phenotypes observed are due to the deletion of the NuMAP gene. To achieve this, the NuMAP-GFP fly strain generated in this study can be used in rescue experiments to assess if expression of NuMAP protein can rescue the phenotypes observed. Preliminary studies of the NuMAP deletion mutant have suggested that the removal of the NuMAP gene affects early development. As NuMAP localises to the mitotic and meiotic spindle microtubules, it will therefore also be interesting to examine spindle microtubule organisation and function in mitosis and meiosis in the NuMAP deletion mutant.

During truncation analysis of NuMAP protein, I observed that NuMAP-GFP over-expression appeared to induce microtubule bundling, suggesting that NuMAP functions to bundle microtubules. NuMAP shows homology to the human protein NuSAP which when over-expressed has been shown to bundle and stabilise microtubules making them resistant to colchicine treatment. Therefore I will treat cells over-expressing NuMAP with colchicine to determine if NuMAP is also capable of stabilising these microtubule bundles, as does NuSAP. This would also help to determine if NuMAP is a potential homologue of the human NuSAP protein.

MAPs play an essential role in the regulation and formation of the mitotic spindle and it is likely that they themselves are under tight regulation. However regulation of MAPs is poorly understood. Biochemical and cytological studies show that NuMAP has a mechanism present during interphase which prevents its

association with microtubules. Phosphorylation is a key cellular post-translational modification used to regulate proteins through the cell cycle and thus it is most likely to also regulate MAPs. In this study, phosphorylation was maintained during MAP purification and this supports the possibility that the regulation of NuMAP may be through phosphorylation. NuMAP has been identified to be phosphorylated in a previous phosphoproteome screen. Systematic mutation of potential phosphorylation sites to alanine, an unphosphorylatable amino acid, may identify key residues in the regulation of the microtubule binding activity of NuMAP. As cell phosphorylation levels increase in mitosis, I expect phosphorylation to enhance the association of NuMAP with microtubules. Therefore I expect an unphosphorylatable mutant of key phosphorylation sites to show mis-localisation in mitosis.

In parallel to systematic mutagenesis, I will use the SILAC tool developed here to identify the changes in the phosphorylation of NuMAP through the cell cycle. Two populations of cells will be cultured, one in 'heavy' media and one in 'light' media. Again these cultures will be used as sources of interphase and mitotic proteins. NuMAP will be purified from mixed extracts and analysed by mass spectrometry to determine phosphorylation ratios. The advantage of using SILAC is that it will identify those modifications which change through the cell cycle and not those which are constitutively phosphorylated. This will provide potential sites which will be subsequently mutated to identify their roles in the localisation and function of NuMAP.

If phosphorylation is shown to regulate NuMAP, it will next be important to identify the kinase responsible. At this point, key phosphorylation sites will be

known and therefore the sequence surrounding the site can be compared to known kinase consensus sequences.

Lastly, the organisation and function of the microtubule network is regulated by the co-ordination of multiple MAPs. The identification of NuMAP interacting proteins and how they function together to regulate microtubule behaviour will indicate the mechanism in which NuMAP functions. I therefore will use immuno-precipitation with mass spectrometry to identify NuMAP-interacting proteins. The mapping of these interactions through truncation analysis or cross linking followed by mass spectrometry will enable me to define the role of the interaction in NuMAP function.

Appendix

During the development of the method for identification of MAPs which associate with microtubules specifically during mitosis, three other side projects arose which resulted in potentially interesting data. In this appendix I will briefly describe these projects.

A.1 Identification of microtubule associated proteins from embryonic extract

Microtubule co-sedimentation using *Drosophila* embryonic extract is a common and effective method for the isolation of MAPs (Kellogg et al., 1989). Before I established microtubule co-sedimentation in Schneider 2 (S2) cells I tested a previous method used by Kellogg et al (1989) using embryonic extract.

Embryonic tissue (0-4hrs) from w^{1118} flies was homogenised from frozen using a Dounce homogeniser using identical buffers as described for S2 cell co-sedimentation. The homogenised product was cleared of debris by centrifugation at 20 krpm for 10 minutes at 4 °C in a Beckman Avanti J-25 with JA-25.50 rotor. The pellet was discarded and centrifugation repeated at 20 krpm. The extract was then centrifuged repeatedly at 55 krpm (100 000g) for 10 min until there was negligible pellet remaining. Latrunculin A and B were added to 2 µg/ml, DTT to 0.1 mM and GTP to 1 mM. The extract was then split into two halves, the control and the sample. Embryonic extract has high tubulin content and enables the polymerisation

of endogenous tubulin in the presence of taxol. To the sample, taxol was added stepwise to achieve a final concentration of 20 μM in order to polymerise microtubules. To the control, colchicine was added to achieve a final concentration of 10 μg/ml. Both the sample and control were then incubated at room temperature for 1 hour. The incubation time allowed for proteins from the extract to bind microtubules. The microtubules were then pelleted through a sucrose cushion twice, bringing with them any associated proteins.

Protein pellets from the sample and control were analysed by SDS-PAGE and coomassie blue staining (Figure A1a). Coomassie blue staining showed a number of proteins in sample pellet. In contrast, the control pellet contained less protein. This indicated that those proteins in the sample pellet were most likely to be microtubule binding proteins and were analysed by mass spectrometry. An SDS-PAGE of the microtubule pellet was cut into two and trypsin digestion was carried out. Both sections were cleaned using a C18 stage tip and run on an LC MS/MS Orbitrap. The data was processed using DTAsupercharge and Mascot software. In total 137 proteins were identified from this process.

To assess the purity of the sample, I compared those proteins identified with a previous microtubule mass spectrometry based screen by Hughes *et al* (2008). Hughes *et al* (2008) considered proteins significant if they scored above 30. Therefore I too only considered those proteins with scores above 30. Of those proteins identified in this present study, 32 % were also identified by Hughes *et al* (2008). Interestingly, 46.5% of those proteins not identified by Hughes *et al* (2008) were only recognized by 1 peptide. This suggests that the mass spectrometry

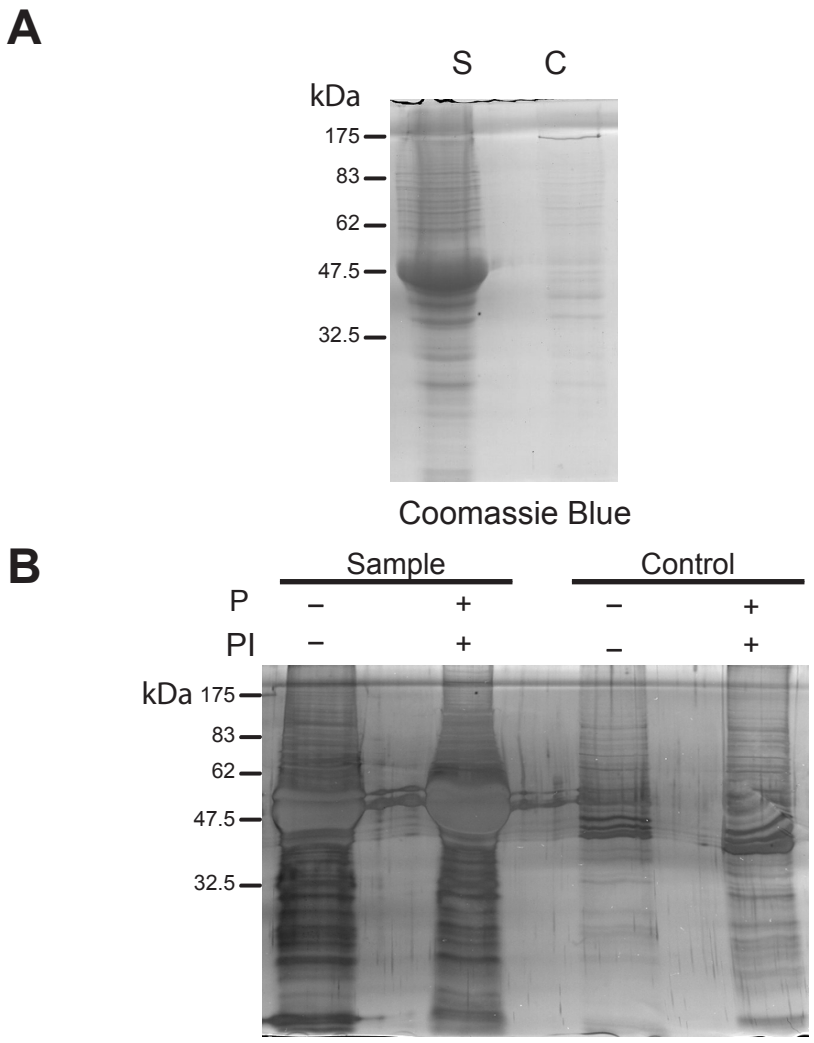

Figure A1 Microtubule co-sedimentation in Drosophila embryonic extract. (A) Coomassie blue staining analysis of microtubule co-sedimentation in embryonic extract. The sample (S) pellet shows significant protein and control (C) minimal protein. **(B)** Silver stain analysis of sample and control protein pellets from microtubule co-sedimentation in the presence and absence of phosphorylation (P). The control pellet,which contained no microtubules, contains minimal protein, indicating those proteins present in sample pellet specifically associate with microtubules.

analysis of my sample was in depth and identified proteins present at low levels different from those identified by Hughes *et al*.

In summary, the microtubule co-sedimentation method tested here is effective for the isolation of MAPs and the mass spectrometry method used is thorough and a suitable tool for the identification of MAPs.

A.2 Identification of MAPs whose microtubule binding is regulated through phosphorylation

To identify MAPs that are cell cycle regulated, major post-translational modifications need to be maintained. Phosphorylation is an abundant reversible post-translational modification that has been shown to affect protein stability, localisation and protein-protein interactions (Pinkse et al., 2004). This tightly controlled modification is recognised to play an essential role in a number of cellular processes such as signal transduction, metabolic maintenance and most importantly the cell cycle (Reinders and Sickmann, 2005). Therefore it is likely that phosphorylation plays a role in regulating MAPs and should be maintained during MAP purification. I therefore identified a combination of phosphatase inhibitors which was compatible with microtubule co-sedimentation and maintained cellular phosphorylation. Using MPM2 antibody to monitor extract phosphorylation, I identified the combination of 15 mM $NaVO_4$, 10 mM p-nitrophenyl phosphate and 1 µM okadaic acid to be suitable.

Although this protocol was developed to specifically identify MAPs which are cell cycle regulated, it also enabled the identification of any MAPs whose

microtubule association is affected by phosphorylation. Therefore as a secondary project I aimed to identify those MAPs regulated by phosphorylation. To achieve this aim I carried out microtubule co-sedimentation in *Drosophila* embryonic extract in both the presence and absence of phosphorylation.

Previously I had noticed that phosphatase inhibitors chemically decrease the association of MAPs with microtubules. This would influence the identification of MAPs regulated by phosphorylation and may result in false positives. To ensure that there was no chemical effect of phosphatase inhibitors, other than the maintenance of phosphorylation, embryonic extract was prepared in the absence of phosphatase inhibitors. This allowed for phosphorylation to be removed by active endogenous phosphatases. Phosphatase inhibitors were then added and co-sedimentation was carried out. In parallel, co-sedimentation was carried out with the addition of phosphatase inhibitors during extract preparation thus maintaining phosphorylation. The two sets of identified MAPs, those purified in the presence of phosphorylation and those purified in the absence of phosphorylation, could then be fairly compared.

Microtubule pellets obtained in the presence and absence of phosphorylation were analysed by silver stain (Figure A1b). Silver staining showed that both pellets contained a similar number of proteins. To identify specific changes in protein profiles between co-sedimentation with and without phosphorylation, LC MS/MS analysis was carried out on microtubule pellets. In total 329 proteins were identified in the microtubule pellet obtained in the absence of phosphorylation and 274 proteins were identified in the microtubule pellet obtained in the presence of phosphorylation. To identify those MAPs whose microtubule association is effected by phosphorylation, I compared the protein profiles of the microtubule pellets. This

comparison showed that 109 proteins were purified only in the absence of phosphorylation and 55 proteins purified only in the presence of phosphorylation.

To confirm that those proteins identified to be affected by phosphorylation, I decided to repeat the experiment and microtubule co-sedimentation was performed as previously described. In total, 420 proteins were identified in the microtubule pellet obtained in the absence of phosphorylation and 390 proteins were identified in the microtubule pellet obtained in the presence of phosphorylation. 103 proteins were purified only in the absence of phosphorylation and 71 proteins were only purified only in the presence of phosphorylation. The two experiments were compared in order to identify those MAPs whose microtubules binding is affected by phosphorylation. 23 proteins were identified to associate with microtubules only in the absence of phosphorylation, suggesting that phosphorylation inhibits their association with microtubules. Only 10 proteins were identified to associate with microtubules only in the presence of phosphorylation, suggesting that phosphorylation enhances their association with microtubules (Table A1).

Using microtubule co-sedimentation I have identified MAPs whose microtubule association is potentially regulated by phosphorylation. However, the purification and analysis of samples was done separately. No single mass spectrometry analysis results in full sample coverage and variance between the qualities of mass spectrum can be large. Therefore comparison of MAPs purified in the presence and absence of phosphorylation is not conclusive evidence that phosphorylation effects their microtubule association. This method of identification could be improved by the use of post-purification labelling mechanism such as

Table A1 Proteins whose microtubule binding is regulated by phosphorylation.

CG Number	Synonym	Number of peptides		Protein score	
		Exp 1	Exp 2		
CG9042	Glycerol 3 phosphate dehydrogenase	5	3	258	111
CG14792	Stubarista	4	4	177	180
CG16817		4	3	148	157
CG5266	Proteasome 25kD subunit	2	2	115	110
CG5784	Mapmodulin	3	1	111	38
CG5289	Proteasome 26S subunit subunit 4 ATPase	2	1	100	96
CG7003	Msh6	3	2	98	67
CG10480	Bj1 protein	1	3	89	133
CG6339	Rad50	1	2	84	102
CG16935		2	3	80	177
CG7414		1	2	76	93
CG2945	Cinnamon	2	3	74	91
CG6625	Soluble NSF attachment protein	1	1	74	77
CG3917	Gamma-tubulin ring protein 84	1	3	69	164
CG3820	Nucleoporin 214	1	1	64	28
CG32858	Singed	1	2	58	83
CG1799	Raspberry	1	6	40	356
CG33106	Multiple ankyrin repeats single KH domain	1	2	36	123
CG11654	Adenosylhomocysteinase at 13	1	5	34	228
CG6535	Telomere fusion	1	1	28	26
CG8491	Kohtalo	1	1	28	31
CG5581	Otefin	1	2	27	100
CG4063	Ebi	1	1	25	42

isostope-coded affinity tags (ICAT) and iTRAQ chemical labelling to enable the analysis of combined samples.

A.3 Optimisation of phosphopeptide enrichment for the identification of phosphorylation sites on MAPs

It is thought that approximately 30 % of mammalian cell content is at one point in its life span phosphorylated. Therefore, great effort has been focused on the development of suitable methods for the identification and characterisation of phosphorylated proteins (McLachlin and Chait, 2001). Mass spectrometry has become one of the most widely used and powerful techniques for proteome-wide experiments and therefore the use of mass spectrometry in the identification of phosphorylation sites would be of great value.

However, there are still limitations to mass spectrometry-based methods in the analysis of phosphorylation. Firstly, no single mass spectrometry approach results in 100 % coverage and consequently regions of interest may be missed. Secondly, the addition of a phosphate group affects both proteolytic cleavage and the ionisation of the protein/peptide and therefore the mass spectrometry signal for phosphopeptides is reduced (Kuroda et al., 2004; Larsen et al., 2005; McLachlin and Chait, 2001). Lastly and probably the most substantial limitation is the presence of non-phosphorylated peptides. Phosphorylation is often sub-stoichiometric, giving a low abundance of phosphopeptides for analysis. This results in the mass spectrometry signal for phosphopeptides being suppressed by the presence of non-phosphopeptides. It is therefore advantageous to enrich phosphopeptides, reducing

the complexity of the mixture and therefore suppression of the phosphopeptide signal.

A variety of methods have been developed to enhance the phosphopeptide sample for mass spectrometry. The more widely applied strategies have been chemical tagging, immobilised metal affinity chromatography (IMAC) and metal oxide chromatography (MOC) (Sugiyama et al., 2007). In recent years titanium dioxide (TiO_2) has been demonstrated to be an effective reagent in the MOC method for phosphopeptide enrichment by the analysis of *B.subtilis* and *E.coli* phosphoproteomes (Macek et al., 2008; Macek et al., 2007).

Larsen et al (2005) showed that the inclusion of 2, 5 dihydroxybenzoic acid (DHB) during phosphopeptide enrichment using TiO_2 was effective at removing acidic non-phosphopeptides. However DHB is not compatible with LC-MS/MS analysis as it interferes with peptide detection and affects the LC MS/MS system (Larsen et al., 2005). During this study, Sugiyama et al (2007) developed a new approach for phosphopeptide enrichment using TiO_2 using aliphatic hydroxyl acids such as lactic acid (Sugiyama et al., 2007). However, I further wanted to develop the method for use with S2 cells specifically.

I needed to optimise the concentration of lactic acid used during phosphopeptide enrichment. To achieve this, I performed phosphopeptide enrichment using peptide mixtures from in-solution digested cycling S2 cell extract using different concentrations of lactic acid. TiO_2 beads were incubated in peptide mixtures and bound peptides eluted. Each digestion was incubated sequentially with three batches of beads. To observe the enrichment of phosphopeptides the

percentage of phosphopeptides identified by mass spectrometry after enrichment was calculated (Number of phosphopeptides/Total number of peptides X 100).

Analysis of S2 cell extract without phosphopeptides results in 0-0.04 % of observed peptides being phosphorylated. The number of phosphopeptides and non-phosphopeptides was plotted against the concentration of lactic acid used (Figure A2). The number of non-phosphopeptides decreases continuously as the concentration of lactic acid is increased. However, the proportion of identified phosphopeptides remained approximately 30 % and rapidly decreased as the concentration of lactic acid was increased to 100 mg/ml. I therefore determined the optimum concentration of lactic acid to be 85 mg/ml.

Using this optimum concentration of 85 mg/ml lactic acid, phosphopeptide enrichment was carried out on in-gel digested Mad3 protein phosphorylated *in vitro* using Mph1 kinase. These samples were provided by Judith Zich from the Hardwick Lab. 14 of the 19 unique peptides identified from Mad3 and Mph1were phosphopeptides. Without phosphopeptide enrichment 68 unique peptides were identified with only being 5 phosphopeptides.

In summary, I have identified a lactic acid concentration of 85 mg/ml to be effective in phosphopeptide enrichment from in-solution and in-gel digested proteins. However, the method needs further testing for its use on the identification of MAP phosphorylation from microtubule co-sedimentation samples.

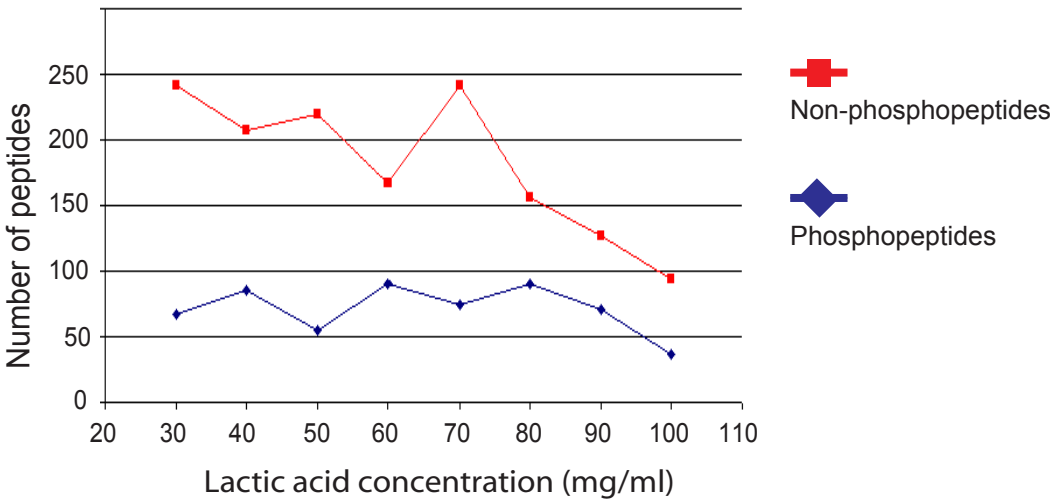

Figure A2. Number of non-phospho and phosphopeptides observed with the use of varying lactic acid concentrations. An increase in the lactic acid concentration used during phosphopeptide enrichment decreases the number of non-phosphopeptides observed. However the number of phosphopeptides also decreases when the concentration of lactic acid reaches 80-90 mg/ml. This indicates the optimum concentration of lactic acid is 85 mg/ml.

A.4 Supplementary tables

Table A2

Table A2 shows proteins from the first relative quantification of MAPs purified from interphase and mitosis extracts. The table lists the 270 proteins quantified in ascending order of 'heavy'/ 'light' ratio. Those proteins in red make it through the more stringent cut off (0.2) and those in blue make it through the less stringent cut off (0.55).

Table A3

Table A3 shows proteins from the second relative quantification of MAPs purified from interphase and mitosis extracts. The table lists the 156 proteins quantified in ascending order of 'heavy'/ 'light' ratio. Those proteins in red make it through the more stringent cut off (0.2) and those in blue make it through the less stringent cut off (0.73).

Table A2 Quantified proteins from the first relative quantification of MAPs from interphase and mitosis.

CG Number	Synonym	Number of peptides	Ratio 'Heavy'/ 'Light'
CG2093	Vacuolar protein sorting 13	1	0.002979
CG9359	β-Tubulin at 85D	16	0.025272
CG9476	α-Tubulin at 85E	13	0.026871
CG3401	β-Tubulin at 60D	13	0.033196
CG10390	Meiosis I arrest	1	0.036992
CG31315		1	0.038591
CG2512	α-Tubulin at 84D	19	0.057841
CG3836	Stonewall	2	0.065102
CG9277	β-Tubulin at 56D	24	0.080957
	Porcine Trypsin	8	0.10706
	Bovine Albumin	14	0.18835
CG9191	Kinesin-like protein at 61F	8	0.1886
CG11120		6	0.19275
CG4869	β-Tubulin at 97EF	12	0.1949
CG4001	Phosphofructokinase	3	0.19811
CG13345	Tumbleweed	2	0.27969
CG10641		4	0.34193
CG1258	Pavarotti	18	0.34382
CG12065		2	0.37367
CG11207	Fascetto	6	0.37713
CG10691	Lethal (2) 37Cc	1	0.41397
CG9193	Mutagen-sensitive 209	2	0.42167
CG10160	Ecdysone-inducible gene L3	2	0.45315
CG1977	α Spectrin	13	0.4625

CG Number	Synonym	Number of peptides	Ratio 'Heavy'/ 'Light'
CG1681		3	0.48269
CG3902		6	0.48675
CG5099	Musashi	2	0.49585
CG7831	Non-claret disjunctional	13	0.50489
CG18076	Short stop	31	0.50812
CG10236	Laminin A	1	0.52101
CG2238	Elongation factor 2b	10	0.52976
CG12165	Inner centromere protein	5	0.53705
CG3415		2	0.53766
CG6647	Porin	7	0.54296
CG1782	Ubiquitin activating enzyme 1	7	0.54343
CG2982		4	0.55765
CG5787		2	0.55797
CG9633	Replication Protein A 70	3	0.60835
CG6756	Translocase of outer membrane 70	2	0.60921
CG9412	Rasputin	2	0.61069
CG14804	Vacuolar protein sorting 26	3	0.61441
CG13387	Embargoed	5	0.62005
CG12030		7	0.63089
CG7438	Myosin 31DF	5	0.6322
CG1616	Disc proliferation abnormal	6	0.63388
CG8893	Glyceraldehyde 3 phosphate dehydrogenase 2	6	0.636
CG12141	Lysyl-tRNA synthetase	3	0.63801
CG9916	Cyclophilin 1	4	0.65189
CG31716		4	0.65291
CG10045	Glutathione S transferase D1	2	0.65698

CG Number	Synonym	Number of peptides	Ratio 'Heavy'/ 'Light'
CG12233	Lethal (1) G0156	4	0.65769
CG10565		3	0.65895
CG10701	Moesin	5	0.66012
CG7008	Tudor-SN	9	0.66286
CG5119	PolyA-binding protein	4	0.67501
CG5108	Mitochondrial ribosomal protein S7	4	0.67572
CG5353	Threonyl-tRNA synthetase	16	0.67811
CG10523	Parkin	1	0.68438
CG4800	Translationally controlled tumor protein	4	0.68553
CG2064		2	0.68556
CG9075	Eukaryotic initiation factor 4a	3	0.68593
CG1591	REG	2	0.68734
CG10161	Eukaryotic initiation factor 3 p66 subunit	3	0.68758
CG1009	Puromycin sensitive aminopeptidase	7	0.69725
CG6944	Lamin	3	0.6973
CG1458		1	0.69846
CG7010	Lethal (1) G0334	2	0.70089
CG10279	Rm62	3	0.70371
CG5784	Mapmodulin	2	0.7056
CG2331	TER94	12	0.70784
CG5730	Annexin IX	5	0.71414
CG8036		5	0.73023
CG12306	Polo	2	0.73051
CG8402	Protein phosphatase D3	2	0.73193
CG31363	Jupiter	2	0.73453

CG Number	Synonym	Number of peptides	Ratio 'Heavy'/ 'Light'
CG14996	Chd64	4	0.73527
CG8947	26-29kD-proteinase	4	0.7373
CG4265	Ubiquitin carboxy-terminal hydrolase	3	0.74103
CG10223	Topoisomerase 2	8	0.74178
CG17064	Mars	3	0.75036
CG3937	Cheerio	28	0.75535
CG1548	CathD	4	0.76086
CG13281	CAS/CSE1 segregation protein	2	0.76208
CG3523		5	0.7637
CG14648	Growl	2	0.76491
CG18572	Rudimentary	5	0.76611
CG11949	Coracle	4	0.76649
CG7461		6	0.76927
CG12163		2	0.77329
CG4027	Actin 5C	9	0.77358
CG15112	Enabled	2	0.78047
CG4747		3	0.78239
CG7113	Scully	3	0.78242
CG16901	Squid	3	0.78389
CG1721	Phosphoglyceromutase	4	0.79004
CG8280	Elongation factor 1α48D	8	0.79892
CG3696	Kismet	2	0.8057
CG4600	Yippee interacting protein 2	4	0.81364
CG1065	Succinyl coenzyme A synthetase α subunit	7	0.82218
CG4466	Heat shock protein 27	2	0.82403
CG8258		8	0.83073

CG Number	Synonym	Number of peptides	Ratio 'Heavy'/ 'Light'
CG1345	Glutamine:fructose-6-phosphate aminotransferase 2	4	0.83285
CG4389		6	0.83359
CG6084		3	0.83485
CG3821	Aspartyl-tRNA synthetase	7	0.83491
CG2171	Triose phosphate isomerase	3	0.83808
CG10363	Thiolester containing protein IV	5	0.84241
CG5170	Dodeca-satellite-binding protein 1	3	0.8431
CG7762	Rpn1	2	0.8446
CG17530	Glutathione S transferase E6	2	0.85603
CG9862	Rae1	2	0.85754
CG6370		2	0.85954
CG2720	Hsp70/Hsp90 organizing protein homolog	5	0.86559
CG14813	δ-coatomer protein	2	0.86651
CG8977	Cctγ	6	0.86652
CG6692	Cysteine proteinase-1	2	0.87049
CG4254	Twinstar	7	0.87323
CG5374	Tcp1-like	3	0.87446
CG12792	Lethal (2) 09851	2	0.87536
CG10333		2	0.87666
CG17259		8	0.88321
CG7144	Lysine ketoglutarate reductase	2	0.88461
CG4082	Minichromosome maintenance 5	2	0.88761
CG3299	Vinculin	6	0.88848
CG8231	T-cp1ζ	10	0.8916
CG1828	Dre4	3	0.91213

CG Number	Synonym	Number of peptides	Ratio 'Heavy'/ 'Light'
CG2248	Rac1	2	0.91715
CG13096		3	0.92144
CG7765	Kinesin heavy chain	12	0.92347
CG8715	Lingerer	5	0.92883
CG6699	B'-coatomer protein	4	0.92956
CG8798		2	0.93269
CG3895	Polyhomeotic distal	2	0.93466
CG1633	Thioredoxin peroxidase 1	5	0.93745
CG15100		7	0.94045
CG10067	Actin 57B	6	0.94097
CG2207	Decondensation factor 31	1	0.94493
CG3725	Calcium ATPase at 60A	5	0.94501
CG7070	Pyruvate kinase	4	0.94672
CG17654	Enolase	3	0.9509
CG5525		2	0.95736
CG5642		2	0.95745
CG6543		2	0.96031
CG1242	Heat shock protein 83	8	0.9624
CG1483	Microtubule-associated protein 205	18	0.96364
CG30122		4	0.96728
CG11963	SkpA associated protein	2	0.97514
CG34417		5	0.97648
CG3762	Vha68-2	3	0.98489
CG13388	A kinase anchor protein 200	3	0.98533
CG4634	Nucleosome remodeling factor - 38kD	2	0.98822
CG11901	Ef1γ	4	0.99033

CG Number	Synonym	Number of peptides	Ratio 'Heavy'/ 'Light'
CG11471	Isoleucyl-tRNA synthetase	9	0.99095
CG6341	Elongation factor 1 β	5	0.99261
CG10600		3	0.99448
CG10840	eIF5B	2	0.99801
CG2050	Modulo	4	0.99932
CG7033		3	0.99945
CG1250	Sec23	2	0.99958
CG17246	Succinate dehydrogenase A	2	1.0023
CG1554	RNA polymerase II 215kD subunit	3	1.0064
CG7261		3	1.0065
CG9579	Annexin X	4	1.0076
CG33130	Short spindle 4	5	1.0081
CG6143	Protein on ecdysone puffs	10	1.0138
CG4276	Arouser	3	1.0161
CG12013	PHGPx	3	1.0311
CG6964	Grunge	2	1.0313
CG8472	Calmodulin	1	1.0388
CG33123		5	1.0393
CG8351	Tcp-1η	7	1.0429
CG3107		3	1.0434
CG8996	Walrus	7	1.0447
CG3186	eIF-5A	6	1.0462
CG10302	Bicoid stability factor	6	1.0511
CG6995		2	1.0531
CG4598		3	1.0561
CG4561	Tyrosyl-tRNA synthetase	3	1.0579

CG Number	Synonym	Number of peptides	Ratio 'Heavy'/ 'Light'
CG4264	Heat shock protein cognate 4	12	1.058
CG4494	Smt3	2	1.0609
CG7823	RhoGDI	1	1.0636
CG11143	Inos	4	1.0686
CG5394	Glutamyl-prolyl-tRNA synthetase	22	1.0688
CG1404	Ran	4	1.0817
CG17255	No circadian temperature entrainment	3	1.0933
CG12819	Slender lobes	6	1.0941
CG1101	Aly	4	1.0993
CG4147	Heat shock protein cognate 3	15	1.1043
CG11027	ADP ribosylation factor 102F	1	1.1066
CG8439	T-complex Chaperonin 5	3	1.1177
CG5094	Small glutamine-rich tetratricopeptide containing protein	3	1.1383
CG9302		5	1.1401
CG13391	Alanyl-tRNA synthetase	9	1.1405
CG7834		3	1.1419
CG5728		3	1.1467
CG2168	Ribosomal protein S3A	5	1.1512
CG5355		8	1.1584
CG7415	Dipeptidyl aminopeptidase III	4	1.1603
CG5771	Rab-protein 11	3	1.1645
CG7752	Putzig	2	1.1652
CG31196	14-3-3ε	11	1.1683
CG6226	FK506-binding protein 1	2	1.1692
CG17870	14-3-3ζ	5	1.1711
CG8732	Acyl-CoA synthetase long-chain	5	1.1758

CG Number	Synonym	Number of peptides	Ratio 'Heavy'/ 'Light'
CG8415	Ribosomal protein S23	2	1.1842
CG7360	Nucleoporin 58	2	1.1851
CG15792	Zipper	17	1.2075
CG13849	Nop56	4	1.2152
CG8542	Heat shock protein cognate 5	12	1.2219
CG17611	eIF6	2	1.2255
CG6871	Catalase	3	1.226
CG6058	Aldolase	8	1.2299
CG2852		5	1.2564
CG5874	NELF-A	3	1.2656
CG32031	Arginine kinase	6	1.2762
CG18495	Proteasome α1 subunit	2	1.2969
CG7145		2	1.3072
CG10206	Nop5	9	1.3138
CG3644	Bicaudal	2	1.3192
CG4062	Valyl-tRNA synthetase	4	1.3295
CG11276	Ribosomal protein S4	6	1.3604
CG7421	Nopp140	2	1.3641
CG9888	Fibrillarin	6	1.3721
CG6988	Protein disulfide isomerase	9	1.3754
CG6453		3	1.396
CG7581	Bub3	3	1.4001
CG8322	ATP citrate lyase	4	1.4005
CG3152	Trap1	4	1.4269
CG8983	ERp60	14	1.4297
CG3333	Nucleolar protein at 60B	2	1.4377

CG Number	Synonym	Number of peptides	Ratio 'Heavy'/ 'Light'
CG4900	Iron regulatory protein 1A	2	1.4489
CG10315	eIF2B-δ	2	1.4807
CG2210	Abnormal wing discs	2	1.4815
CG4164		3	1.4833
CG6603	Hsc70Cb	5	1.4963
CG3001	Hexokinase A	2	1.517
CG5174		3	1.5394
CG4038		2	1.5828
CG14066	La related protein	2	1.6217
CG6459		2	1.6308
CG10122	RNA polymerase I subunit	2	1.6384
CG2918		6	1.6562
CG7998		2	1.6685
CG1883	Ribosomal protein S7	3	1.6983
CG7917	Nucleoplasmin	5	1.7222
CG5520	Glycoprotein 93	6	1.7404
CG5258	NHP2	1	1.7813
CG12101	Heat shock protein 60	8	1.7908
CG6684	Ribosomal protein S25	2	1.8463
CG4233	Glutamate oxaloacetate transaminase 2	1	1.9097
CG32549		2	1.9174
CG33129		1	1.9368
CG5809	CaBP1	2	1.9371
CG6850	UDP-glucose-glycoprotein glucosyltransferase	5	2.0494
CG12918		2	2.0562

CG Number	Synonym	Number of peptides	Ratio 'Heavy'/ 'Light'
CG14998	Ensconsin	9	2.0782
CG17489	Ribosomal protein L5	2	2.0953
CG9342	Microsomal triacylglycerol transfer protein	1	2.1017
CG5020	Cytoplasmic linker protein 190	37	2.1905
CG1112	α-Esterase-7	2	2.1922
CG10687	Asparaginyl-tRNA synthetase	4	2.1981
CG6287		4	2.2609
CG4464	Ribosomal protein S19a	2	2.387
CG4143	multiprotein bridging factor 1	1	2.4496
CG7013	Mesencephalic astrocyte-derived neurotrophic factor	2	2.4551
CG1516		4	2.58
CG9244	Aconitase	5	2.9101
CG4460	Heat shock protein 22	2	3.2741
CG4463	Heat shock protein 23	2	3.3766
CG4183	Heat shock protein 26	2	3.8974

Table A3 Quantified proteins from the second relative quantification of MAPs from interphase and mitosis.

CG Number	Synonym	Number of peptides	Ratio "Heavy"/"Light"
CG9476	α-Tubulin at 85E	10	0.007349
CG3401	β-Tubulin at 60D	11	0.011363
CG9359	β-Tubulin at 85D	14	0.014124
	Porcine Trypsin	6	0.022402
CG9277	β-Tubulin at 56D	19	0.036572
CG2512	α-Tubulin at 84D	17	0.054269
CG1399		1	0.064963
CG4869	β-Tubulin at 97EF	10	0.1787
CG9191	Kinesin-like protein at 61F	12	0.24925
CG11120		5	0.30307
CG10849	Sc2	1	0.36331
CG11840	Signal peptide protease	1	0.40762
CG2064		5	0.53082
CG6214		5	0.53321
CG6370		3	0.55058
CG6455		2	0.55654
CG10223	Topoisomerase 2	4	0.55816
CG10236	Laminin A	4	0.56329
CG10630		2	0.57865
CG17064	mars	2	0.59691
CG3902		3	0.61395
CG6030	ATP synthase, subunit d	1	0.63072
CG16944	stress-sensitive B	5	0.64475

CG Number	Synonym	Number of peptides	Ratio "Heavy"/"Light"
CG5020	Cytoplasmic linker protein 190	30	0.65623
CG10882	stenosis	3	0.66675
CG13387	embargoed	4	0.67608
CG1371		4	0.67833
CG3321		1	0.69523
CG11856	Nucleoporin 358	2	0.71339
CG8947	26-29kD-proteinase	1	0.7241
CG8996	walrus	6	0.72644
CG4389		4	0.74697
CG6647	porin	5	0.75254
CG4494	smt3	1	0.75495
CG17856		1	0.7586
CG6699	β'-coatomer protein	2	0.7676
CG12819	slender lobes	7	0.76819
CG1528	γ-coatomer protein	3	0.77387
CG4817	Structure specific recognition protein	2	0.77863
CG8798		5	0.78031
CG15792	zipper	2	0.78047
CG1258	pavarotti	9	0.78087
CG14066	La related protein	3	0.78934
CG10206	nop5	9	0.79366
CG1828	dre4	2	0.79643
CG7752	putzig	4	0.79769
CG5991		2	0.798
CG5366		4	0.80104

CG Number	Synonym	Number of peptides	Ratio "Heavy"/"Light"
CG13345	tumbleweed	3	0.81321
CG11958	Calnexin 99A	6	0.81516
CG8479	optic atrophy 1-like	1	0.81677
CG7834		1	0.81682
CG10811	eukaryotic translation initiation factor 4G	2	0.8203
CG7961	α-coatomer protein	6	0.83729
CG1483	Microtubule-associated protein 205	12	0.84507
CG1059	Karyopherin β 3	2	0.84843
CG7765	Kinesin heavy chain	12	0.85004
CG4169		4	0.85264
CG11471	Isoleucyl-tRNA synthetase	10	0.85432
CG10691	lethal (2) 37Cc	2	0.8558
CG33129		7	0.85632
CG13281	CAS/CSE1 segregation protein	4	0.85654
CG12165	Inner centromere protein	2	0.85674
CG5099	musashi	2	0.8571
CG12276	Aos1	2	0.85713
CG6223	β-coatomer protein	3	0.85879
CG6815	belphegor	4	0.86303
CG11624	Ubiquitin-63E	1	0.86467
CG4276	arouser	4	0.86772
CG3937	cheerio	3	0.86792
CG5728		4	0.87119
CG5394	Glutamyl-prolyl-tRNA synthetase	11	0.87227
CG9020	Arginyl-tRNA synthetase	2	0.87778

CG Number	Synonym	Number of peptides	Ratio "Heavy"/"Light"
CG9012	Clathrin heavy chain	3	0.88279
CG7113	scully	2	0.88549
CG3333	Nucleolar protein at 60B	3	0.8894
CG1065	Succinyl coenzyme A synthetase α subunit	4	0.89237
CG1404	ran	4	0.8947
CG9805	eIF3-S10	4	0.8966
CG2098	ferrochelatase	2	0.90307
CG6453		3	0.9038
CG6988	Protein disulfide isomerase	3	0.90959
CG4769		1	0.91579
CG11207	fascetto	2	0.9258
CG5170	Dodeca-satellite-binding protein 1	6	0.93227
CG7831	non-claret disjunctional	17	0.95124
CG7261		3	0.95161
CG7434	Ribosomal protein L22	2	0.95545
CG33123		9	0.96168
CG4307	Oligomycin sensitivity-conferring protein	1	0.97106
CG4254	twinstar	2	0.98271
CG5258	NHP2	1	0.98375
CG8402	Protein phosphatase D3	2	0.98473
CG12008	karst	4	0.9901
CG18076	short stop	42	0.99025
CG6341	Elongation factor 1 β	4	0.99096
CG12233	lethal (1) G0156	4	0.995

CG Number	Synonym	Number of peptides	Ratio "Heavy"/"Light"
CG5520	Glycoprotein 93	8	0.99749
CG7490	Ribosomal protein LP0	4	1.0042
CG4912	eEF1δ	4	1.01
CG8542	Heat shock protein cognate 5	2	1.0154
CG9302		2	1.0205
CG9888	Fibrillarin	4	1.0236
CG6684	Ribosomal protein S25	2	1.0249
CG4046	Ribosomal protein S16	1	1.0271
CG8732	Acyl-CoA synthetase long-chain	3	1.0311
CG12306	polo	5	1.0318
CG7070	Pyruvate kinase	2	1.037
CG11876		1	1.0373
CG8983	ERp60	2	1.0439
CG6944	Lamin	3	1.0561
CG5854		2	1.0665
CG2918		2	1.0704
CG12030		7	1.0765
CG7421	Nopp140	2	1.0869
CG10279	Rm62	2	1.0905
CG12055	Glyceraldehyde 3 phosphate dehydrogenase 1	3	1.0949
CG4264	Heat shock protein cognate 4	11	1.0955
CG6512		1	1.0974
CG4147	Heat shock protein cognate 3	7	1.0997
CG8280	Elongation factor 1α48D	2	1.0997
CG4027	Actin 5C	4	1.1004

CG Number	Synonym	Number of peptides	Ratio "Heavy"/"Light"
CG11276	Ribosomal protein S4	1	1.1069
CG8893	Glyceraldehyde 3 phosphate dehydrogenase 2	3	1.107
CG8274	Megator	7	1.1119
CG17870	14-3-3ζ	3	1.1175
CG3373	Hemomucin	2	1.1178
CG8258		5	1.1214
CG6773	sec13	1	1.1223
CG4463	Heat shock protein 23	3	1.1284
CG13849	Nop56	6	1.1444
CG4878	eIF3-S9	2	1.1507
CG1242	Heat shock protein 83	11	1.1595
CG1345	Glutamine:fructose-6-phosphate aminotransferase 2	2	1.17
CG3821	Aspartyl-tRNA synthetase	5	1.1705
CG15100		5	1.1742
CG14897		3	1.1887
CG8415	Ribosomal protein S23	1	1.1891
CG8231	T-cp1ζ	4	1.1894
CG1101	Aly	2	1.1918
CG2168	Ribosomal protein S3A	2	1.2248
CG5353	Threonyl-tRNA synthetase	9	1.2253
CG14648	growl	4	1.2287
CG10712	Chromator	3	1.2334
CG12101	Heat shock protein 60	3	1.2494
CG10687	Asparaginyl-tRNA synthetase	6	1.261

CG Number	Synonym	Number of peptides	Ratio "Heavy"/"Light"
CG7917	Nucleoplasmin	2	1.2667
CG13391	Alanyl-tRNA synthetase	3	1.2712
CG6143	Protein on ecdysone puffs	6	1.2951
CG33910	His2B:CG33910	2	1.3004
CG8977	Cctγ	6	1.3111
CG1977	α Spectrin	8	1.345
CG34417		3	1.4354
CG13096		2	1.4881
CG31196	14-3-3ε	1	1.5008
CG4183	Heat shock protein 26	2	1.6029
CG4460	Heat shock protein 22	2	1.666
CG14998	ensconsin	16	1.8021
CG5870	β Spectrin	2	1.9627

Cited Literature

Alberts, B., Johnson, A., Lewis, J., Raff, M., Roberts, K., Walter, P. 2002. Molecular biology of the cell. Garland Science, New York.

Allen, C., and G.G. Borisy. 1974. Structural polarity and directional growth of microtubules of Chlamydomonas flagella. *J Mol Biol*. 90:381-402.

Amos, L., and A. Klug. 1974. Arrangement of subunits in flagellar microtubules. *J Cell Sci*. 14:523-49.

Amos, L.A., and R.A. Cross. 1997. Structure and dynamics of molecular motors. *Curr Opin Struct Biol*. 7:239-46.

Andersen, J.S., C.J. Wilkinson, T. Mayor, P. Mortensen, E.A. Nigg, and M. Mann. 2003. Proteomic characterization of the human centrosome by protein correlation profiling. *Nature*. 426:570-4.

Aravind, L., and E.V. Koonin. 2000. SAP - a putative DNA-binding motif involved in chromosomal organization. *Trends Biochem Sci*. 25:112-4.

Ashburner, M. 2005. Drosophila A laboratory handbook. Cold Spring Harbour Laboratory press, New York.

Baas, P.W., T. Slaughter, A. Brown, and M.M. Black. 1991. Microtubule dynamics in axons and dendrites. *J Neurosci Res*. 30:134-53.

Bauer, A., and B. Kuster. 2003. Affinity purification-mass spectrometry. Powerful tools for the characterization of protein complexes. *Eur J Biochem*. 270:570-8.

Belmont, L.D., A.A. Hyman, K.E. Sawin, and T.J. Mitchison. 1990. Real-time visualization of cell cycle-dependent changes in microtubule dynamics in cytoplasmic extracts. *Cell*. 62:579-89.

Belmont, L.D., and T.J. Mitchison. 1996. Identification of a protein that interacts with tubulin dimers and increases the catastrophe rate of microtubules. *Cell*. 84:623-31.

Biernat, J., N. Gustke, G. Drewes, E.M. Mandelkow, and E. Mandelkow. 1993. Phosphorylation of Ser262 strongly reduces binding of tau to microtubules: distinction between PHF-like immunoreactivity and microtubule binding. *Neuron*. 11:153-63.

Biernat, J., and E.M. Mandelkow. 1999. The development of cell processes induced by tau protein requires phosphorylation of serine 262 and 356 in the repeat

domain and is inhibited by phosphorylation in the proline-rich domains. *Mol Biol Cell*. 10:727-40.

Bodenmiller, B., J. Malmstrom, B. Gerrits, D. Campbell, H. Lam, A. Schmidt, O. Rinner, L.N. Mueller, P.T. Shannon, P.G. Pedrioli, C. Panse, H.K. Lee, R. Schlapbach, and R. Aebersold. 2007. PhosphoPep--a phosphoproteome resource for systems biology research in Drosophila Kc167 cells. *Mol Syst Biol*. 3:139.

Bonaldi, T., T. Straub, J. Cox, C. Kumar, P.B. Becker, and M. Mann. 2008. Combined use of RNAi and quantitative proteomics to study gene function in Drosophila. *Mol Cell*. 31:762-72.

Borisy, G.G., J.M. Marcum, J.B. Olmsted, D.B. Murphy, and K.A. Johnson. 1975. Purification of tubulin and associated high molecular weight proteins from porcine brain and characterization of microtubule assembly in vitro. *Ann N Y Acad Sci*. 253:107-32.

Brady, S.T., K.K. Pfister, and G.S. Bloom. 1990. A monoclonal antibody against kinesin inhibits both anterograde and retrograde fast axonal transport in squid axoplasm. *Proc Natl Acad Sci U S A*. 87:1061-5.

Brand, A.H., and N. Perrimon. 1993. Targeted gene expression as a means of altering cell fates and generating dominant phenotypes. *Development*. 118:401-15.

Bulinski, J.C., and G.G. Gundersen. 1991. Stabilization of post-translational modification of microtubules during cellular morphogenesis. *Bioessays*. 13:285-93.

Burns, R.G. 1991. Alpha-, beta-, and gamma-tubulins: sequence comparisons and structural constraints. *Cell Motil Cytoskeleton*. 20:181-9.

Cahu, J., A. Olichon, C. Hentrich, H. Schek, J. Drinjakovic, C. Zhang, A. Doherty-Kirby, G. Lajoie, and T. Surrey. 2008. Phosphorylation by Cdk1 increases the binding of Eg5 to microtubules in vitro and in Xenopus egg extract spindles. *PLoS One*. 3:e3936.

Caplow, M. 1992. Microtubule dynamics. *Curr Opin Cell Biol*. 4:58-65.

Caplow, M., R.L. Ruhlen, and J. Shanks. 1994. The free energy for hydrolysis of a microtubule-bound nucleotide triphosphate is near zero: all of the free energy for hydrolysis is stored in the microtubule lattice. *J Cell Biol*. 127:779-88.

Caplow, M., and J. Shanks. 1990. Mechanism of the microtubule GTPase reaction. *J Biol Chem*. 265:8935-41.

Carazo-Salas, R.E., G. Guarguaglini, O.J. Gruss, A. Segref, E. Karsenti, and I.W. Mattaj. 1999. Generation of GTP-bound Ran by RCC1 is required for chromatin-induced mitotic spindle formation. *Nature*. 400:178-81.

Carlier, M.F., and D. Pantaloni. 1981. Kinetic analysis of guanosine 5'-triphosphate hydrolysis associated with tubulin polymerization. *Biochemistry*. 20:1918-24.

Caudron, M., G. Bunt, P. Bastiaens, and E. Karsenti. 2005. Spatial coordination of spindle assembly by chromosome-mediated signaling gradients. *Science*. 309:1373-6.

Chretien, D., S.D. Fuller, and E. Karsenti. 1995. Structure of growing microtubule ends: two-dimensional sheets close into tubes at variable rates. *J Cell Biol*. 129:1311-28.

Compton, D.A., and C. Luo. 1995. Mutation of the predicted p34cdc2 phosphorylation sites in NuMA impair the assembly of the mitotic spindle and block mitosis. *J Cell Sci*. 108 (Pt 2):621-33.

Cox, J., and M. Mann. 2008. MaxQuant enables high peptide identification rates, individualized p.p.b.-range mass accuracies and proteome-wide protein quantification. *Nat Biotechnol*. 26:1367-72.

Cox, J., I. Matic, M. Hilger, N. Nagaraj, M. Selbach, J.V. Olsen, and M. Mann. 2009. A practical guide to the MaxQuant computational platform for SILAC-based quantitative proteomics. *Nat Protoc*. 4:698-705.

Dasso, M. 2002. The Ran GTPase: theme and variations. *Curr Biol*. 12:R502-8.

David-Pfeuty, T., H.P. Erickson, and D. Pantaloni. 1977. Guanosinetriphosphatase activity of tubulin associated with microtubule assembly. *Proc Natl Acad Sci U S A*. 74:5372-6.

Davis, F.M., T.Y. Tsao, S.K. Fowler, and P.N. Rao. 1983. Monoclonal antibodies to mitotic cells. *Proc Natl Acad Sci U S A*. 80:2926-30.

Desai, A., and T.J. Mitchison. 1997. Microtubule polymerization dynamics. *Annu Rev Cell Dev Biol*. 13:83-117.

Detrich, H.W., 3rd, and M.A. Jordan. 1986. Mechanism of assembly of sea urchin egg tubulin. *Ann N Y Acad Sci*. 466:529-42.

Diaz, J.F., E. Pantos, J. Bordas, and J.M. Andreu. 1994. Solution structure of GDP-tubulin double rings to 3 nm resolution and comparison with microtubules. *J Mol Biol*. 238:214-25.

Drechsel, D.N., A.A. Hyman, M.H. Cobb, and M.W. Kirschner. 1992. Modulation of the dynamic instability of tubulin assembly by the microtubule-associated protein tau. *Mol Biol Cell*. 3:1141-54.

Drechsel, D.N., and M.W. Kirschner. 1994. The minimum GTP cap required to stabilize microtubules. *Curr Biol*. 4:1053-61.

Drubin, D.G., S.C. Feinstein, E.M. Shooter, and M.W. Kirschner. 1985. Nerve growth factor-induced neurite outgrowth in PC12 cells involves the coordinate induction of microtubule assembly and assembly-promoting factors. *J Cell Biol*. 101:1799-807.

Enos, A.P., and N.R. Morris. 1990. Mutation of a gene that encodes a kinesin-like protein blocks nuclear division in A. nidulans. *Cell*. 60:1019-27.

Erickson, H.P. 1974. Microtubule surface lattice and subunit structure and observations on reassembly. *J Cell Biol*. 60:153-67.

Eshel, D., L.A. Urrestarazu, S. Vissers, J.C. Jauniaux, J.C. van Vliet-Reedijk, R.J. Planta, and I.R. Gibbons. 1993. Cytoplasmic dynein is required for normal nuclear segregation in yeast. *Proc Natl Acad Sci U S A*. 90:11172-6.

Esmaeli-Azad, B., J.H. McCarty, and S.C. Feinstein. 1994. Sense and antisense transfection analysis of tau function: tau influences net microtubule assembly, neurite outgrowth and neuritic stability. *J Cell Sci*. 107 (Pt 4):869-79.

Evans, L., T. Mitchison, and M. Kirschner. 1985. Influence of the centrosome on the structure of nucleated microtubules. *J Cell Biol*. 100:1185-91.

Fan, J., A.D. Griffiths, A. Lockhart, R.A. Cross, and L.A. Amos. 1996. Microtubule minus ends can be labelled with a phage display antibody specific to alpha-tubulin. *J Mol Biol*. 259:325-30.

Gaglio, T., A. Saredi, and D.A. Compton. 1995. NuMA is required for the organization of microtubules into aster-like mitotic arrays. *J Cell Biol*. 131:693-708.

Garrett, S., K. Auer, D.A. Compton, and T.M. Kapoor. 2002. hTPX2 is required for normal spindle morphology and centrosome integrity during vertebrate cell division. *Curr Biol*. 12:2055-9.

Gatti, M., and B.S. Baker. 1989. Genes controlling essential cell-cycle functions in Drosophila melanogaster. *Genes Dev*. 3:438-53.

Gehmlich, K., L. Haren, and A. Merdes. 2004. Cyclin B degradation leads to NuMA release from dynein/dynactin and from spindle poles. *EMBO Rep*. 5:97-103.

Gliksman, N.R., S.F. Parsons, and E.D. Salmon. 1992. Okadaic acid induces interphase to mitotic-like microtubule dynamic instability by inactivating rescue. *J Cell Biol*. 119:1271-6.

Gliksman, N.R., R.V. Skibbens, and E.D. Salmon. 1993. How the transition frequencies of microtubule dynamic instability (nucleation, catastrophe, and rescue) regulate microtubule dynamics in interphase and mitosis: analysis using a Monte Carlo computer simulation. *Mol Biol Cell*. 4:1035-50.

Goldstein, L.S., R.A. Laymon, and J.R. McIntosh. 1986. A microtubule-associated protein in Drosophila melanogaster: identification, characterization, and isolation of coding sequences. *J Cell Biol*. 102:2076-87.

Gonczy, P., S. Pichler, M. Kirkham, and A.A. Hyman. 1999. Cytoplasmic dynein is required for distinct aspects of MTOC positioning, including centrosome separation, in the one cell stage Caenorhabditis elegans embryo. *J Cell Biol*. 147:135-50.

Goshima, G., F. Nedelec, and R.D. Vale. 2005. Mechanisms for focusing mitotic spindle poles by minus end-directed motor proteins. *J Cell Biol*. 171:229-40.

Goshima, G., and R.D. Vale. 2005. Cell cycle-dependent dynamics and regulation of mitotic kinesins in Drosophila S2 cells. *Mol Biol Cell*. 16:3896-907.

Goshima, G., R. Wollman, S.S. Goodwin, N. Zhang, J.M. Scholey, R.D. Vale, and N. Stuurman. 2007. Genes required for mitotic spindle assembly in Drosophila S2 cells. *Science*. 316:417-21.

Groen, A.C., T.J. Maresca, J.C. Gatlin, E.D. Salmon, and T.J. Mitchison. 2009. Functional overlap of microtubule assembly factors in chromatin-promoted spindle assembly. *Mol Biol Cell*. 20:2766-73.

Gruss, O.J., R.E. Carazo-Salas, C.A. Schatz, G. Guarguaglini, J. Kast, M. Wilm, N. Le Bot, I. Vernos, E. Karsenti, and I.W. Mattaj. 2001. Ran induces spindle assembly by reversing the inhibitory effect of importin alpha on TPX2 activity. *Cell*. 104:83-93.

Gruss, O.J., M. Wittmann, H. Yokoyama, R. Pepperkok, T. Kufer, H. Sillje, E. Karsenti, I.W. Mattaj, and I. Vernos. 2002. Chromosome-induced microtubule assembly mediated by TPX2 is required for spindle formation in HeLa cells. *Nat Cell Biol*. 4:871-9.

Hans, F., and S. Dimitrov. 2001. Histone H3 phosphorylation and cell division. *Oncogene*. 20:3021-7.

Hartman, J.J., J. Mahr, K. McNally, K. Okawa, A. Iwamatsu, S. Thomas, S. Cheesman, J. Heuser, R.D. Vale, and F.J. McNally. 1998. Katanin, a

microtubule-severing protein, is a novel AAA ATPase that targets to the centrosome using a WD40-containing subunit. *Cell*. 93:277-87.

Hayden, J.H., S.S. Bowser, and C.L. Rieder. 1990. Kinetochores capture astral microtubules during chromosome attachment to the mitotic spindle: direct visualization in live newt lung cells. *J Cell Biol*. 111:1039-45.

Heck, M.M., A. Pereira, P. Pesavento, Y. Yannoni, A.C. Spradling, and L.S. Goldstein. 1993. The kinesin-like protein KLP61F is essential for mitosis in Drosophila. *J Cell Biol*. 123:665-79.

Holy, T.E., and S. Leibler. 1994. Dynamic instability of microtubules as an efficient way to search in space. *Proc Natl Acad Sci U S A*. 91:5682-5.

Holzinger, A., and U. Lutz-Meindl. 2002. Kinesin-like proteins are involved in postmitotic nuclear migration of the unicellular green alga Micrasterias denticulata. *Cell Biol Int*. 26:689-97.

Horio, T., and H. Hotani. 1986. Visualization of the dynamic instability of individual microtubules by dark-field microscopy. *Nature*. 321:605-7.

Hotani, H., and T. Horio. 1988. Dynamics of microtubules visualized by darkfield microscopy: treadmilling and dynamic instability. *Cell Motil Cytoskeleton*. 10:229-36.

Howard, W.D., and S.N. Timasheff. 1986. GDP state of tubulin: stabilization of double rings. *Biochemistry*. 25:8292-300.

Hughes, J.R., A.M. Meireles, K.H. Fisher, A. Garcia, P.R. Antrobus, A. Wainman, N. Zitzmann, C. Deane, H. Ohkura, and J.G. Wakefield. 2008. A microtubule interactome: complexes with roles in cell cycle and mitosis. *PLoS Biol*. 6:e98.

Inoue, S., and H. Sato. 1967. Cell motility by labile association of molecules. The nature of mitotic spindle fibers and their role in chromosome movement. *J Gen Physiol*. 50:Suppl:259-92.

Kalab, P., A. Pralle, E.Y. Isacoff, R. Heald, and K. Weis. 2006. Analysis of a RanGTP-regulated gradient in mitotic somatic cells. *Nature*. 440:697-701.

Kalab, P., R.T. Pu, and M. Dasso. 1999. The ran GTPase regulates mitotic spindle assembly. *Curr Biol*. 9:481-4.

Kalab, P., K. Weis, and R. Heald. 2002. Visualization of a Ran-GTP gradient in interphase and mitotic Xenopus egg extracts. *Science*. 295:2452-6.

Kalderon, D., B.L. Roberts, W.D. Richardson, and A.E. Smith. 1984. A short amino acid sequence able to specify nuclear location. *Cell*. 39:499-509.

Kallajoki, M., J. Harborth, K. Weber, and M. Osborn. 1993. Microinjection of a monoclonal antibody against SPN antigen, now identified by peptide sequences as the NuMA protein, induces micronuclei in PtK2 cells. *J Cell Sci*. 104 (Pt 1):139-50.

Kallajoki, M., K. Weber, and M. Osborn. 1991. A 210 kDa nuclear matrix protein is a functional part of the mitotic spindle; a microinjection study using SPN monoclonal antibodies. *EMBO J*. 10:3351-62.

Kellogg, D.R., C.M. Field, and B.M. Alberts. 1989. Identification of microtubule-associated proteins in the centrosome, spindle, and kinetochore of the early Drosophila embryo. *J Cell Biol*. 109:2977-91.

Kikkawa, M., T. Ishikawa, T. Nakata, T. Wakabayashi, and N. Hirokawa. 1994. Direct visualization of the microtubule lattice seam both in vitro and in vivo. *J Cell Biol*. 127:1965-71.

Koffa, M.D., C.M. Casanova, R. Santarella, T. Kocher, M. Wilm, and I.W. Mattaj. 2006. HURP is part of a Ran-dependent complex involved in spindle formation. *Curr Biol*. 16:743-54.

Kuroda, I., Y. Shintani, M. Motokawa, S. Abe, and M. Furuno. 2004. Phosphopeptide-selective column-switching RP-HPLC with a titania precolumn. *Anal Sci*. 20:1313-9.

Larsen, M.R., T.E. Thingholm, O.N. Jensen, P. Roepstorff, and T.J. Jorgensen. 2005. Highly selective enrichment of phosphorylated peptides from peptide mixtures using titanium dioxide microcolumns. *Mol Cell Proteomics*. 4:873-86.

Lawrence, C.J., R.K. Dawe, K.R. Christie, D.W. Cleveland, S.C. Dawson, S.A. Endow, L.S. Goldstein, H.V. Goodson, N. Hirokawa, J. Howard, R.L. Malmberg, J.R. McIntosh, H. Miki, T.J. Mitchison, Y. Okada, A.S. Reddy, W.M. Saxton, M. Schliwa, J.M. Scholey, R.D. Vale, C.E. Walczak, and L. Wordeman. 2004. A standardized kinesin nomenclature. *J Cell Biol*. 167:19-22.

Lindwall, G., and R.D. Cole. 1984. Phosphorylation affects the ability of tau protein to promote microtubule assembly. *J Biol Chem*. 259:5301-5.

Lupas, A., M. Van Dyke, and J. Stock. 1991. Predicting coiled coils from protein sequences. *Science*. 252:1162-4.

Lydersen, B.K., and D.E. Pettijohn. 1980. Human-specific nuclear protein that associates with the polar region of the mitotic apparatus: distribution in a human/hamster hybrid cell. *Cell*. 22:489-99.

Macek, B., F. Gnad, B. Soufi, C. Kumar, J.V. Olsen, I. Mijakovic, and M. Mann. 2008. Phosphoproteome analysis of E. coli reveals evolutionary conservation of bacterial Ser/Thr/Tyr phosphorylation. *Mol Cell Proteomics*. 7:299-307.

Macek, B., I. Mijakovic, J.V. Olsen, F. Gnad, C. Kumar, P.R. Jensen, and M. Mann. 2007. The serine/threonine/tyrosine phosphoproteome of the model bacterium Bacillus subtilis. *Mol Cell Proteomics*. 6:697-707.

Mack, G.J., and D.A. Compton. 2001. Analysis of mitotic microtubule-associated proteins using mass spectrometry identifies astrin, a spindle-associated protein. *Proc Natl Acad Sci U S A*. 98:14434-9.

Mandelkow, E.M., E. Mandelkow, and R.A. Milligan. 1991. Microtubule dynamics and microtubule caps: a time-resolved cryo-electron microscopy study. *J Cell Biol*. 114:977-91.

Margolis, R.L., and L. Wilson. 1978. Opposite end assembly and disassembly of microtubules at steady state in vitro. *Cell*. 13:1-8.

Margolis, R.L., and L. Wilson. 1981. Microtubule treadmills--possible molecular machinery. *Nature*. 293:705-11.

Matthias, P., M. Yoshida, and S. Khochbin. 2008. HDAC6 a new cellular stress surveillance factor. *Cell Cycle*. 7:7-10.

McIntosh, J.R., U.P. Roos, B. Neighbors, and K.L. McDonald. 1985. Architecture of the microtubule component of mitotic spindles from Dictyostelium discoideum. *J Cell Sci*. 75:93-129.

McLachlin, D.T., and B.T. Chait. 2001. Analysis of phosphorylated proteins and peptides by mass spectrometry. *Curr Opin Chem Biol*. 5:591-602.

McNally, F.J., K. Okawa, A. Iwamatsu, and R.D. Vale. 1996. Katanin, the microtubule-severing ATPase, is concentrated at centrosomes. *J Cell Sci*. 109 (Pt 3):561-7.

McNally, F.J., and R.D. Vale. 1993. Identification of katanin, an ATPase that severs and disassembles stable microtubules. *Cell*. 75:419-29.

Melki, R., M.F. Carlier, and D. Pantaloni. 1990. Direct evidence for GTP and GDP-Pi intermediates in microtubule assembly. *Biochemistry*. 29:8921-32.

Melki, R., S. Fievez, and M.F. Carlier. 1996. Continuous monitoring of Pi release following nucleotide hydrolysis in actin or tubulin assembly using 2-amino-6-mercapto-7-methylpurine ribonucleoside and purine-nucleoside phosphorylase as an enzyme-linked assay. *Biochemistry*. 35:12038-45.

Merdes, A., K. Ramyar, J.D. Vechio, and D.W. Cleveland. 1996. A complex of NuMA and cytoplasmic dynein is essential for mitotic spindle assembly. *Cell*. 87:447-58.

Miki, H., Y. Okada, and N. Hirokawa. 2005. Analysis of the kinesin superfamily: insights into structure and function. *Trends Cell Biol*. 15:467-76.

Mitchison, T., and M. Kirschner. 1984. Dynamic instability of microtubule growth. *Nature*. 312:237-42.

Mitchison, T.J. 1993. Localization of an exchangeable GTP binding site at the plus end of microtubules. *Science*. 261:1044-7.

Morales-Mulia, S., and J.M. Scholey. 2005. Spindle pole organization in Drosophila S2 cells by dynein, abnormal spindle protein (Asp), and KLP10A. *Mol Biol Cell*. 16:3176-86.

Morishima-Kawashima, M., M. Hasegawa, K. Takio, M. Suzuki, H. Yoshida, K. Titani, and Y. Ihara. 1995. Proline-directed and non-proline-directed phosphorylation of PHF-tau. *J Biol Chem*. 270:823-9.

Mortensen, P., J.W. Gouw, J.V. Olsen, S.E. Ong, K.T. Rigbolt, J. Bunkenborg, J. Cox, L.J. Foster, A.J. Heck, B. Blagoev, J.S. Andersen, and M. Mann. 2010. MSQuant, an open source platform for mass spectrometry-based quantitative proteomics. *J Proteome Res*. 9:393-403.

Muller, H., D. Schmidt, S. Steinbrink, E. Mirgorodskaya, V. Lehmann, K. Habermann, F. Dreher, N. Gustavsson, T. Kessler, H. Lehrach, R. Herwig, J. Gobom, A. Ploubidou, M. Boutros, and B.M. Lange. Proteomic and functional analysis of the mitotic Drosophila centrosome. *EMBO J*. 29:3344-57.

Nachury, M.V., T.J. Maresca, W.C. Salmon, C.M. Waterman-Storer, R. Heald, and K. Weis. 2001. Importin beta is a mitotic target of the small GTPase Ran in spindle assembly. *Cell*. 104:95-106.

Nakamura, K., H. Ida, and M. Yamaguchi. 2008. Transcriptional regulation of the Drosophila moira and osa genes by the DREF pathway. *Nucleic Acids Res*. 36:3905-15.

Nakano, A., H. Kato, T. Watanabe, K.D. Min, S. Yamazaki, Y. Asano, O. Seguchi, S. Higo, Y. Shintani, H. Asanuma, M. Asakura, T. Minamino, K. Kaibuchi, N. Mochizuki, M. Kitakaze, and S. Takashima. 2010. AMPK controls the speed of microtubule polymerization and directional cell migration through CLIP-170 phosphorylation. *Nat Cell Biol*. 12:583-90.

Nogales, E., M. Whittaker, R.A. Milligan, and K.H. Downing. 1999. High-resolution model of the microtubule. *Cell*. 96:79-88.

Ohba, T., M. Nakamura, H. Nishitani, and T. Nishimoto. 1999. Self-organization of microtubule asters induced in Xenopus egg extracts by GTP-bound Ran. *Science*. 284:1356-8.

Ong, S.E., B. Blagoev, I. Kratchmarova, D.B. Kristensen, H. Steen, A. Pandey, and M. Mann. 2002. Stable isotope labeling by amino acids in cell culture, SILAC, as a simple and accurate approach to expression proteomics. *Mol Cell Proteomics*. 1:376-86.

Ong, S.E., L.J. Foster, and M. Mann. 2003. Mass spectrometric-based approaches in quantitative proteomics. *Methods*. 29:124-30.

Ozlu, N., F. Monigatti, B.Y. Renard, C.M. Field, H. Steen, T.J. Mitchison, and J.J. Steen. 2010. Binding partner switching on microtubules and aurora-B in the mitosis to cytokinesis transition. *Mol Cell Proteomics*. 9:336-50.

Perkins, D.N., D.J. Pappin, D.M. Creasy, and J.S. Cottrell. 1999. Probability-based protein identification by searching sequence databases using mass spectrometry data. *Electrophoresis*. 20:3551-67.

Pinkse, M.W., P.M. Uitto, M.J. Hilhorst, B. Ooms, and A.J. Heck. 2004. Selective isolation at the femtomole level of phosphopeptides from proteolytic digests using 2D-NanoLC-ESI-MS/MS and titanium oxide precolumns. *Anal Chem*. 76:3935-43.

Plattner, F., M. Angelo, and K.P. Giese. 2006. The roles of cyclin-dependent kinase 5 and glycogen synthase kinase 3 in tau hyperphosphorylation. *J Biol Chem*. 281:25457-65.

Raemaekers, T., K. Ribbeck, J. Beaudouin, W. Annaert, M. Van Camp, I. Stockmans, N. Smets, R. Bouillon, J. Ellenberg, and G. Carmeliet. 2003. NuSAP, a novel microtubule-associated protein involved in mitotic spindle organization. *J Cell Biol*. 162:1017-29.

Rappsilber, J., Y. Ishihama, and M. Mann. 2003. Stop and go extraction tips for matrix-assisted laser desorption/ionization, nanoelectrospray, and LC/MS sample pretreatment in proteomics. *Anal Chem*. 75:663-70.

Rechsteiner, M., and S.W. Rogers. 1996. PEST sequences and regulation by proteolysis. *Trends Biochem Sci*. 21:267-71.

Reinders, J., and A. Sickmann. 2005. State-of-the-art in phosphoproteomics. *Proteomics*. 5:4052-61.

Ribbeck, K., A.C. Groen, R. Santarella, M.T. Bohnsack, T. Raemaekers, T. Kocher, M. Gentzel, D. Gorlich, M. Wilm, G. Carmeliet, T.J. Mitchison, J. Ellenberg, A. Hoenger, and I.W. Mattaj. 2006. NuSAP, a mitotic RanGTP target that stabilizes and cross-links microtubules. *Mol Biol Cell*. 17:2646-60.

Ribbeck, K., T. Raemaekers, G. Carmeliet, and I.W. Mattaj. 2007. A role for NuSAP in linking microtubules to mitotic chromosomes. *Curr Biol*. 17:230-6.

Robinson, J.M., and D.D. Vandre. 1995. Stimulus-dependent alterations in macrophage microtubules: increased tubulin polymerization and detyrosination. *J Cell Sci*. 108 (Pt 2):645-55.

Rodionov, V.I., and G.G. Borisy. 1997. Microtubule treadmilling in vivo. *Science*. 275:215-8.

Rogers, S.L., G.C. Rogers, D.J. Sharp, and R.D. Vale. 2002. Drosophila EB1 is important for proper assembly, dynamics, and positioning of the mitotic spindle. *J Cell Biol*. 158:873-84.

Rorth, P. 1998. Gal4 in the Drosophila female germline. *Mech Dev*. 78:113-8.

Roth, P., N. Xylourgidis, N. Sabri, A. Uv, M. Fornerod, and C. Samakovlis. 2003. The Drosophila nucleoporin DNup88 localizes DNup214 and CRM1 on the nuclear envelope and attenuates NES-mediated nuclear export. *J Cell Biol*. 163:701-6.

Sambrook, J., Fritsch, E.F. and Maniatis, T. 1989. Molecular cloning: A laboratory manual. Cold Spring Harbour Laboratory Press, New York.

Sauer, G., R. Korner, A. Hanisch, A. Ries, E.A. Nigg, and H.H. Sillje. 2005. Proteome analysis of the human mitotic spindle. *Mol Cell Proteomics*. 4:35-43.

Sawin, K.E., and T.J. Mitchison. 1995. Mutations in the kinesin-like protein Eg5 disrupting localization to the mitotic spindle. *Proc Natl Acad Sci U S A*. 92:4289-93.

Saxton, W.M., D.L. Stemple, R.J. Leslie, E.D. Salmon, M. Zavortink, and J.R. McIntosh. 1984. Tubulin dynamics in cultured mammalian cells. *J Cell Biol*. 99:2175-86.

Schatz, C.A., R. Santarella, A. Hoenger, E. Karsenti, I.W. Mattaj, O.J. Gruss, and R.E. Carazo-Salas. 2003. Importin alpha-regulated nucleation of microtubules by TPX2. *EMBO J*. 22:2060-70.

Sengupta, A., J. Kabat, M. Novak, Q. Wu, I. Grundke-Iqbal, and K. Iqbal. 1998. Phosphorylation of tau at both Thr 231 and Ser 262 is required for maximal inhibition of its binding to microtubules. *Arch Biochem Biophys*. 357:299-309.

Sengupta, A., M. Novak, I. Grundke-Iqbal, and K. Iqbal. 2006. Regulation of phosphorylation of tau by cyclin-dependent kinase 5 and glycogen synthase kinase-3 at substrate level. *FEBS Lett*. 580:5925-33.

Sharp, D.J., K.L. McDonald, H.M. Brown, H.J. Matthies, C. Walczak, R.D. Vale, T.J. Mitchison, and J.M. Scholey. 1999. The bipolar kinesin, KLP61F, cross-links microtubules within interpolar microtubule bundles of Drosophila embryonic mitotic spindles. *J Cell Biol*. 144:125-38.

Shevchenko, A., M. Wilm, O. Vorm, and M. Mann. 1996. Mass spectrometric sequencing of proteins silver-stained polyacrylamide gels. *Anal Chem*. 68:850-8.

Simon, J.R., S.F. Parsons, and E.D. Salmon. 1992. Buffer conditions and non-tubulin factors critically affect the microtubule dynamic instability of sea urchin egg tubulin. *Cell Motil Cytoskeleton*. 21:1-14.

Simon, J.R., and E.D. Salmon. 1990. The structure of microtubule ends during the elongation and shortening phases of dynamic instability examined by negative-stain electron microscopy. *J Cell Sci*. 96 (Pt 4):571-82.

Sisson, J.C., C. Field, R. Ventura, A. Royou, and W. Sullivan. 2000. Lava lamp, a novel peripheral golgi protein, is required for Drosophila melanogaster cellularization. *J Cell Biol*. 151:905-18.

Skop, A.R., H. Liu, J. Yates, 3rd, B.J. Meyer, and R. Heald. 2004. Dissection of the mammalian midbody proteome reveals conserved cytokinesis mechanisms. *Science*. 305:61-6.

Solomon, F., M. Magendantz, and A. Salzman. 1979. Identification with cellular microtubules of one of the co-assemlbing microtubule-associated proteins. *Cell*. 18:431-8.

Song, L., and M. Rape. 2010. Regulated degradation of spindle assembly factors by the anaphase-promoting complex. *Mol Cell*. 38:369-82.

Spiegelman, B.M., S.M. Penningroth, and M.W. Kirschner. 1977. Turnover of tubulin and the N site GTP in Chinese hamster ovary cells. *Cell*. 12:587-600.

Sugiyama, N., T. Masuda, K. Shinoda, A. Nakamura, M. Tomita, and Y. Ishihama. 2007. Phosphopeptide enrichment by aliphatic hydroxy acid-modified metal oxide chromatography for nano-LC-MS/MS in proteomics applications. *Mol Cell Proteomics*. 6:1103-9.

Sun, Q.Y., and H. Schatten. 2006. Role of NuMA in vertebrate cells: review of an intriguing multifunctional protein. *Front Biosci*. 11:1137-46.

Suryadinata, R., M. Sadowski, and B. Sarcevic. 2010. Control of cell cycle progression by phosphorylation of cyclin-dependent kinase (CDK) substrates. *Biosci Rep*. 30:243-55.

Tanaka, E.M., and M.W. Kirschner. 1991. Microtubule behavior in the growth cones of living neurons during axon elongation. *J Cell Biol*. 115:345-63.

Trieselmann, N., S. Armstrong, J. Rauw, and A. Wilde. 2003. Ran modulates spindle assembly by regulating a subset of TPX2 and Kid activities including Aurora A activation. *J Cell Sci*. 116:4791-8.

Tsai, M.Y., C. Wiese, K. Cao, O. Martin, P. Donovan, J. Ruderman, C. Prigent, and Y. Zheng. 2003. A Ran signalling pathway mediated by the mitotic kinase Aurora A in spindle assembly. *Nat Cell Biol*. 5:242-8.

Tsou, A.P., C.W. Yang, C.Y. Huang, R.C. Yu, Y.C. Lee, C.W. Chang, B.R. Chen, Y.F. Chung, M.J. Fann, C.W. Chi, J.H. Chiu, and C.K. Chou. 2003. Identification of a novel cell cycle regulated gene, HURP, overexpressed in human hepatocellular carcinoma. *Oncogene*. 22:298-307.

Tulu, U.S., C. Fagerstrom, N.P. Ferenz, and P. Wadsworth. 2006. Molecular requirements for kinetochore-associated microtubule formation in mammalian cells. *Curr Biol*. 16:536-41.

Valiron, O., N. Caudron, and D. Job. 2001. Microtubule dynamics. *Cell Mol Life Sci*. 58:2069-84.

Vallee, R.B. 1982. A taxol-dependent procedure for the isolation of microtubules and microtubule-associated proteins (MAPs). *J Cell Biol*. 92:435-42.

Vallee, R.B., and G.S. Bloom. 1983. Isolation of sea urchin egg microtubules with taxol and identification of mitotic spindle microtubule-associated proteins with monoclonal antibodies. *Proc Natl Acad Sci U S A*. 80:6259-63.

Verde, F., M. Dogterom, E. Stelzer, E. Karsenti, and S. Leibler. 1992. Control of microtubule dynamics and length by cyclin A- and cyclin B-dependent kinases in Xenopus egg extracts. *J Cell Biol*. 118:1097-108.

Walker, R.A., E.T. O'Brien, N.K. Pryer, M.F. Soboeiro, W.A. Voter, H.P. Erickson, and E.D. Salmon. 1988. Dynamic instability of individual microtubules analyzed by video light microscopy: rate constants and transition frequencies. *J Cell Biol*. 107:1437-48.

Walker, R.A., N.K. Pryer, and E.D. Salmon. 1991. Dilution of individual microtubules observed in real time in vitro: evidence that cap size is small and independent of elongation rate. *J Cell Biol*. 114:73-81.

Wegner, A. 1976. Head to tail polymerization of actin. *J Mol Biol*. 108:139-50.

Weisenberg, R.C., G.G. Borisy, and E.W. Taylor. 1968. The colchicine-binding protein of mammalian brain and its relation to microtubules. *Biochemistry*. 7:4466-79.

Wen, W., J.L. Meinkoth, R.Y. Tsien, and S.S. Taylor. 1995. Identification of a signal for rapid export of proteins from the nucleus. *Cell*. 82:463-73.

Wiese, C., A. Wilde, M.S. Moore, S.A. Adam, A. Merdes, and Y. Zheng. 2001. Role of importin-beta in coupling Ran to downstream targets in microtubule assembly. *Science*. 291:653-6.

Wilson, P.G., M.T. Fuller, and G.G. Borisy. 1997. Monastral bipolar spindles: implications for dynamic centrosome organization. *J Cell Sci*. 110 (Pt 4):451-64.

Wittmann, T., H. Boleti, C. Antony, E. Karsenti, and I. Vernos. 1998. Localization of the kinesin-like protein Xklp2 to spindle poles requires a leucine zipper, a microtubule-associated protein, and dynein. *J Cell Biol*. 143:673-85.

Wittmann, T., M. Wilm, E. Karsenti, and I. Vernos. 2000. TPX2, A novel xenopus MAP involved in spindle pole organization. *J Cell Biol*. 149:1405-18.

Wong, J., and G. Fang. 2006. HURP controls spindle dynamics to promote proper interkinetochore tension and efficient kinetochore capture. *J Cell Biol*. 173:879-91.

Yang, C.H., and M. Snyder. 1992. The nuclear-mitotic apparatus protein is important in the establishment and maintenance of the bipolar mitotic spindle apparatus. *Mol Biol Cell*. 3:1259-67.

Yang, X.J., and E. Seto. 2008. Lysine acetylation: codified crosstalk with other posttranslational modifications. *Mol Cell*. 31:449-61.

Yu, C.T., J.M. Hsu, Y.C. Lee, A.P. Tsou, C.K. Chou, and C.Y. Huang. 2005. Phosphorylation and stabilization of HURP by Aurora-A: implication of HURP as a transforming target of Aurora-A. *Mol Cell Biol*. 25:5789-800.

Zhang, X., Z. Yuan, Y. Zhang, S. Yong, A. Salas-Burgos, J. Koomen, N. Olashaw, J.T. Parsons, X.J. Yang, S.R. Dent, T.P. Yao, W.S. Lane, and E. Seto. 2007. HDAC6 modulates cell motility by altering the acetylation level of cortactin. *Mol Cell*. 27:197-213.

Zhao, J.Y., J. Kuang, R.C. Adlakha, and P.N. Rao. 1989. Threonine phosphorylation is associated with mitosis in HeLa cells. *FEBS Lett*. 249:389-95.